5-1-2014

The Application of Zircon (U-Th)/He Thermochronology to Determine the Timing and Slip Rate on the Willard Thrust, Sevier Fold and Thrust Belt, Northern Utah

Bryan Eleogram
University of Nevada, Las Vegas, eleogram@unlv.nevada.edu

THE APPLICATION OF ZIRCON (U-TH)/HE THERMOCHRONOLOGY TO DETERMINE THE TIMING AND SLIP RATE ON THE WILLARD THRUST, SEVIER FOLD AND THRUST BELT, NORTHERN UTAH

By

Bryan Ruston Eleogram

Bachelor of Science -- Geology
University of Nevada, Las Vegas
December 2011

A Thesis to be submitted in partial fulfillment
of the requirement for the

Masters of Science – Geology

Department of Geoscience
College of Sciences
The Graduate College

University of Nevada, Las Vegas
May 2014

UNLV
UNIVERSITY OF NEVADA LAS VEGAS

THE GRADUATE COLLEGE

We recommend the thesis prepared under our supervision by

Bryan Ruston Eleogram

entitled

The Application of Zircon (U-Th)/He Thermochronology to Determine the Timing and Slip Rate on the Willard Thrust, Sevier Fold and Thrust Belt, Northern Utah

is approved in partial fulfillment of the requirements for the degree of

Master of Science - Geoscience

Department of Geoscience

Michael Wells, Ph.D., Committee Chair

Adolph Yonkee, Ph.D., Committee Member

Andrew Hanson, Ph.D., Committee Member

Paul Forster, Ph.D., Graduate College Representative

Kathryn Hausbeck Korgan, Ph.D., Interim Dean of the Graduate College

May 2014

Abstract

Although the Sevier fold-thrust belt is one of the best-studied foreland systems in the world, timing of motion on the dominant western thrust sheets that carry thick Neoproterozoic to Paleozoic strata remains incompletely understood. Zircon (U-Th)/He thermochrometry (ZHe) studies of the hanging wall of the Willard thrust sheet (WTS) in northern Utah are used to constrain the timing and rate of thrust slip. Previous interpretations of the age of initial slip on the Willard thrust vary widely from 150 to 115 Ma, reflecting ambiguous relations with foreland basin strata and limited geochronologic data. The large displacement on the Willard thrust (~60 km net slip), the wide range of exposed levels (>8 km vertical structural relief), and the wide aerial extent (>60 km horizontal length) provide an ideal setting for application of ZHe to evaluate thrust timing. Samples were collected and analyzed for 40 sites along three pseudo-vertical transects that spanned the eastern, east-central, and central parts of the WTS (with sample spacing of ~0.5 to 1 km structural depth) and along three stratigraphic-parallel (pseudo-horizontal) traverses at intermediate levels across the sheet. Due to relatively slow cooling rates and multi-kinetic zircon populations, grains were prescreened based on similar U-Pb ages and U/Th contents, with 6 grains selected for ZHe analysis at each sample site. Vertical transects captured an Early Cretaceous partial retention zone (PRZ) with slow cooling starting at ~130 Ma. Cooling ages are systematically younger downward in the east-central and central vertical transects, yielding an average exhumation rate of 0.12 mm/yr (assuming steady state geothermal conditions) from ~125 to 90 Ma; only part of the PRZ is preserved along the eastern

leading edge of the sheet. Cooling ages are systematically younger westward along a horizontal traverse near the base of the Geertsen Canyon Formation, yielding an average slip rate of 1.7 mm/yr from ~125 to 90 Ma. The estimated exhumation rate is consistent with uplift and erosion above a moderately (average ~10°) dipping, composite thrust ramp, and the estimated slip rate and duration are roughly consistent with a net slip of ~60 km. The WTS was subsequently passively uplifted and exhumed during Late Cretaceous development of the Wasatch anticlinorium, recorded by cooling ages at deeper levels.

TABLE OF CONTENTS

List of Figures

Introduction

Determining the ages and the rates of shortening in continental retroarc fold-thrust belts is critical towards addressing a number of fundamental questions in continental tectonics, including: (1) what is the relationship between plate boundary-forearc tectonic processes and retroarc deformation; (2) how is the deformation history of the metamorphic hinterland related to that of the external fold-thrust belt; and (3) what is the role of large displacement, dominant thrusts in the evolution of retroarc thrust wedges? The retroarc Cordilleran thrust belt and foreland basin of North America extends greater than 3000 km from Mexico to Canada and accumulated substantial crustal shortening in the Mesozoic (Dickinson, 2004; DeCelles, 2004). Shortening in the retroarc Cordilleran orogen of the western U.S. can be seen in multiple contractional belts from Early Jurassic to Paleogene time. These belts, which include the Luning-Fencemaker belt, Central Nevada thrust belt, Sevier fold-thrust belt, and the Laramide foreland province display an overall eastward propagation of deformation (Taylor et al., 2000; DeCelles, 2004; Dickinson, 2004; DeCelles and Coogan, 2006). Major thrusts have slip on the order of 10's of km and were active over time scales on the order of 10's of m.y. By conducting thermochronologic analysis of these structures geologists can reconstruct thermal histories, interpret deformation histories, and evaluate thermal maturation of hydrocarbons.

Although multiple techniques exist for dating rocks, determining the timing and rates of crustal shortening remains a challenge. Provenance studies, subsidence analysis, depositional environments of syn-thrusting strata preserved in foreland basins,

and cross cutting to onlapping relationships between proximal strata and structures may widely bracket ages of fault slip (DeCelles and Giles, 1996; Braun et al., 2006). Thermochronology, the interpretation of the thermal history of rocks based on accumulation of daughter isotopes and temperature dependent diffusion, partly reflects deformation histories accompanied by exhumation and changes in temperature (Braun et al., 2006). In rare cases, minerals that grew below their closure temperature and in specific structural settings can be isotopically dated to directly constrain deformation timing. Variations in cooling ages of different isotopic systems in footwalls of normal faults have been previously interpreted to record uplift and exhumation, and used to estimate the timing and rates of fault slip (Farley, 2002). Variations in cooling ages in hanging walls above thrust ramps are less well studied, but can potentially be used to estimate the timing and rates of fault slip. In this work, thermochronology is applied to the Willard thrust sheet (WTS), northern Utah, a dominant thrust sheet in the Cretaceous to mid Paleogene Sevier fold-thrust belt (FTB). The timing of displacement along the Willard thrust is incompletely understood and estimates for timing of thrust initiation vary widely from ~150 to 115 Ma (Heller et al., 1986; Burtner and Nigrini, 1994; DeCelles et al., 1995; Yonkee et al., 1989, 1997; Sears, 2001; Stockli et al., 2001; Currie, 2002; DeCelles, 2004).

Upper crustal shortening in the thin-skin Sevier FTB is related to middle to lower crustal thickening in the hinterland, and to synorogenic deposition in the Sevier foreland basin (DeCelles, 2004). Direct measurements of the timing of thrust motion are important in developing coupled models of thrust sheet exhumation and foreland basin

sedimentation. Although timing relations of sedimentation of the Sevier foreland basin strata are reasonably well understood (DeCelles, 1994; DeCelles and Currie 1996; Liu et al, 2005), few direct measurements are available on the timing of in situ exhumation of the thrust sheets. This study presents new (U-Th)/He zircon (ZHe) thermochronologic data from the WTS, which constrains timing of thrust initiation, rate of exhumation, and fault slip rate. The ZHe system was chosen because zircon-bearing strata are widely exposed within the WTS and the closure temperature (~160-200 °C) for this system is appropriate for determining exhumation timing in the upper crust (depths~ 5-8 km) (Reiners, 2005).

The WTS is well exposed in northern Utah where younger uplift and erosion have exposed a wide range of structural levels across the thrust sheet, providing an exceptional opportunity to apply modern thermochronologic methods to determine a poorly understood deformation history for an important part of the Sevier FTB. Results from this study, along with existing age constraints of the WTS, help to provide an improved understanding of: (1) the age of inception, rate, and duration of fault slip along the dominant Willard thrust sheet; (2) the timing relations between thrust faults of the Wyoming salient; (3) temporal correlations between other “dominant” western thrust systems of the Sevier FTB and on a broader scale; (4) the relationship between thrusting in the FTB and crustal shortening/extension in the metamorphic hinterland.

Regional Geology

Neoproterozoic to Cambrian rifting of the supercontinent Rodinia, and subsequent deposition of a westward-thickening sedimentary wedge along the passive margin of western Laurentia, established the tectonic and stratigraphic framework for subsequent development of the Cordilleran orogen of the western United States (Stewart, 1972; Dickinson, 2004). By the end of the middle Paleozoic, subduction initiated and volcanic arc systems emerged near the continental margin (Dickinson, 2004). During the Antler and Sonoma orogenies, oceanic allochthons were thrust eastward over the passive margin strata and accreted to the continent (Speed and Sleep, 1982; Burchfiel and Royden, 1991; Dickinson, 2004). In Triassic to Middle Jurassic time the fringing arcs and interarc basins developed along and were eventually accreted onto the western margin of the Cordillera. In Late Jurassic and through Paleogene time, convergence of the Farallon and Kula oceanic plates with the North American plate controlled the tectonic evolution of western North America (DeCelles, 2004). The convergent margin developed the classic elements of an Andean-style orogen including the Franciscan accretionary wedge, Great Valley forearc basin, Sierra Nevada magmatic arc, metamorphic hinterland, Sevier retroarc fold-thrust belt, and a foreland basin system (Figure 1) (Ernst, 1970; Constenius, 2000; Saleeby and Busby-Spera, 1992; Dickinson, 2004, DeCelles, 2004).

The Sevier orogeny was a continent-scale mountain building event that extended more than 3,000 km, from Canada in the north to Mexico in the south, with thin-skin folding and overall top-to-east thrusting of the sedimentary wedge above Precambrian basement (Figure 1) (DeCelles and Coogan, 2006). Sedimentary rocks were shortened by

~150-300 km across the Sevier belt, resulting in upper crustal thickening, thrust loading, and isostatic flexural subsidence in the foreland basin (Yonkee, 1992; DeCelles, 2004; Yonkee, 2005). An increase in convergence rates (likely exceeding the rate of trench retreat) between the Farallon and North American plates, influenced by the opening of the Atlantic ocean in mid Jurassic time and the subduction of young lithosphere, may have led to the intraplate shortening (Royden, 1993). Although the age of thrusting is roughly bracketed from the Late Jurassic to early Paleogene, most shortening in occurred during the Cretaceous (Camilleri et al., 1997; DeCelles, 2004; Heller et al., 1986). The Sevier orogenic system can be divided into four parts: a hinterland, western thrust system, eastern thrust system, and foreland basin.

The hinterland has a metamorphic core wherein crustal thickening occurred during the Late Jurassic to middle Cretaceous (Smith et al., 1993; Hoisch et al., 2014), leading to substantial tectonic burial of supracrustal rocks (e.g., McGrew et al., 1992; Harris et al., 2007). Although the hinterland experienced significant crustal thickening during much of the Cretaceous (e.g., McGrew et al., 1992; Harris et al., 2007), by the Late Cretaceous metamorphic cores experienced alternating periods of extension and shortening (tectonic mode switches) (Wells et al., 1990; Wells, 1997; Wells and Hoisch, 2008). The timing of tectonic mode switches of the hinterland partly overlap with the timing of crustal shortening of the Sevier FTB to the east. Final alternation between contraction and extension and out-of-sequence thrusting in the hinterland occurred at 53-51 MA, synchronous with final thrusting in the Sevier belt and uplift of basement arches in the Laramide belt (Camilleri and Chamberlain, 1997; Wells et al., 2012; Lacy et

al., 2013; Wells et al., 2013). The hinterland subsequently underwent extension and cooling during the Paleogene (McGrew et al., 2000; Wells et al., 2000; Rahl et al., 2002; Sullivan and Snoke, 2007).

The western thrust fault system carries thick Neoproterozoic to Paleozoic passive margin strata, includes the "dominant" Paris, Willard, Canyon Range, Wah Wah, and Wheeler Pass thrusts, and was mostly active during the Early Cretaceous (Yonkee and Weil, 2011). These thrusts have ramp-flat geometries, large fault-bend and fault-propagation folds, and exhibit a thin-skinned structural style (DeCelles and Coogan, 2006). These thrusts have variable, large displacements (~60 km of net slip on the WTS), significant stratigraphic throw across ramps, and play a key role in the total shortening budget of the orogenic wedge. The eastern thrust system carried a thinner sequence of Paleozoic strata, includes the Crawford, Absaroka, Hogsback, and Charleston thrusts, and was dominantly active during the Late Cretaceous to Early Eocene. Thrusts faults in western and eastern systems, along with their associated foredeep basins, propagated eastward over time.

Synorogenic sediments were deposited in the foreland basin that lay east of the Sevier FTB (DeCelles and Currie, 1996; DeCelles, 2004). The foreland basin extended laterally more than 3000 km from Canada southward toward Mexico, and eastward up to 1000 km from the orogenic front (DeCelles, 2004). The system included foredeep, forebulge and backbulge depozones, which migrated to the east as thrust systems of the Sevier belt propagated eastward (DeCelles and Giles, 1996; DeCelles, 2004). The basin was flooded by the Western Interior Seaway in the Late Cretaceous to early Paleogene

(Kauffman, 1977). The Sevier foreland was broken into smaller basins within parts of Wyoming to New Mexico by Laramide foreland uplifts and basins from Campanian to Paleogene time (~80 Ma to 55 Ma) (Dickinson et al., 1988).

Geology of the Willard Thrust Sheet

The Sevier FTB contains systematically curved sections, including the Wyoming salient that is bound by the Gros Ventre uplift to the north and the Uinta uplift to the south (Yonkee and Weil, 2010). Major thrusts in the Wyoming salient include: the related Willard, Paris, and Meade thrust faults that form a western system, the Crawford, Absaroka, Hogsback-Darby-Prospect thrust faults that form an eastern system, and the Precambrian basement cored Wasatch anticlinorium marking the transition between the two (Figure 2) (Royse, 1993a; DeCelles, 2004; Yonkee and Weil, 2011). The western system has a decollement in Neoproterozoic strata and the eastern system has a decollement in middle Cambrian shale. Large-scale fault-propagation and fault-bend folds are associated with thrust faults. Total shortening from large-scale thrust faulting and folding is about 150 km in the center of the Wyoming salient and decreases toward the ends of the salient.

The Willard thrust sheet is prominently exposed in northern Utah due to uplift and tilting about the Wasatch anticlinorium and in footwalls of Cenozoic normal faults (Figure 2). The sheet carries 10-15 km of passive margin strata that can be separated into three structural levels with different lithologies and structural styles. The lower level is comprised of micaceous Neoproterozoic strata, the middle level includes strong quartzite-rich upper Neoproterozoic to lower Cambrian strata, and the upper level is

dominantly comprised of Paleozoic carbonate-rich strata. The main thrust has western flat in Neoproterozoic micaceous strata, a ramp through quartzite-rich strata, a central flat in middle Cambrian strata, a ramp in upper Cambrian to lower Jurassic strata, and an eastern flat in middle Jurassic strata (Figure 3) (Yonkee 2005). The ramps generally cross cut competent stratigraphic layers, whereas flats are in incompetent layers.

The Willard thrust has about 50 km of top-to-the-east-southeast slip in northern Utah, with another 10 km of shortening from associated folds and imbricate faults (Yonkee, 2005). In the central part of the salient the Willard splays into the Paris and Meade thrusting respectively with ~20 km and ~40 km of top-to-east slip (DeCelles et al., 1993). The large displacement on the WTS, the wide range of exposed levels (>8 km vertical structural relief), the widely exposed aerial extent (>60 km E-W horizontal length), and the presence of zircon-bearing siliciclastic strata provide an ideal setting for application of zircon (U-Th)/He thermochronology (ZHe) to evaluate thrust timing. Late Cretaceous to Paleogene strata unconformably overly the southeastern part of the Willard sheet and were deposited after major slip transferred to the eastern system (Figure 2) (Yonkee and Weil, 2011). The WTS was tilted around the northern margin of the Wasatch anticlinorium, leading to variable regional dip directions ranging from overall west-northwest to northeast. The WTS was also cut by Cenozoic normal faults, which imparted additional eastward tilt in the footwall of the Wasatch normal fault. Growth of the anticlinorium during the Late Cretaceous to Paleogene was related to slip and duplexing along the Ogden and basal thrusts (Yonkee, 1992; DeCelles, 1994). Apatite fission track data of basement rocks in the Wasatch anticlinorium reported by

Naeser and others (1983) include clusters at 90-85 Ma, 85-75 Ma, and 65-50 Ma, interpreted to record pulses of uplift in the anticlinorium that were linked to slip along the Crawford, Absaroka, and Hogsback thrusts to the east (Figure 4) (DeCelles, 1994).

Previous interpretations for the age of initiation of slip in the Sevier FTB vary widely from ~150 to 115 Ma, reflecting ambiguous relations with foreland basin strata and limited geochronologic and thermochronologic data (Heller et al., 1986; Burtner and Nigrini, 1994; DeCelles et al., 1995; Yonkee et al., 1989, 1997; Sears, 2001; Stockli et al., 2001; Currie, 2002; DeCelles, 2004). The Upper Jurassic Morrison Formation accumulated in the retroarc region of Colorado to Montana (Currie, 1998). Regionally, the top of the Morrison has a major unconformity recording up to a ~25 m.y. hiatus (DeCelles 2004). Multiple models have been proposed for the tectonic setting of the Morrison Formation. Paleocurrent and detrital zircon data support derivation from a western source and deposition in a foreland setting (DeCelles, 2004). Heller and others (1986) argued that the Morrison Formation does not thicken westward as expected for a flexural foreland basin and was instead deposited during regional tectonothermal subsidence. The Morrison Formation may have been deposited in a backbulge depozone with an Late Jurassic “phantom foredeep” to the west associated with thickening in the Sevier hinterland (Royse, 1993b; DeCelles and Currie, 1996; Currie, 1997).

A thick sequence of Jurassic strata, including the Twin Creek, Sundance, and Morrison formations, were deposited in the Utah-Idaho trough. Using stratigraphic and subsidence analysis, Bjerrum and Dorsey (1995) interpreted the Utah-Idaho trough as a retroarc foreland basin for a Middle Jurassic thrust belt to the west. Episodic thrusting in

this belt may have caused unconformities and stratigraphic geometries seen in the Utah-Idaho trough (Bjerrum and Dorsey, 1995). Their results are interpreted to record a ~163 to ~157 Ma thrust front in western Utah followed by a slowing in the rate of subsidence; this stands as the establishment of a period of quiescence until the initiation of the Sevier FTB.

Previous studies have variously interpreted initial slip the WTS from 140 to 115 Ma, based on limited geochronologic and thermochronologic isotopic data and relations of foreland basin deposits. Deposits include the Early Cretaceous Gannet Group that likely record early slip of the Willard-Paris-Meade thrusts (DeCelles et al., 1993), and the overlying Bear River to Frontier Formations that record continued erosion of the thrust sheet (Schmitt, 1992; Liu et al., 2005). Recently, Gentry et al. (2013) reported detrital zircon data from Aptian to Turonian (~125-90 Ma) synorogenic strata, interpreted to record protracted exhumation of upper levels of the WTS. Isotopic data include several apatite fission track ages from the Paris and Mead thrust sheets (Burtner and Nigrini, 1994) and $^{40}Ar/^{39}Ar$ fusion ages of muscovite from veins in the hanging wall of the Willard thrust (Yonkee et al., 1989). Recently, Giallorenzo (2013) reported $^{40}Ar/^{39}Ar$ UV laser ablation ages of ~145-130 Ma for mica in the western, basal part of the WTS, interpreted to record early alteration and internal deformation that preceded large-scale thrust slip.

Stratigraphy and Targeted Formations

The WTS carries a thick package of sedimentary rocks that include: (1) Neoproterozoic to Early Cambrian micaceous to quartz-rich strata; (2) Early Paleozoic

carbonate-rich strata; (3) Late Paleozoic mixed carbonate and siliciclastic strata (Figure 5 and 6). Neoproterozoic to lower Cambrian strata are separated into an up to 3 km thick sequence of upper Neoproterozoic glaciomarine sedimentary rocks with local volcanic rocks and a ~2-4 km sequence of upper Neoproterozoic to lower Cambrian siliciclastic and rare volcanic rocks (DeCelles, 2004; Dickinson, 2004). Neoproterozoic strata include the Perry Canyon Formation, Maple Canyon Formation, and the Kelley Canyon Formation, which display lateral changes in thickness related to rifting (Christie-Blick, 1982; Crittenden et al., 1972). The upper Neoproterozoic to lower Cambrian strata thicken westward and include the Caddy Canyon Formation, Mutual Formation, Browns Hole Formation, and Geertsen Canyon Quartzite (Yonkee and Weil, 2011). Lower Paleozoic strata are up to 6 km thick and consist mostly of shallow water carbonate rocks with thinner intervals of siliciclastic rocks deposits during episodic regressions, including the Cambrian Worm Creek Member of the St. Charles Formation, Ordovician Swan Peak Formation, and parts of the Devonian Water Canyon and Beirdneau formations (Poole et al., 1992). The Pennsylvanian to Permian Oquirrh Group is up to 6 km thick and was deposited in the subsiding Oquirrh basin in northwest Utah in time (Dickinson and Gehrels, 2003; Yonkee and Weil, 2011). Triassic and Jurassic strata have mostly been eroded from the WTS (Yonkee and Weil, 2011).

Sampling and Analytical Methods

Sample Collection

Approximately 40 samples of quartzose sedimentary rocks were collected from the hanging wall of the Willard thrust in northeastern Utah for zircon (U-Th)/He analysis (Appendix A). Samples were collected along both down-plunge structural (pseudo-vertical) transects through the thrust sheet, and along stratigraphic-parallel (pseudo-horizontal) traverses from west to east. The three vertical transects will be referred to as Monte Cristo for the eastern part, Browns Hole to Bear River for the east-central part, and Wellsville for the central part of the WTS (Figure 3). Samples collected along these transects were from Neoproterozoic to Devonian siliciclastic strata of the Perry Canyon, Maple Canyon, Kelley Canyon, Caddy Canyon, Mutual, Browns Hole, Geertsen Canyon, Worm Creek Member of the St. Charles Formation, Swan Peak, Water Canyon, and Beirdneau formations. For the three stratigraphic-parallel traverses, samples were collected from the Perry Canyon Formation, Browns Hole to basal Geertsen Canyon formation, and the Worm Creek Member. Additional samples were collected in the footwall of the Willard thrust from the Cambrian Tintic Quartzite and Paleoproterozoic Farmington Canyon Complex to better assess the tectonic significance of cooling ages across the Willard thrust. Samples on vertical transects were collected at 0.5 to 1 km intervals in structural depth. Samples collected for this study were augmented by zircon separates of previously collected samples from Carol Dehler (Utah State University) and Paul Link (Idaho State University). Additional work is underway to increase sample density along horizontal traverses and add another vertical transect in the western part of the WTS. Sampling locations for the pseudo-vertical and stratigraphic-parallel transects are shown in Figure 7.

Mineral Separation and Preparation Techniques

Samples were crushed using a BICO rock crusher and disk pulverizer and then sieved to separate the 345µm to 53µm size fraction. Sieved material was then passed over a water table to obtain concentrates of denser mineral grains, followed by density separation using methylene iodide (MI) (specific gravity =3.32). Franz isodynamic magnetic separation was used to further concentrate zircon grains, which were then hand-picked to obtain zircon grains free of visible fractures, zonation under polarized light, inclusions, and metamictization.

Zircon (U-Th)/He Thermochronology

The zircon (U-Th)/He (ZHe) thermochronologic system was used to constrain the cooling history of the Willard thrust sheet. The cooling history is assumed to be mostly related to erosional exhumation resulting from rock uplift due to displacement of the thrust sheet up a ramp. The (U-Th)/He system determines cooling ages of rocks by looking at production and trapping of ^{4}He from the decay of ^{238}U, ^{235}U and ^{232}Th. ^{4}He is also produced at negligible amounts by the decay of ^{147}Sm and ^{143}Nd (Reiners et al., 2002). The thermochronologic age of a rock or mineral is an apparent age that represents the time that a daughter isotope becomes immobile or locked into a crystal lattice (Dodson, 1973). The daughter isotope becomes immobile at a temperature interval known as the closure temperature (Tc). The closure temperature is dependent on the thermochronologic system, that is the radiogenic isotopic decay process and mineral where the daughter isotope resides, and to a lesser extent on the grain size and cooling rate (Farley, 2002). At temperatures above the Tc, radiogenic daughter products

diffuse out of the mineral lattice as quickly as they are produced, and therefore they do not accumulate. When the mineral cools below Tc the daughter particles escape at a negligible level, allowing accumulation (Dodson, 1973; Farley, 2002). This study uses zircon (U-Th)/He thermochronometry, which for typical zircon, has a Tc of 180˚ to 200˚C contingent on the cooling rate, grain size, and radiation damage. For typical geothermal gradients, rocks exceed the Tc for ZHe when deeper than 8-10 km (Farley, 2002; Reiners, 2005). When the rocks are exhumed above 8-10 km, the zircon will cool below the Tc and ^{4}He will begin to accumulate. This system is therefore sensitive to cooling at low temperatures and is useful to date events that influence the thermal structure of the upper crust, such as erosion.

The change from readily diffusing ^{4}He from a mineral grain to being locked into the crystal lattice does not occur at a specific temperature; rather, it changes over a distinct temperature interval called the partial retention zone (PRZ) (Reiners, 2005). The Tc lies within the PRZ (near its base), so rocks above the PRZ have already cooled through the Tc and record an earlier tectonic event. When there is rapid uplift and exhumation from thrust faulting, the PRZ may be preserved as a "fossil" PRZ (Braun et al., 2006). This can be seen on age vs. depth profiles where age decreases rapidly with depth. The breaks in slope serve as the top and bottom of the PRZ and indicate changes in cooling rate which may translate to the timing of important tectonic transitions, such as the initiation of thrusting (Figure 7) (Braun et al., 2006).

A study by Reiners (2005) showed that radiation damage does not effectively change ^{4}He diffusivity until radiation dosages are higher than 2-4 x 10^{18} α/g. At high

dosages radiation damage enhances He loss from zircon crystals. Based on a study by Damon and Kulp (1957) radiation damage only occurs when zircon has cooled below ~250˚C. Zircons that have cooled below this temperature for less than a few hundred million years are assumed to not have substantial radiation damage.

ZHe analysis was conducted at the (U-Th)/He Geo- and Thermochronology Lab in the Jackson School of Geosciences at the University of Texas, Austin. Zircon separates were hand-picked to obtain grains with euhedral tetragonal shapes, grain widths between 70-150 µm, clarity, and lack of visible zonation, inclusions, and metamictization (Farley, 2002; Reiners, 2005; see (U-Th)/He Geo- and Thermochronology Lab at UT Austin webpage). In almost all cases zircon with widths <60 µm are not dated because of the large alpha ejection corrections that these crystals require. Large alpha ejection corrections can potentially produce large errors in the ZHe age if U/Th concentrations in the crystals are zoned. Alternatively, grains >200 µm are not used because of the greater difficulty of He diffusion over larger lengths leading to a potential need for multiple gas extractions (Reiners, 2005).

To lessen the potential variability of T_c among the multi-kinetic detrital zircon populations within and between samples, zircons were prescreened prior to He analysis. Thirty hand-picked grains per sample were prescreened prior to ZHe analysis using the U/Th-Pb system to assess crystallization ages, uranium and thorium contents, and potential zonation (Figure 5 and 6; Appendix B). Grains were mounted onto adhesive pucks and analyzed using Laser Ablation Inductively Coupled Plasma Mass Spectrometry (LA-ICPMS), with a beam size of 30 µm and profile depths of 18 µm. After analysis,

zircon grains with greater than 300 ppm U and U-Pb ages older than ~1.8 Ga were rejected. U/Th zonation in grains was evaluated using Iolite software for reduction of data obtained by LA-ICPMS (www.iolite.org.au). Zoned zircon grains were rejected from further analysis.

Subsequent to (U-Th)/He investigation, alpha damage calculations were made for each aliquot to further test the integrity of the helium age. Radiation damage can compromise the kinetics of helium diffusivity reducing the reliability of ZHe dating. When U and Th decay to He, alpha particles (^{4}He) are naturally formed. Alpha-parent recoil produces linear defects (radiation damage) that are accountable for metamictization of the mineral (Nasdala et al., 2004). Radiation damage can also occur from spontaneous fission, which produces fission tracks, and the alpha particles themselves (Guenthner et al., 2013). Radiation damage can alter the rate of diffusion of ^{4}He depending on track density, connectivity, and time (Reiners et al., 2002). Radiation damage is annealed at elevated temperature and over time (Nasdala et al., 2004). The extent of single grain radiation damage can be roughly calculated by time-integrated self-irradiation doses (Alpha Doses) (Nasdala et al., 2004; Reiners, 2005; Guenther et al., 2013). Reproducibility of ZHe cooling ages declines at an effective radiation damage greater than 2.00 x 10^{18} α/g - 4.00 x 10^{18} α/g (Reiners, 2005; Guenthner et al., 2013). This implies that an upper dosage boundary for reproducible ZHe ages is 2.00 x 10^{18} α/g. Effective radiation damage was calculated for all Willard hanging wall aliquots that were run for ZHe. For the 202 analyzed aliquots, effective radiation damage ranges from 2.46 x 10^{16} to 2.86 x 10^{18} α/g (Figure 8). From these prescreened grains only two rose above

the upper dosage boundary of 2.00 x 10^{18} α/g (Figure 8, red diamonds). Ninety nine percent of all ZHe ages in this study do not surpass the reproducible boundary, but may still have complications and variations greater than expected for analytical uncertainties.

Six prescreened grains per sample, with ages of ~1.0 - 1.8 Ga and Uranium contents below 300 ppm, were selected for ZHe analysis. Previous studies, including Dickinson and Gehrels (2003) have used He-Pb double dating to supplement thermochronologic research, and in our case were used to prescreen the samples to minimize alpha damage variability, grain inhomogeneity, and zonation. It has been calculated that for U-Th zoned zircons ZHe ages may increase in error by up to ~30% if not accurately accounted for in alpha ejection corrections (Hourigan et al., 2005). Selected grains were photographed and measured on two perpendicular planes that are parallel to the a1 and a2 axes. Following methods by Farley (2002) and Reiners (2005), alpha ejection corrections, based on the dimensions of each individual grain, were assigned to account for ^{4}He lost from the crystal by stopping distances of alpha particles. Stopping distances are calculated to be ~19.3 µm (^{238}U), ~19.6 µm (^{235}U), and ~19.3 µm (^{232}Th) (Farley et al., 1996; Hourigan et al., 2005; Reiners, 2005).

U and Th amounts can vary widely between crystals so measurements of parent and daughter nuclides are calculated on the same aliquot. Once the desired grains have been chosen they are packed into Pt foil tubes, loaded into a Cu planchette, and degassed. The ^{4}He is extracted using an ultra-high vacuum noble gas extraction and purification line by heating of the Pt tubes with a focused 10µm laser beam to 1100-

1250 ˚C for 15 minute extraction intervals. Aliquots are subject to multiple ^{4}He extractions. U-Th concentrations, thermal history, and radiation damage are not obviously related to ^{4}He retentivity during degassing (Reiners, 2005). After laser degassing, He is spiked and analyzed using a computer-automated ultra-high vacuum He extraction line that is equipped with precise volume aliquot systems, a cryogenic gas purification system, and a Blazers Prisma QMS-200 quadrupole mass spectrometer to determine ^{4}He/^{3}He ratios. After degassing, the grain is unpacked then dissolved with a mixture of HF-HNO_3 at high temperatures and pressures. The aliquots are unpacked from the Pt tubes due to Pt dissolution and subsequent contamination of the ICP-MS. The aliquots are spiked with an isotopically distinctive known concentration U-Th spike. Aliquot solutions are then analyzed for U, Th, and Sm using the Thermo Element2 HR-ICP-MS, fitted with a CETAC micro-concentric nebulizer and ESI auto sampler (see (U-Th)/He Geo- and Thermochronology Lab at UT Austin webpage).

Thermal Modeling

Inverse time-temperature (t-T) modeling of measured ZHe thermochronologic data was conducted using the Helium modeling program (HeMP) (R2010beta; Hager and Stockli, 2009; Lee et al., 2011) for the Bear River to Browns Hole and the Wellsville vertical transects. HeMP derives a series of t-T paths that are user constrained and assume a constant geothermal gradient. The measured ZHe ages, sample depths, together with user defined geothermal gradients produce model ages and model t-T paths. The model ages are compared to measured ages in evaluating the suitability of the model t-T paths for the measured ZHe data. Generally, more than one thermal

history is consistent with the given conditions, so an inverse model contains large sets of acceptable thermal histories that fit with the measured data. It is important to note that the inverse models are only as good as the analytical data and geologic interpretations behind them (e.g., Ketcham, 2005).

Zircon (U-Th)/He Results

Samples from the WTS were strategically collected along three pseudo-vertical transects that spanned the eastern (Monte Cristo), east-central (Browns Hole-Bear River), and central (Wellsville) parts of the WTS, and along three different stratigraphic-parallel traverses along the Worm Creek Member of the St. Charles, Brows Hole to basal Geertsen Canyon, and Perry Canyon formations across the sheet (Figure 3 and 7). The WTS developed with westward-thickening passive margin strata, and thus formation thicknesses and depths increase westward. Paleodepths of samples were estimated from regional stratigraphic thickness patterns, and pre-thrusting positions were palinspastically restored by removing effects of thrusting (Figure 9). Horizontal distances for samples were measured with respect to the palinspastically restored west end of the section (Promontory Point). Individual grain ages were assigned a 1σ measurement uncertainty (error) of ± 8% the estimated age (i.e. ± 8 Ma for a 100 Ma grain), based on age variance of standard samples at the University of Texas U/Th-He Geo- and Thermochronometry Lab (http://www.jsg.utexas.edu/he-lab/procedures/). Site mean ZHe ages were estimated from individual grain ages, and 95% confidence intervals approximated using a t test (which assumes normally distributed sample measurement

errors). Outlier grains, defined as those grains that give >2 sigma from the mean age, were not included in calculations of mean ages. Mean ages were not calculated for sites with more than two outlier grains. Supplementary samples were collected from the footwall of the sheet. The following results can be seen in Appendix B.

Monte Cristo Transect

The Monte Cristo pseudo-vertical transect lies at the eastern part of the WTS and spans a paleodepth interval from 5.3 to 7.5 km, with samples from the Worm Creek Member, the upper and middle Geertsen Canyon, Browns Hole, and Caddy Canyon formations (Figure 10). A sample from the Worm Creek Member had an estimated at 5.3 km paleodepth and mean ZHe age of 159.3 ± 8.2 Ma (n/N = 4/5, where N is total number of grains analyzed and n is number of grains used to estimate the site mean age). A sample from the upper part of the Geertsen Canyon Quartzite had an estimated 6 km depth and a mean ZHe age of 159.6 ± 15.2 Ma (n/N = 4/6), along with one older grain and one anomalously young grain with very low [U]e (effective uranium). A sample from the middle part of the Geertsen Canyon Quartzite contained mostly older grains with ages of 174 to 247 Ma. A sample from the Browns Hole Formation, located at a paleodepth of 7.1 km, had a mean ZHe age of 159.7 ± 10.3 Ma (n/N = 4/6), along with two older grains. Two samples from the Caddy Canyon Quartzite located at 7.3 and 7.4 km paleodepths had average ZHe ages respectively of 166.2 ± 10.9 Ma (n/N =6/6) and 174.2 ± 37.9 Ma (n/N =4/6). The presence of older grains in most samples is interpreted to reflect a location within the PRZ for ZHe.

Bear River to Browns Hole Transect

The Bear River- Browns Hole transect lies on the east central part of the WTS and spans a paleodepth interval from 5.6 to 10.8 km, with samples from the Beirdneau Formation, Worm Creek Member of the St Charles, upper and middle Geertsen Canyon, Browns Hole, Mutual, Caddy Canyon, and Maple Canyon formations (Figure 11). Two samples from Devonian strata had different age patterns. A southern sample had an estimated paleodepth of 5.6 km and contained mostly older grains (four grains had ages of 140 to 200 Ma), indicating it was located within the PRZ. A northern sample at slightly greater estimated depth of 5.8 km had a mean age of 108.8 ± 9.2 Ma (n/N =4/6) along with two older grains. This younger age for this sample is anomalous compared to ages other samples from Devonian strata, and may reflect presence of unusually non-retentive zircon grains, or local heating of the sample, possibly from hydrothermal fluids. Mean ages for other samples display systematic variations with depth. A sample from the Worm Creek Member, paleodepth of 6.5 km, had an age of 126.8 ± 4.7 Ma (n/N =4/5), along with one older grain. Samples from the upper Geertsen Canyon Quartzite, depth of 7.7 km, and the underlying Browns Hole Formation, depth of 9.0 km, had mean ZHe ages of 112.4 ± 7.6 Ma (n/N =5/6) and 105.6 ± 2.9 Ma (n/N =6/6) respectively. Samples from the Mutual Formation, depth of 9.5 km, and Caddy Canyon Quartzite, depth of 10 km, had mean ZHe ages of 96.2 ± 8.9 (n/N =5/6), and 100.1 ± 12.4 Ma (n/N =5/6) respectively (Figure 11). A sample from the middle Geertsen Canyon Quartzite was not used due to anonymously large dispersion in grain ages and high [U]e for some grains. A sample from the Maple Canyon Formation at the base of the transect, depth of 10.8 km, only yielded a single ZHe age due to loss of other grains

during analysis; this formation has been resampled for future analysis. Two samples from the Swan Peak Quartzite did not yield usable zircon grains.

Wellsville Transect

The Wellsville transect lies in the central part of the WTS and spans paleodepths from 6.3 to 13.5 km with samples from the Beirdneau, Swan Peak, upper and middle Geertsen Canyon, Browns Hole, Mutual, Caddy Canyon, Perry Canyon, and Facer formations. The upper part of the transect includes samples from the Beirdneau Formation (depth of 6.3 km) and the Swan Peak Quartzite (depth of 7.0 km) with ZHe mean ages of 128.8 ±14.5 Ma (n/N =5/6) and 129.5 ± 11.1 Ma (n/N =6/6). Samples from the Upper Geertsen Canyon Quartzite (depth of 9.1 km) and underlying Browns Hole Formation (depth of 10.2 km) yielded mean ZHe ages of 109.5 ± 9.4 Ma (n/N =4/6) along with one older and one younger grain, and 97 ± 5.8 Ma (n/N =6/6) respectively. Samples from the Mutual Formation (depth of 10.8 km) and Caddy Canyon Quartzite (depth of 11.4 km) had mean ages of 86.9 ± 9.1 Ma (n/N =5/6) and 94.5 ± 10.2 Ma (n/N =4/6) respectively (Figure 12). A gneiss sample from the Facer Formation at a 13.5 km paleodepth had a bimodal distribution with grain age groups of 95.2 ± 5.5 Ma (n=3) and 62.8 ± 3.9 Ma (n=3). The younger age group is interpreted to record less retentive zircons for a new PRZ that developed after Willard thrusting and prior to ~60-65 Ma uplift of the Wasatch anticlinorium during younger Absaroka thrusting. The deepest structural level on the transect lies in a repeated section of the Perry Canyon Formation below an imbricate thrust at the base of Facer Formation. A sample from this lower panel of Perry Canyon Formation at the base of the WTS yielded a mean age of 24.0

±6.4 Ma (n/N =6/6). A sample from the middle Geertsen Canyon Quartzite (9.6 km) yielded a wide range of ages and was not used for thermal modeling.

Worm Creek Traverse

The pseudo-horizontal traverse along the Worm Creek Member includes 4 samples and covers a distance from 22 to 57 km relative to prominatory point on a palinspastically restored section. Mean ZHe ages are 111.3 ± 8.9 Ma (WT12-40, 22 km), 149.4 ± 17.5 Ma (WT12-41, 26 km), 126.8 ± 4.7 Ma (WT12-3, 36 km), and 166.23 ± 17.6 Ma (NCAT-9, 57 km). Too few sample sites were collected along the Worm Creek traverse to estimate slip rate (Figure 13).

Geertsen Canyon Traverse

The horizontal traverse along the basal Geertsen Canyon Quartzite to underlying Browns Hole Formation includes 6 samples and covers horizontal distances from -3 km to 63 km on a palinspastically restored section. Sample WT12-19 along the eastern edge of the WT (distance 63 km) yielded an age of 179.5 ± 30.2 Ma (n=4/6) and is interpreted to be within the PRZ. Samples that span a traverse distance from 41 km to 3 km yield mean ZHe ages that range correspondingly from 119.4 ± 8.9 Ma to 87.5 ± 8.8 Ma. Assuming a constant geothermal gradient, the traverse yields an average slip rate of ~1.7 mm/yr. from ~ 125 to 90 Ma (Figure 14). Sample CAT-15 only had two usable grains and will need additional sampling.

Perry Canyon Traverse

The stratigraphic traverse along the Perry Canyon Formation includes 5 samples. Four of the samples, EAB10-18 and EAB10-11 (-1 km), WT12-49 (7 km), and WT12-43

(33 km) have ZHe ages that range from 66.7 ± 5.3 Ma to 67.8 ± 5.4 Ma. The samples along this level did not cool through the PRZ until the latest Cretaceous, likely during subsequent uplift above the Wasatch anticlinorium (Figure 15). Sample WT12-47 (24 km), which is located in the footwall of an imbricate thrust and thus at a deeper structural level, has a younger ZHe age of 24.0 ± 1.9 Ma and did not cool through the PRZ until Neogene extension.

Footwall

Samples were collected from the Tintic Quartzite and underlying basement of the Farmington Canyon Complex in the footwall of the Willard thrust along the Wellsville transect to better assess the tectonic significance of the ages of exhumation. The intent was to distinguish whether the exhumation signature of the samples collected from the lower hanging wall to footwall recorded slip along the Willard thrust, uplift of the basement-cored Wasatch anticlinorium, or Neogene extension. Footwall samples have mean ZHe ages ranging from 14.0 ± 0.4 Ma 4.7 ± 0.4 Ma to, recording cooling related to exhumation along the Wasatch normal fault (Figure 20). All samples collected from the footwall remained too deep for He closure during the Cretaceous or were reset in the Neogene.

Inverse Modeling of Arrays of Zircon (U-Th)/He Data Using HeMP and Interpretation of Age Versus Depth Data Arrays

Bear River to Browns Hole

Inverse models run in HeMP were assigned initial t-T constraints of 170 °C to 220 °C from 150 Ma to 200 Ma for the structurally highest sample below the PRZ. HeMP models yielded acceptable fits for geothermal gradients ranging mostly between 10 and 25 °C/km. Modeling suggests slow cooling (~2 °C/m.y. to ~10°C/m.y.) initiated by ~127 Ma, and continued until 90 Ma with an average exhumation rate of ~0.12 mm/yr. (Figures 11 and 16).

Wellsville

Inverse models run in HeMP were assigned initial t-T constraints of 170 °C to 220 °C from 150 Ma to 200 Ma for the structurally highest sample below the PRZ. HeMP models yielded acceptable fits for geothermal gradients ranging mostly from 14 - 25 °C/km. Modeling suggests that the central Wellsville transect underwent slow cooling (~2 °C/m.y. to ~10°C/m.y.) from ~134 – 90 Ma with an average exhumation rate of ~0.11 mm/yr. (Figures 12 and 17). Thermal gradients with the largest number of fits for the Bear River to Browns Hole and Wellsville transects are slightly lower than the range of 20-30°C/km initial thermal gradients modeled by Yonkee et al. (1989).

Interpretation and Discussion

Early Cretaceous Cooling of the Willard Thrust Sheet

Mechanisms for upper crustal cooling signatures from ZHe data include top-down cooling, and bottom-up cooling. Bottom-up cooling mechanisms include refrigeration due to flat-slab subduction, post-magmatic thermal relaxation following magmatic intrusion, and thermal relaxation following prior heating from lithosphere

delamination. Top-down cooling mechanisms include enhanced erosion leading to exhumation or the ingress of meteoric fluids. Upper crustal cooling mechanisms are described below.

Cooling of the crust may occur by refrigeration due to flat slab subduction. Evidence of refrigeration from thermochronologic data has been presented from the North American Cordillera during the Laramide orogeny and is interpreted to be caused by the shallowing of the subducting Farallon plate under North America (Dumitru et al., 1991). Thermal gradients are high in magmatic arcs due to heat transfer from underlying asthenosphere (Dumitru et al., 1991). When the angle of the subducting Farallon slab decreased (at ~80 Ma) it displaced hot asthenosphere from under part of the plate margin and replaced it with cold subducting slab (Dumitru et al., 1991). Although refrigeration may have occurred during the Laramide orogeny this event does not overlap in timing with cooling of the WTS. There is no evidence for shallowing of the Farallon slab during the Early Cretaceous.

Delamination or the convective removal of part of the lower lithosphere can occur in convergent belts from thickening of the continental lithosphere (Wells and Hoisch, 2008). Following removal of the lithospheric root there can be an associated increase in the geothermal gradient and in igneous and metamorphic events (Platt and England, 1993). Thermal relaxation and cooling will occur when the lithosphere readjusts back to equilibrium thickness by basal accretion. Although Wells and Hoisch (2008) have suggested that there was removal of a lithospheric root beneath the North American Cordillera immediately prior to the shallowing of the Farallon slab at the start

of the Laramide orogeny, there are no delamination features such as extensional structures and magmatic and metamorphic rocks of appropriate ages within this study area to explain the Early Cretaceous cooling evident in the Willard thrust sheet.

Geothermal gradients can increase due to magmatic intrusions. Subsequent post-magmatic thermal relaxation can potentially modify isotopic cooling signatures. A zircon and apatite FT thermochronology study by Adriasola et al. (2006) in the Andean Cordillera showed different time-temperature cooling histories due to post-magmatic cooling and is directly related to relative distance from the intrusion. Although the magmatic arc was active during calculated cooling events of the Willard, the eastern extent of Late Jurassic to Early Cretaceous magmatism lay sufficiently far to the west that significant thermal perturbations related to these plutons are unlikely (Barton, 1990; Wright and Wooden, 1991).

Top down cooling mechanisms include enhanced erosion leading to exhumation, such as uplift along a thrust ramp causing cooling due to exhumation and erosion or uplift of footwalls during normal faulting. The slow cooling event signatures of the Willard thrust sheet are interpreted to be a result of erosion and exhumation due to translation up ramps in the Willard thrust.

First-order thermal models used in this study use constant thermal gradients. During rapid fault slip heat may be transferred advectivley with change to thermal gradients. With subsequent thermal relaxation as heat flows conductively from the hanging wall to the footwall thermal gradients equilibrate. However, if thrust slip rate is relatively slow, conductive heat transfer keeps pace with thrusting, resulting in

approximate thermal equilibrium and constant geothermal gradients. A simplified approximation of ratio of advective to conductive heat transfer is given by $P_e = \frac{hv}{\alpha}$, where P_e is the Peclet number, h is thrust sheet thickness, v is the vertical component of slip rate along a thrust ramp, and α is thermal diffusivity (Turcotte and Schubert, 2002). An approximate P_e of .25 for the WTS is estimated for typical α ~30 km^2/m.y., h ~15 km, v ~0.5 km/m.y., corresponding to an average slip rate of 1.7 km/m.y. and ramp angle of about 15 degrees. This calculation indicates conductive heat transport was most important, and an assumption of a constant geothermal gradient is a reasonable first order approximation.

Age of Inception of the Willard Thrust

The Bear River to Browns Hole ZHe ages capture a Late Jurassic to Early Cretaceous PRZ, with slow cooling (~2 °C/m.y. to ~10°C/m.y.) starting at ~127 Ma (Figure 11). Cooling ages systematically increase upward in the stratigraphy of the thrust sheet, yielding an average exhumation rate of 0.12 mm/yr. assuming steady state geothermal conditions (Figure 16). An inflection in the age vs. depth profile shows a ~97 Ma event that may record onset of additional uplift of the Wasatch anticlinorium induced by footwall imbrication and increase in rate of Willard fault slip.

The Wellsville ZHe ages record initiation of slow cooling (~2 °C/m.y. to ~10°C/m.y.) by ~134 Ma (Figure 12). Cooling ages systematically increase upward in the thrust sheet, yielding an average exhumation rate of 0.11 mm/yr. assuming steady state geothermal conditions (Figure 17). An inflection in the age vs. depth profile of the Wellsville transect at ~97 Ma may record initial uplift of the Wasatch anticlinorium or

increase in slip rate on the Willard thrust. The ZHe ages from the Wellsville and Bear River to Browns Hole vertical transects indicate thrusting in the Sevier FTB in northern Utah initiated by ~130 Ma.

Samples from the Monte Cristo transect appear to be within the PRZ based on the relatively wide dispersion of grain ZHe ages within individual samples that are also older than 130 Ma. The Monte Cristo transect is therefore interpreted as being too shallow to record cooling due to slip on the Willard thrust and data were not modeled with HeMP (Figure 10). However, many grains had ZHe ages between 140 and 180 Ma (Figure 18), which may record a period of enhanced but incomplete He loss during either: (1) burial beneath Jurassic strata that are up to 1.5 km Crawford thrust sheet, followed by cooling during erosion and development of a regional Early Cretaceous unconformity (DeCelles, 2004); or (2) influx of warmer fluids possibly related to shortening in the Sevier hinterland in the Jurassic, followed by influx of cooler meteoric waters. More retentive zircon grains retained significant He and have older ages.

Slip Rate of the Willard Thrust

The slip rate along the Willard thrust was estimated using three horizontal traverses at different levels of the thrust sheet. Ideally samples should have been initially located beneath the PRZ and then cooled sufficiently during thrust slip and erosion to move through the syn-thrusting PRZ. Slip rate could not be estimated for the stratigraphically highest traverse along the Worm Creek Member due to poor zircon yields and eastern samples being within the PRZ (Figure 13). Slip could also not be determined for the stratigraphically lowest traverse in the Perry Canyon Formation, as

most samples along this traverse did not cool through the PRZ until the latest Cretaceous, after cessation of slip along the Willard thrust. Late Cretaceous cooling is interpreted to record renewed exhumation of the WTS during growth of the Wasatch anticlinorium and passive uplift of the WTS, synchronous with slip along the Absaroka thrust (Figure 15). The stratigraphically-intermediate traverse along the basal Geertsen Canyon Quartzite to Browns Hole Formation beneath the pre-thrust PRZ and above the post-Willard PRZ and thus could be used to estimate slip rate. The distance vs. age profile for this level yields an average slip rate of 1.7 mm/yr. from ~125 to 90 Ma (assuming steady state geothermal conditions), which is consistent with the estimated net slip of ~60 km (Figure 14). An identical average shortening rate of 1.7 mm/yr. was calculated by Allmendinger (1992) for the entire Wyoming Salient using an age vs. cumulative displacement plot. Structurally restored sections of major thrust faults of the Wyoming Salient conducted by Royse (1993a) estimate total shortening to be ~160 km, yielding an average shortening rate of ~2 mm/yr.

Total shortening across the entire Sevier FTB has been calculated by other authors to better assess links between the FTB and the processes along the Cordilleran margin. Shortening estimates range from ~150 to 300 km (Royse, 1993a; Yonkee et al., 1997; DeCelles and Coogan, 2006). DeCelles and Coogan (2006) calculated total shortening along a transect at the latitude of the Canyon Range. Their total estimation of shortening in the Sevier FTB is 220 km at an average rate of ~3 mm/yr. and is comparable to Currie's (2002) estimate of a minimum of ~230 km of displacement in central Utah using a similar reconstruction strategy.

Timing Relations of the Wyoming Salient

ZHe data from this study constrain the timing of fault initiation, rate of thrust slip, and exhumation history of the WTS. These data help to inform our overall understanding of the tectonic evolution of the Sevier fold-and-thrust belt. Regional timing relations of the thrust belt discussed below are shown on Figure 19. Data presented here indicate the WTS had a protracted deformation history with thrust motion initiating ~130 Ma and continuing until ~90 Ma with an average slip rate of ~1.7 mm/year. During this time, rocks along the central and east-central parts of the sheet experienced slow cooling due to rock exhumation and erosion that averaged ~0.12 mm/yr. $^{40}Ar/^{39}Ar$ UV laser ablation ages of muscovite and biotite in the western basal part of the WTS are ~145-125 Ma, recording mica growth during early low-grade metamorphism, fluid flow, and internal deformation that mostly preceded large-scale thrust slip (Giallorenzo, 2013). $^{40}Ar/^{39}Ar$ ages are consistent with ZHe data from this study that indicate onset of cooling at ~130 Ma. The timing of Willard thrusting predates development of the basement cored Wasatch anticlinorium and the eastern thrust system of the salient. The ZHe ages generated by this study record continuous cooling from ~130-90 Ma.

Exhumation of the thrust sheet is also recorded by synorogenic deposits of the Gannett Group, Bear River Formation, Aspen Formation, and Frontier Formation. Detrital zircon analysis of these deposits have yielded, 110 to 90 Ma reworked volcanic grains that give maximum depositional ages, young stratigraphically upward, and closely date deposition, except for the basal part of the Gannett Group that lacked volcanic

grains (Gentry et al., 2013). Zircon fission track ages from the lower parts of the WTS, yielding 120-95 Ma cooling ages, also support erosional exhumation of the WTS at this time (Shari Kelley, personal communication, 2013).

The WTS was uplifted and rotated by the basement cored Wasatch anticlinorium. The anticlinorium is interpreted to have experienced multiple pulses of growth from ~90 to 60 Ma, recorded by apatite fission track ages from basement rocks, structural relations and characteristics of wedge top to fordeep basins (Naeser et al., 1983; Yonkee, 1992; DeCelles, 1994; DeCelles et al., 1995; Yonkee and Weil, 2010). Pulses of uplift are linked to episodes of slip along the Crawford, Absaroka, and Hogsback thrusts (DeCelles, 1994). ZHe ages from the structurally deeper footwall of the WTS from this study record cooling events at ~5 Ma related to exhumation in the footwall of the Wasatch normal fault (Figure 20).

The eastern system has a well-established record of progressive deformation due to preserved structures in synorogenic strata and clear relationships between synorogenic strata and thrust motion (DeCelles, 1994; Royse, 1993a; Wiltscko and Door, 1983). Structural relationships with the Mead thrust indicate that the Crawford is younger than the Willard-Paris-Mead thrusts (Coogan, 1992). Slip along the Crawford is recorded in growth structures of the synorogenic Weber Canyon Conglomerate at 90-85 Ma (DeCelles, 1994). Slip along the WTS had largely stopped by 90 Ma, but parts continued to be exhumed during uplift above the Wasatch anticlinorium (DeCelles, 1994; Yonkee et al., 1997; Yonkee and Weil, 2010), as recorded by the Evanston Formation, which lies unconformably on the WTS (DeCelles, 1994). Continued

exhumation of the WTS is also interpreted to occur from further development of the eastern thrust system. Evidence for this can be seen in ZHe data presented in this study from the Perry Canyon Formation, which records a ~65 Ma event interpreted as a phase of slip along the Absaroka thrust. As deformation progressed eastward, the Absaroka thrust had two phases of slip at 85-75 Ma and 70-65 Ma; both events are recorded by deposition of synorogenic conglomerates (Royse et al., 1975; DeCelles, 1994). The Hogsback-Darby-Prospect thrusts are the eastern leading thrust faults in the Wyoming Salient and slip along them likely continued into the Eocene (Wiltchko and Dorr, 1983; Solum and van der Pluijm, 2007; Yonkee and Weil, 2011).

Correlations Between Western Thrust Systems of the Sevier FTB

Correlations between western thrust systems of the Sevier FTB have been proposed based on similarities in stratigraphic relationships, structural positions within the FTB, inferred timing, and displacement estimates. With a better understanding of fault timing of the WTS, a better assessment can be made regarding thrust correlation and whether displacement along these thrusts was synchronous or diachronous. Extensive dominant thrusts in the Sevier FTB displaced Neoproterozoic to Paleozoic sedimentary rocks ca. 50-100 km eastward during the Early Cretaceous and/or the Late Jurassic (DeCelles, 2004). These include the Hawley Creek thrust in southwestern Montana, the Willard thrust of the Wyoming salient, the Sheeprock thrust in the Nebo-Charleston salient, the Canyon Range thrust in central Utah, the Wah Wah thrust in southern Utah, and the Wheeler Pass thrust in the Spring Mountains in southern Nevada (Figure 21) (DeCelles, 2004).

Located in central Utah, the Canyon Range, Pavant, Paxton, and Gunnison thrust system makes up the type area for the Sevier FTB. The Canyon Range thrust carries up to an estimated 12 km thick sequence of Neoproterozoic to Jurassic sedimentary rocks. Although the age of thrusting is not well constrained, the Canyon Range thrust is thought to have been active in the Early Cretaceous (DeCelles and Coogan, 2006). The synorogenic Canyon Range conglomerate records thrust slip along the Canyon Range thrust at ~96 Ma and apatite fission track modeling suggests possible thrust initiation at ~145 Ma (Ketcham, 1996; Stockli et al., 2001). A correlation between the Canyon Range thrust and the Wah Wah thrust to the south is commonly accepted (DeCelles et al., 1995; Currie, 2002; Friedrich and Bartley, 2003). Similarly, a correlation has been proposed for the Canyon Range thrust and the Willard thrust to the north, supported by similarities in thrust sheet stratigraphy and synorogenic deposits (Allmendinger, 1992; Burtner and Nigrini, 1994; DeCelles et al., 1995; Yonkee et al., 1997; Currie, 2002; Friedrich and Bartley, 2003; DeCelles, 2004; DeCelles and Coogan, 2006). Thermochronologic evidence of the WTS presented here support this prior correlation.

Slip along the Wheeler Pass thrust sheet (WPS) from ca. 160 Ma to 150 Ma is suggested by recent thermochronologic studies (Giallorenzo et al., 2013; Giallorenzo, 2013). According to this study, slip along the WPS was initiated up to 30 m.y. prior to motion on other dominant western thrust faults in the Sevier FTB, calling into question the correlation between the WPS in southern Nevada and the WTS in northern Utah, as coeval thrust sheets. Based upon stratigraphic relationships and structural position within the thrust belt, the Wheeler Pass and Gass Peak thrusts have been proposed as

correlative across the Las Vegas valley shear zone (Armstrong, 1968). It is debatable whether the Wheeler Pass/Gass Peak thrust follows the trend of the Sevier FTB into Utah or continues into southern Nevada (Royse, 1993a; Taylor et al., 2000).

Hinterland Relationships

Supracrustal rocks in the hinterland show evidence for only minor Late Jurassic to Early Cretaceous shortening. Miller and Hoisch (1995) summarize Jurassic tectonism within areas of the northeastern Great Basin. Thrust faults and folds predated or were coeval with Jurassic plutonism in the Pilot Range, Knoll Mountain, Gold Hill, and the Ruby, Silver Island, Newfoundland, Oquirrh, and Dolly Varden mountains (Miller and Hoisch, 1995). A minor episode of crustal shortening in the hinterland of the Sevier FTB in the Late Jurassic is also interpreted in studies by Smith et al. (1993) and Miller et al. (1988). Shortening, metamorphism, and plutonism have been recorded at ~153 Ma in the Ruby Mountains by Hudec (1992).

Metamorphic rocks in the core complexes of the Sevier hinterland record burial of supracrustal rocks to mid-crustal depths by stacking of thrust sheets and/or fold nappes within the Sevier orogenic wedge (McGrew et al., 2000; Harris et al., 2007; Cooper et al., 2010; Hoisch et al., 2014). This causes metamorphism and garnet growth that can be evaluated to determine P-T paths and dated by Lu-Hf to determine timing of thrust burial metamorphism (e.g., Wells et al., 2012; Hoisch et al., 2014). In the Albion Mountains-Raft River Mountains-Grouse Creek Mountains, Snake Range, and Ruby Mountains-East Humboldt Range, contractional deformation is thought to have initially occurred in Late Jurassic time (Sullivan and Snoke, 2007). Lu–Hf isochron ages from

multiple garnet fractions and whole-rock analyses from both the hanging wall and the footwall of the Basin-Elba fault in southern Idaho and northwestern Utah record episodic contraction and exhumation at ~138-132 Ma (Kelly et al., 2013; Cruz-Uribe et al., in review). Burial ages as old as 149.9 ± 1.2 Ma and 158.2 ±2.6 Ma have been determined from the Raft River Mountains in northwestern Utah and in the Funeral Mountains in eastern California, respectively (Hoisch et al., 2014; Wells et al., 2013). Renewed crustal shortening has been recorded in the hinterland from burial ages of 85.5 ± 1.9 Ma in the Grouse Creek Mountains in northeastern Utah and 82.8 ± 1.1 Ma in the Wood Hills in eastern Nevada (Hoisch et al., 2013; Wells et al., 2012; 2013). The metamorphic rocks of the core complexes provide clear evidence for Late Jurassic to Early Cretaceous crustal shortening and metamorphism. Thrust timing of the WTS determined from this study and age relationships discussed in the above section are consistent with an in-sequence eastward propagation of initial shortening within the Sevier orogen (Figure 19).

Conclusions

ZHe analysis on approximately 240 grains from three transport-parallel traverses and three vertical transects across the Willard thrust sheet in northern Utah record the timing of cooling interpreted to result from erosion and exhumation due to rock uplift above thrust ramps. Vertical transects capture an Early Cretaceous PRZ with thrust slip occurring ca. 130 to 90 Ma. Cooling ages increase systematically upward in the east-central and central transects, yielding an average exhumation rate of 0.12 mm/yr.

assuming steady state geothermal conditions; all samples from the eastern leading edge of the sheet are within the PRZ. Ages across a transport parallel traverse yield an average slip rate of 1.7 mm/yr. from ~125 to 90 Ma, and assuming that cooling kept pace with displacement. The WTS was subsequently passively uplifted and partially exhumed during Late Cretaceous development of the Wasatch anticlinorium. Age relationships with the hinterland are consistent with in-sequence thrust propagation during development of the orogenic wedge. The thermochronologic methodology presented in this study effectively allows for quantification of timing, rate, and magnitude of hanging-wall exhumation due to thrust faulting, and may adequately be used as a case study for similar thermochronologic studies on thrust systems around the world.

Figure Captions

Figure 1. Simplified map of the North American Cordillera during the early Cretaceous showing the location of the Wyoming Salient and major elements of the western Cordillera. Modified from Yonkee and Weil (2011).

Figure 2. Regional geologic map of the Wyoming Salient in northern Utah showing geographic locations of the Willard, Crawford, Absaroka and Hogsback thrusts and the Wasatch anticlinorium. Modified from Yonkee and Weil (2010).

Figure 3. (A) Geologic map of the Willard thrust sheet and the Wasatch anticlinorium in northern Utah. (B) Generalized geologic cross-section of the Willard thrust from W to E. The Willard has large folds, imbricate faults, and displays a ramp-flat geometry. Vertical transects are indicated in green. Modified from Adolph Yonkee personal communication.

Figure 4. Tectonic model for development of the Wasatch anticlinorium and the eastern thrust system in the Wyoming salient. Modified from Yonkee and Weil (2011)

Figure 5. Probability density plots of single-grain detrital zircon U/Pb ages for early Neoproterozoic through Devonian strata from the Willard thrust sheet. Only concordant ages (< 15% discordance) are plotted. Relevant stratigraphic units are Facer Formation, Farmington Canyon, Tintic Quartzite, formation of Perry Canyon, Kelley Canyon Formation, Caddy Canyon Quartzite, Mutual Formation, Browns Hole Formation, Geertsen Canyon Quartzite, Worm Creek, Swan Peak Quartzite, and Beirdneau Formation. Separated into two figures for space. Colors indicate phases of sedimentation. Simplified stratigraphic column from Yonkee and Weil (2011).

Figure 6. Probability density plots of single-grain detrital zircon U/Pb ages for early Neoproterozoic through Devonian strata from the Willard thrust sheet. Only concordant ages (< 15% discordance) are plotted. Relevant stratigraphic units are Facer Formation, Farmington Canyon, Tintic Quartzite, formation of Perry Canyon, Kelley Canyon Formation, Caddy Canyon Quartzite, Mutual Formation, Browns Hole Formation, Geertsen Canyon Quartzite, Worm Creek, Swan Peak Quartzite, and Beirdneau Formation. Separated into two figures for space. Colors indicate phases of sedimentation. Simplified stratigraphic column from Yonkee and Weil (2011).

Figure 7. Thermochronology sampling strategy with idealized output. (A) Conceptual diagrams showing 3 sequential periods of evolution (t_0, t_1, t_2) for a large-displacement, single-thrust ramp with erosion. Proposed sampling strategies for thermochronometry indicated in A, with idealized output shown in B-D. Age-temperature (B), age-depth (C), and age-distance (D) plots to be used to estimate timing of initiation of thrusting (inflections in D, E, and F), cooling rate (B), exhumation rate (C), and slip rate (D). PRZ = Partial Retention Zone for zircon He. Modified from Michael Wells, personal communication.

Figure 8. Plot of He concentration vs. effective alpha damage for all grains that were U-Pb prescreened prior to ZHe analysis. Blue diamonds represent zircon grains whose calculated alpha damage is below the ~2 $\times 10^{18}$ α/g threshold (Reiners, 2005) and red

diamonds represent zircon grains which exceed the threshold. Zircon grains that exceed Reiners' threshold have accumulated enough lattice defects to disturb the ZHe age.

Figure 9. Restored section of the western part of the Willard sheet. Restored positions of vertical transect samples and ZHe ages are indicated. Modified from Adolph Yonkee personal communication.

Figure 10. ZHe age vs. relative paleodepth plot from samples collected along the Monte Cristo transect of the WTS hanging wall (Figure 3). Large red circles represent sample average ZHe age and small circles represent ZHe ages for individual grains.

Figure 11. ZHe age vs. relative paleodepth plot from samples collected along the Bear River to Browns Hole transect of the WTS (Figure 3). Large red circles represent sample average ZHe ages and small circles represent ZHe ages for individual grains. Grey lines represent exhumation curves that were generated from HeMP modeling software using sample average ZHe ages. Results from modeling shows tectonic exhumation was initiated ~126 ± 4.69 Ma that was preceded by a Cretaceous PRZ.

Figure 12. ZHe age vs. relative paleodepth plot from samples collected along the Wellsville transect of the WTS hanging wall (Figure 3). Large red circles represent sample average ZHe ages and small red circles represent ZHe ages for individual grains. Grey lines represent exhumation curves that were generated from HeMP modeling software using sample average ZHe ages. Results from modeling shows tectonic exhumation was initiated ~134.2 ± 7.98 Ma.

Figure 13. Age vs. Distance plot for the Worm Creek traverse. Large circles represent sample average ZHe ages and small circles represent ZHe ages for individual grains.

Figure 14. Age vs. Distance plot for the Geertsen Canyon traverse. Large circles represent sample average ZHe ages and small circles represent ZHe ages for individual grains. Solid black line represents a best fit line for the traverse. Results indicate an average slip rate of 1.7 mm/yr.

Figure 15. Age vs. Distance plot for the Perry Canyon traverse. Large circles represent sample average ZHe ages and small circles represent ZHe ages for individual grains.

Figure 16. Time-Temperature plot (t-T) showing grey HeMP cooling curves for the Bear River to Browns Hole transect of the WTS hanging wall (Figure 3). Chosen initial t-T constraints are represented by a black box. Warmer colors represent higher geothermal gradients.

Figure 17. Time-Temperature plot (t-T) showing HeMP cooling curves for the Wellsville transect of the WTS hanging wall (Figure 3). Chosen initial t-T constraints are represented by a black box. Warmer colors represent higher geothermal gradients.

Figure 18. ZHe age probability diagram for the vertical Monte Cristo Transect.

Figure 19. Diagram showing regional timing relationships between the Sevier hinterland, fold-thrust belt, and the foreland. Modified from DeCelles, 1994; Yonkee et al., 1997; Wells et al., 2013; Druschke et al., 2009; Giallorenzo, 2013; Hoisch et al., 2014.

Figure 20. (A) Age probability plot for the samples collected from the footwall of the WTS. (B) Age vs. Paleodepth plot for the Wellsville transect including the samples collected from the footwall of the WTS.

Figure 21. Map showing dominant western thrusts in the Sevier FTB. Modified from DeCelles (2004)

Figures

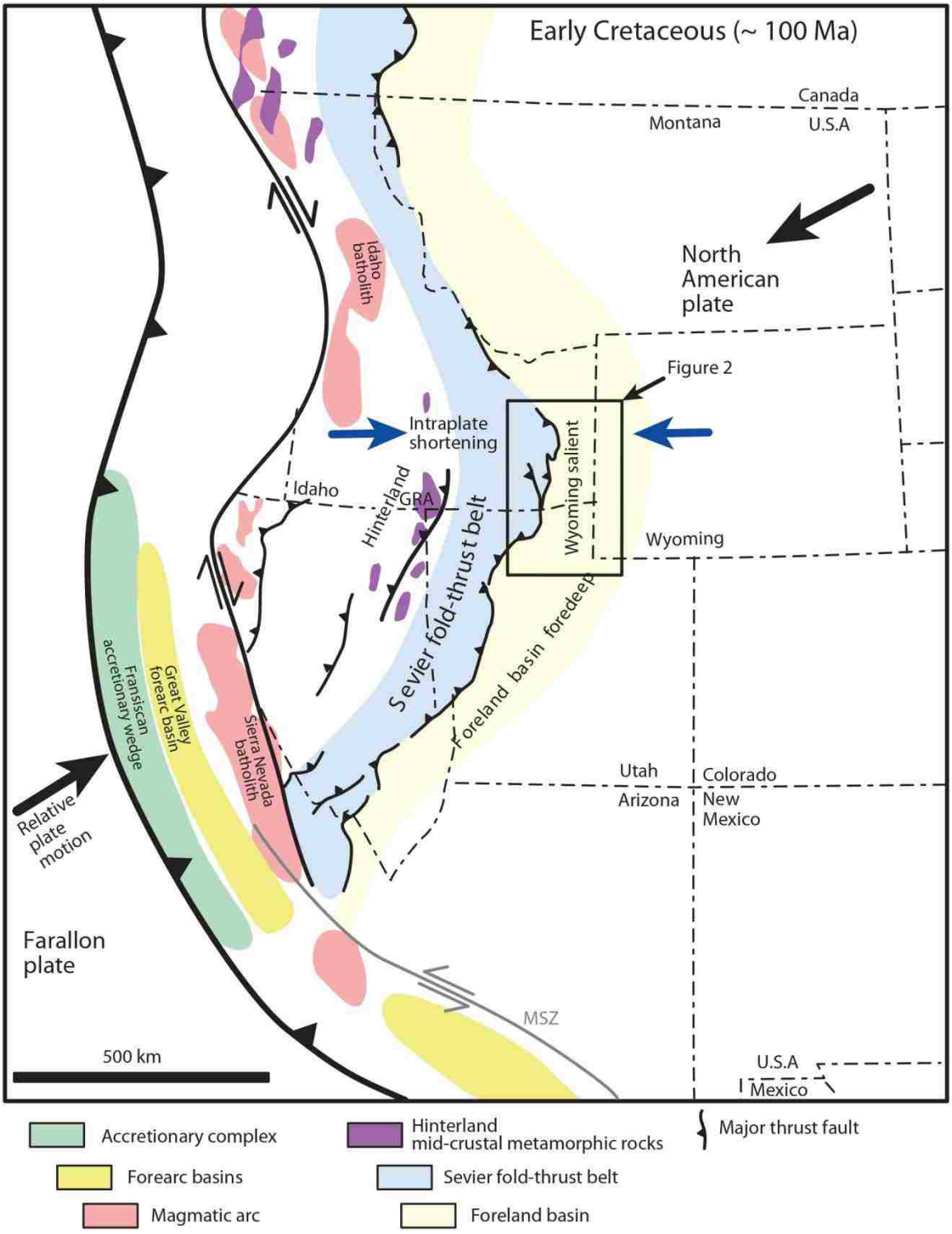

Figure 1. Simplified Tectonic Map of the Western North American Cordilleran

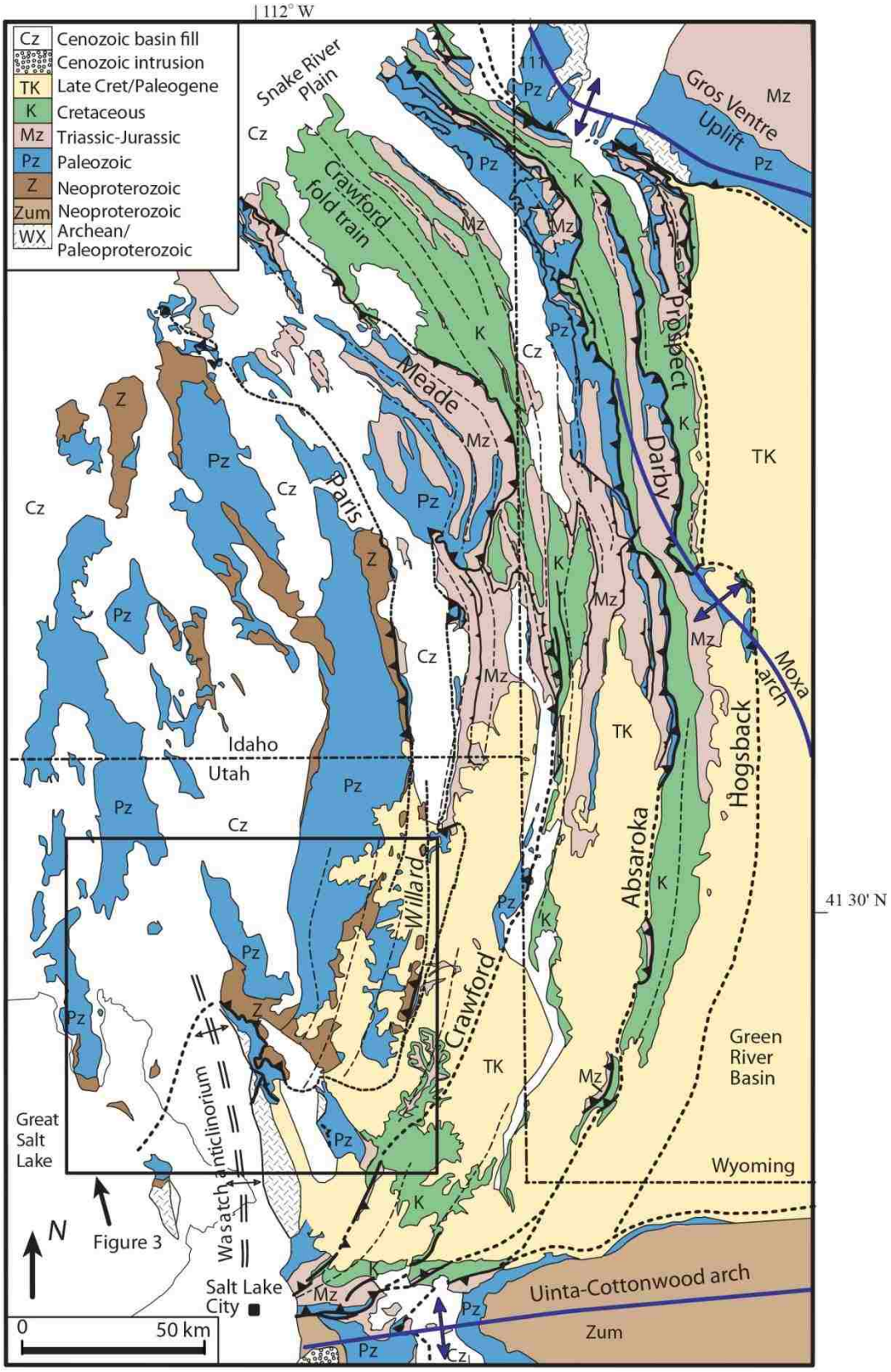

Figure 2. Geologic Map of the Wyoming Salient

Figure 8

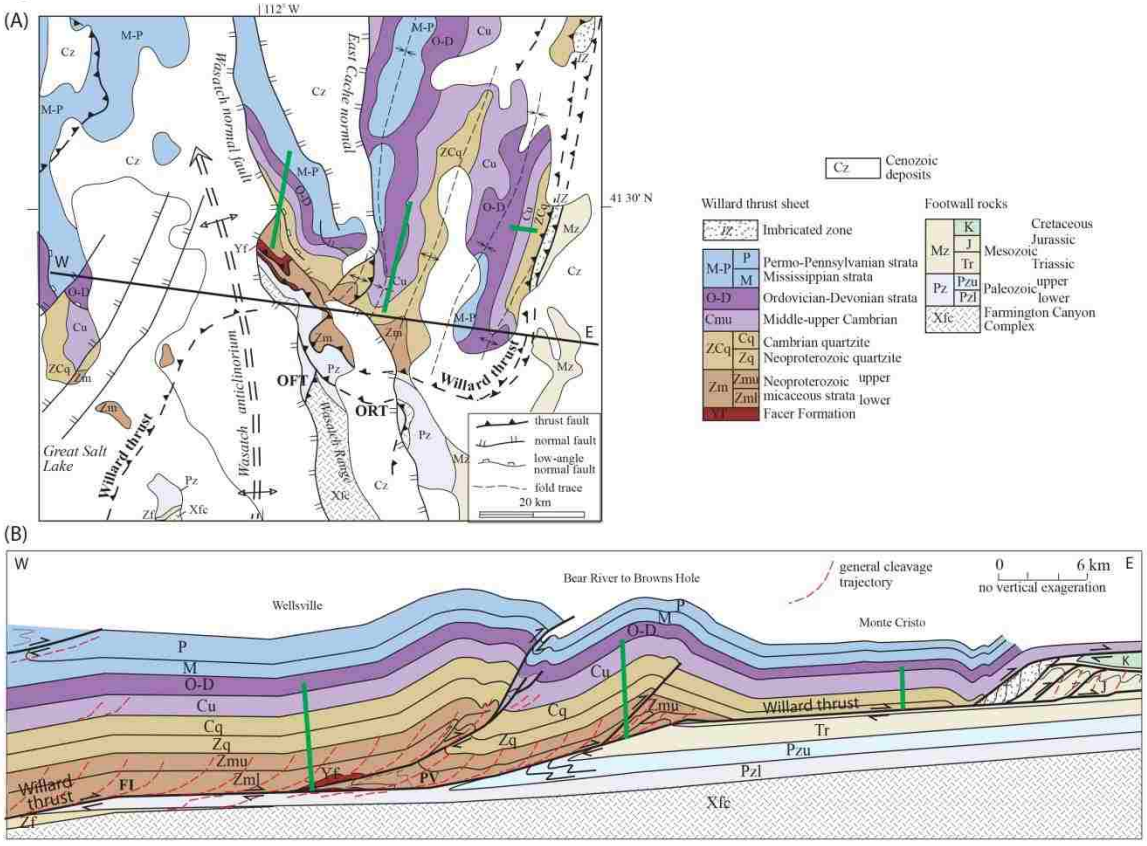

Figure 3. Geologic Map and Cross Section of the Willard Thrust Sheet Including Vertical Transects

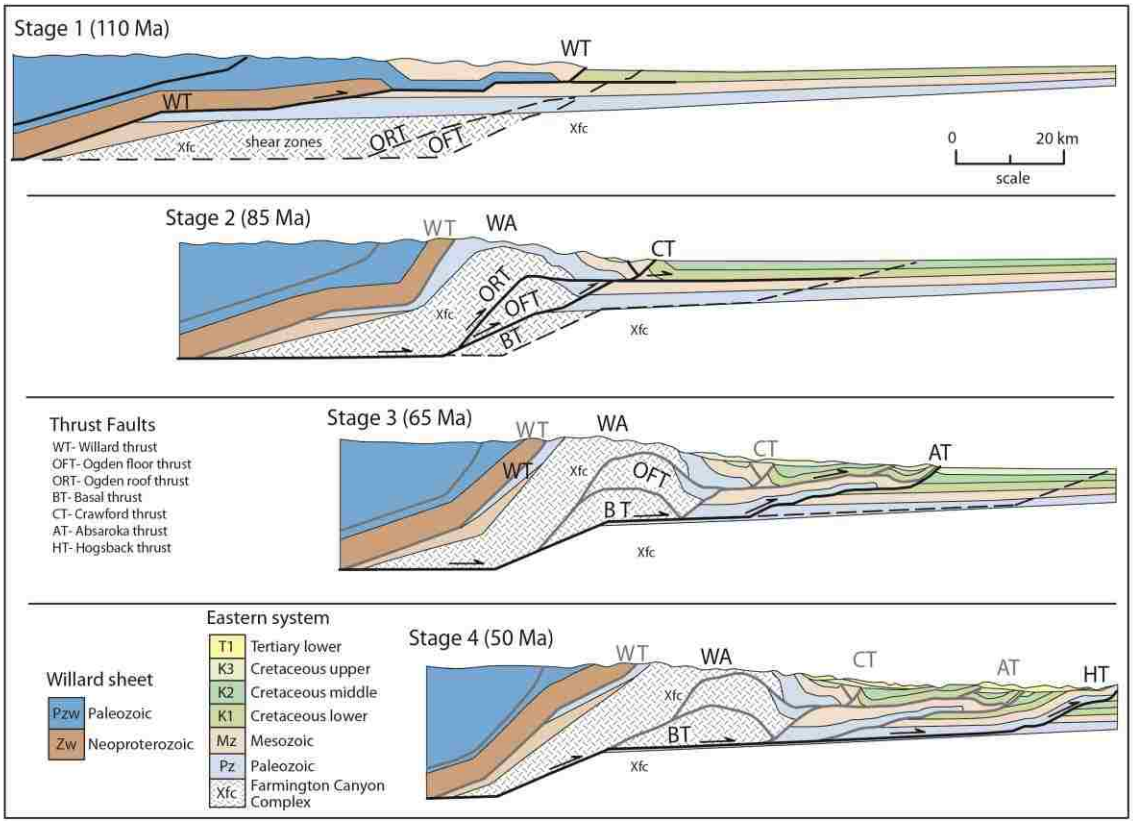

Figure 4. Model for the Development of the Wasatch Anticlinorium

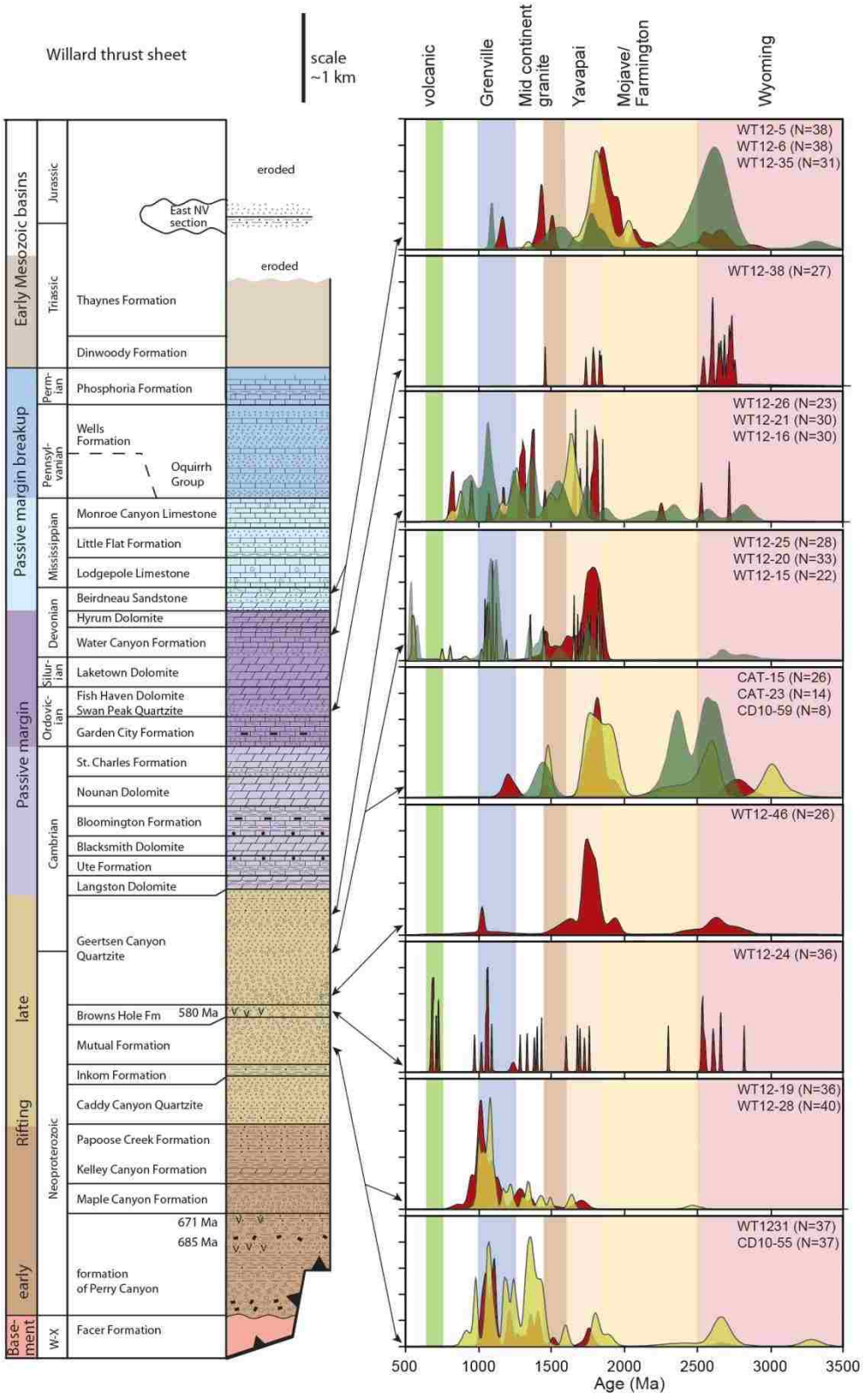

Figure 5. Willard Strat Column with U/Pb Diagrams A

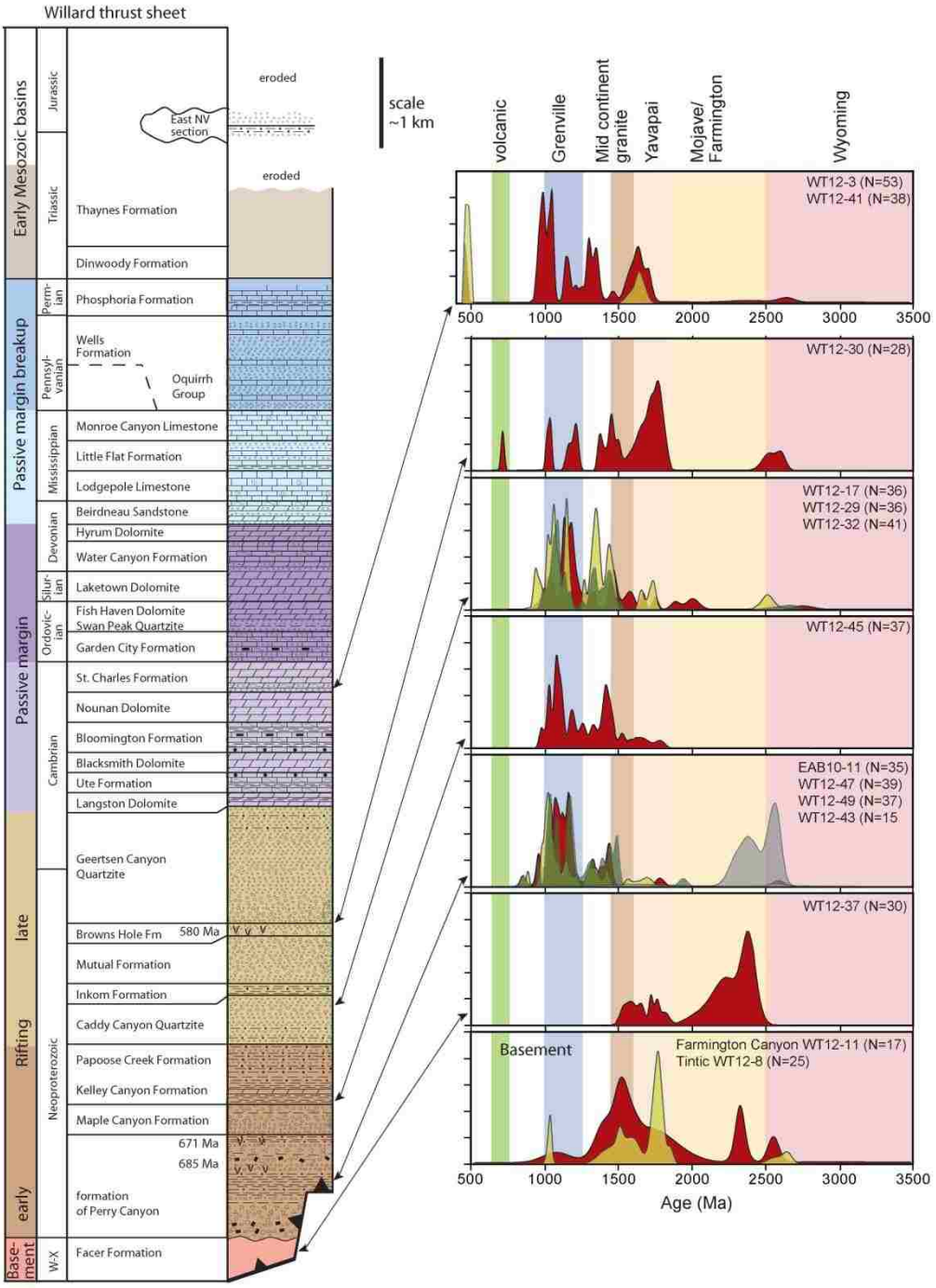

Figure 6. Willard Strat Column with U/Pb Diagrams B

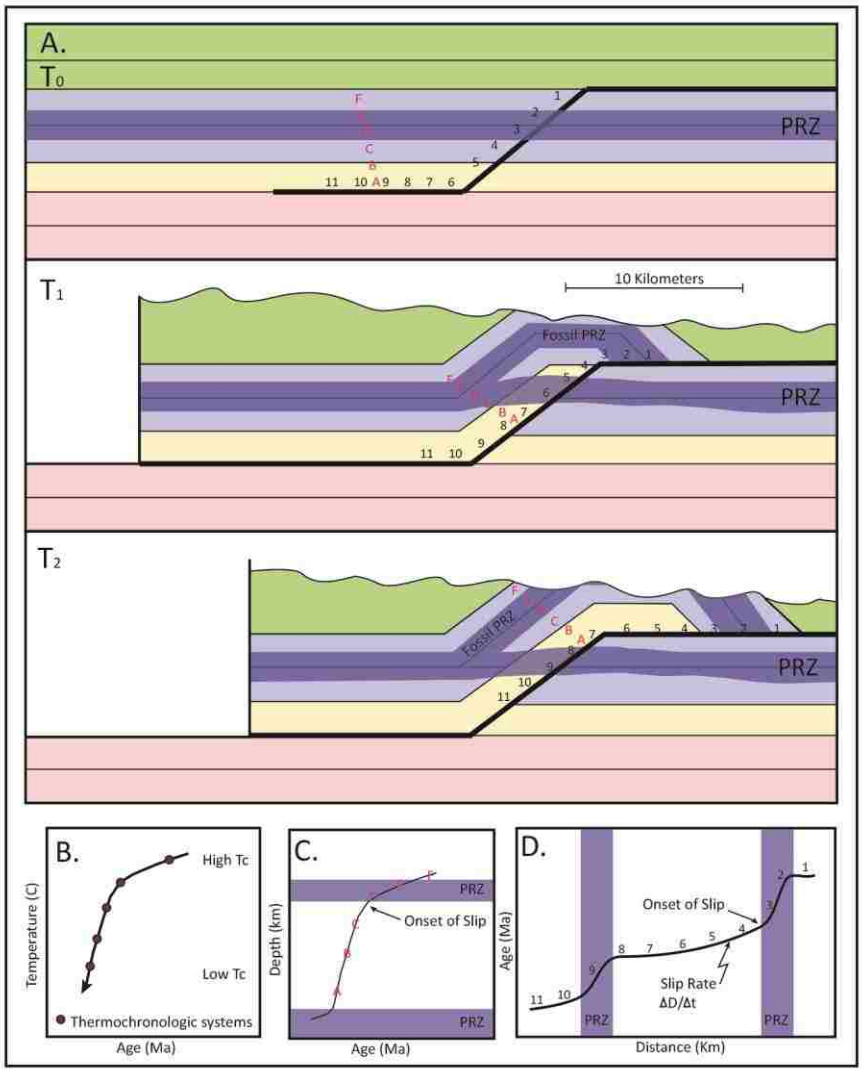

Figure 7. Thermochronologic Sampling Stategy

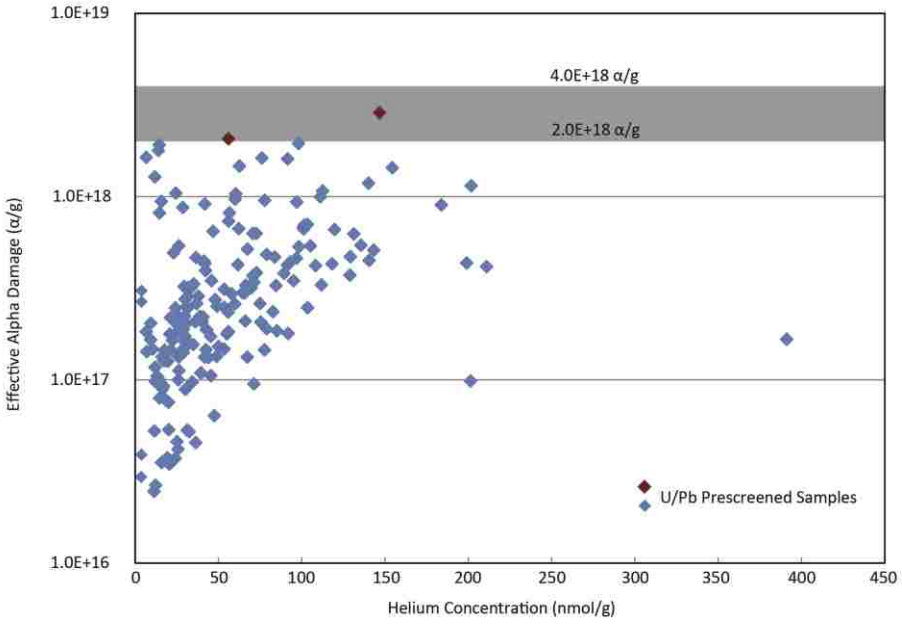

Figure 8. Plot of He Concentration vs. Effective Alpha Damage

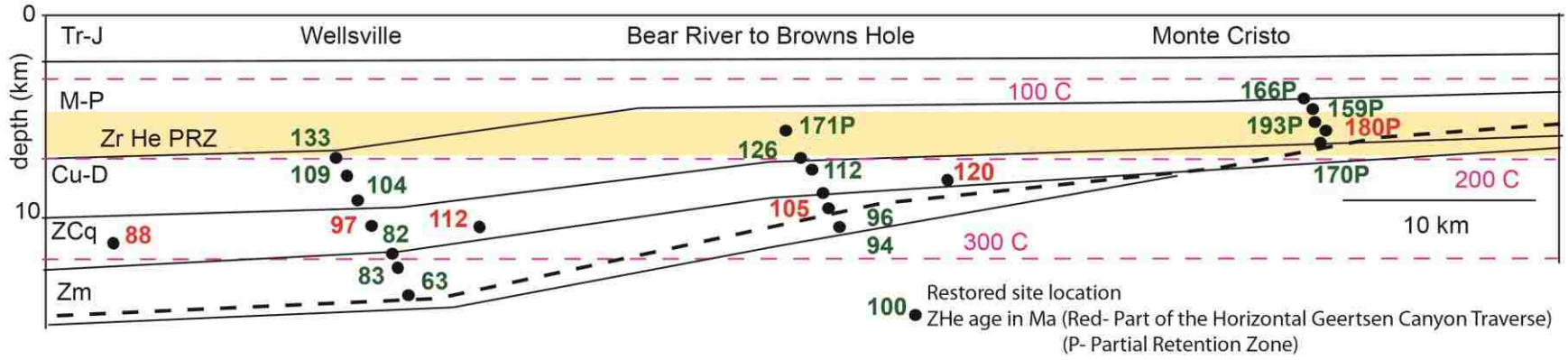

Figure 9. Restored Willard Cross-Section with Zhe Ages

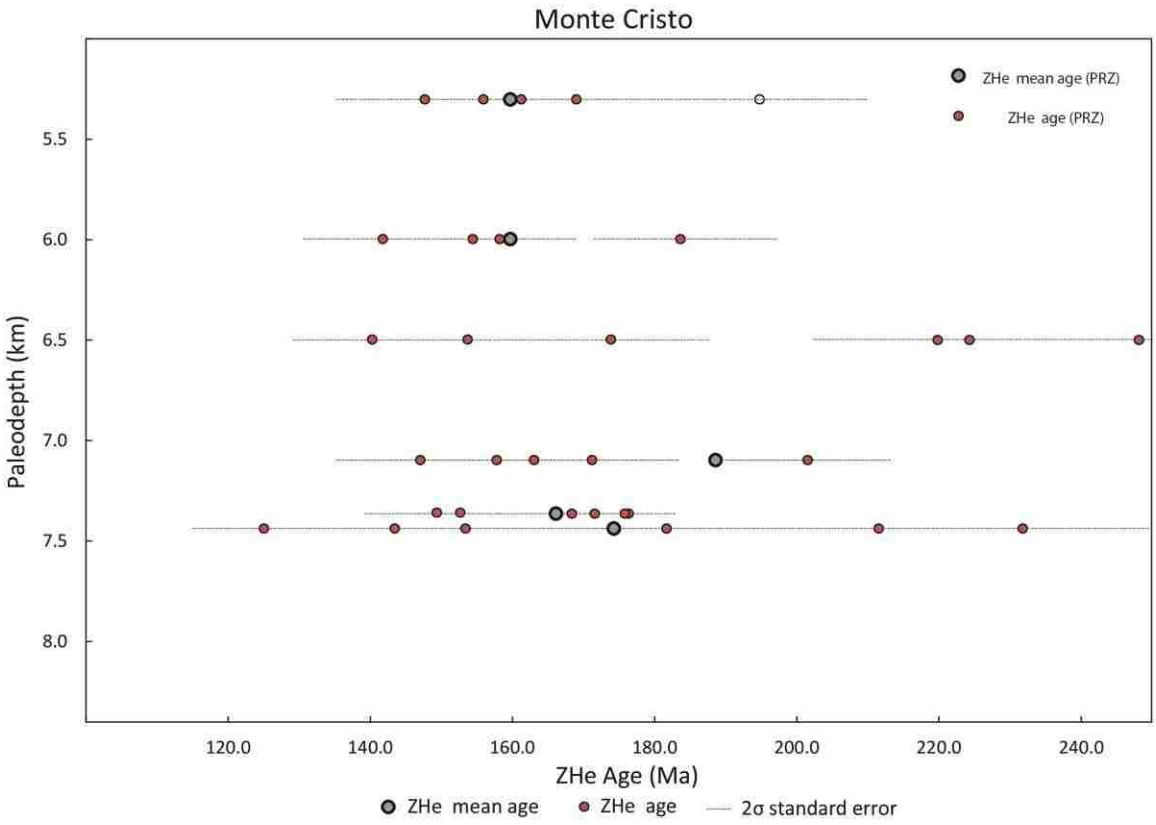

Figure 10. Monte Cristo Age vs. Depth Diagram

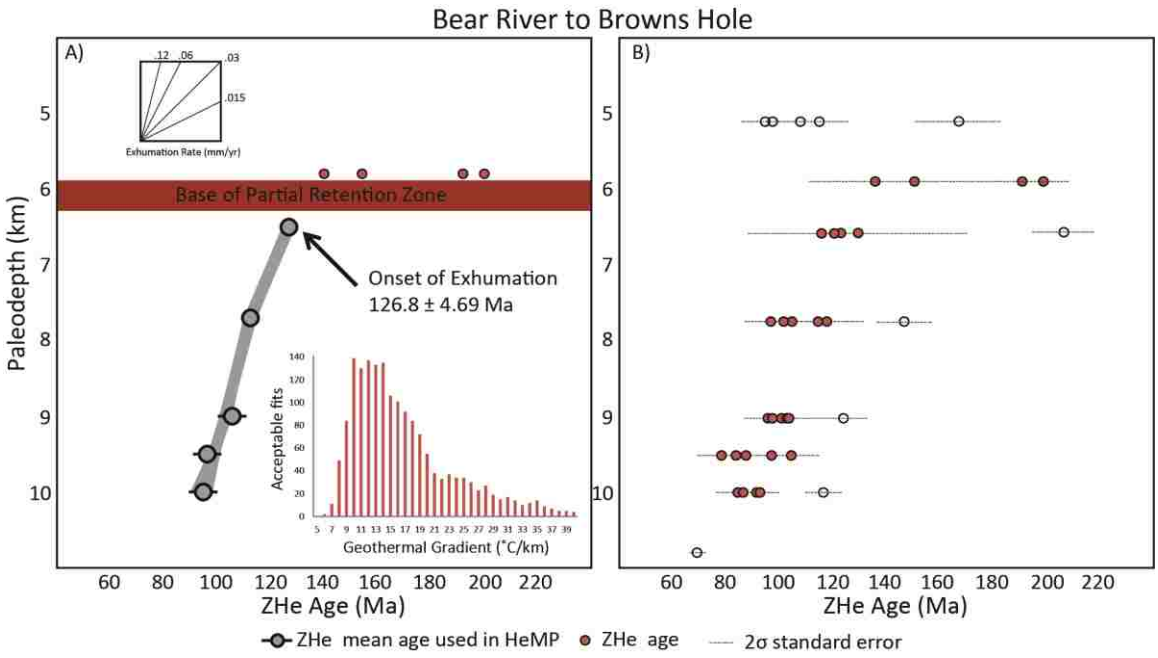

Figure 11. Bear River to Browns Hole Age vs. Depth Diagram

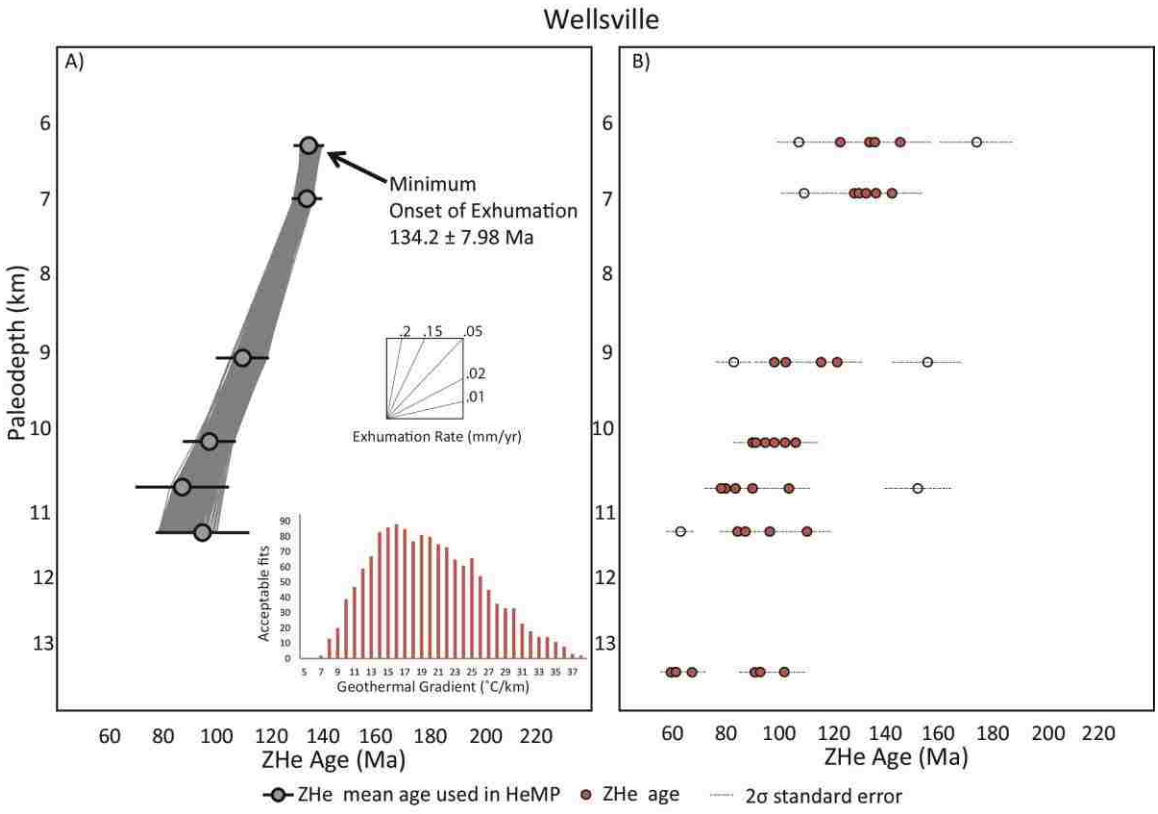

Figure 12. Wellsville Age vs. Depth Diagram

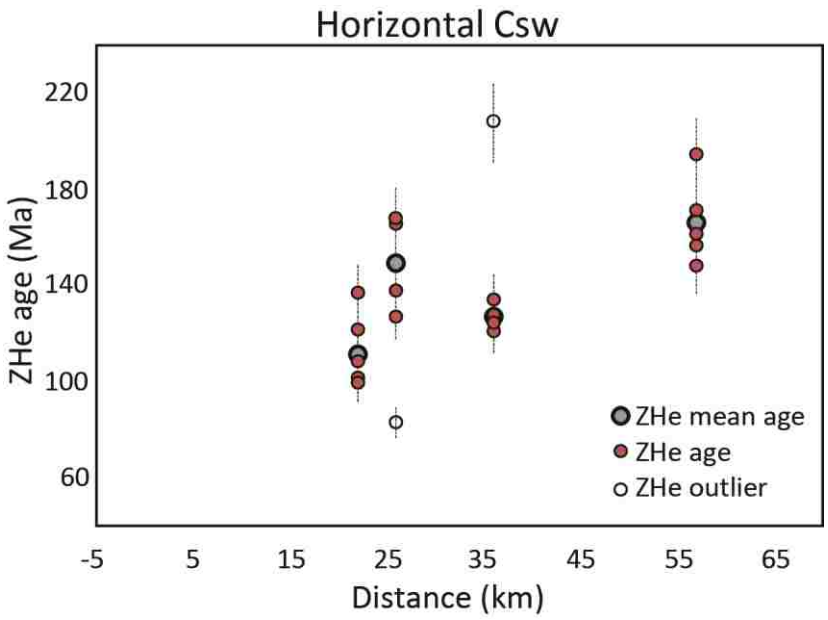

Figure 13. Worm Creek Age vs. Distance Diagram

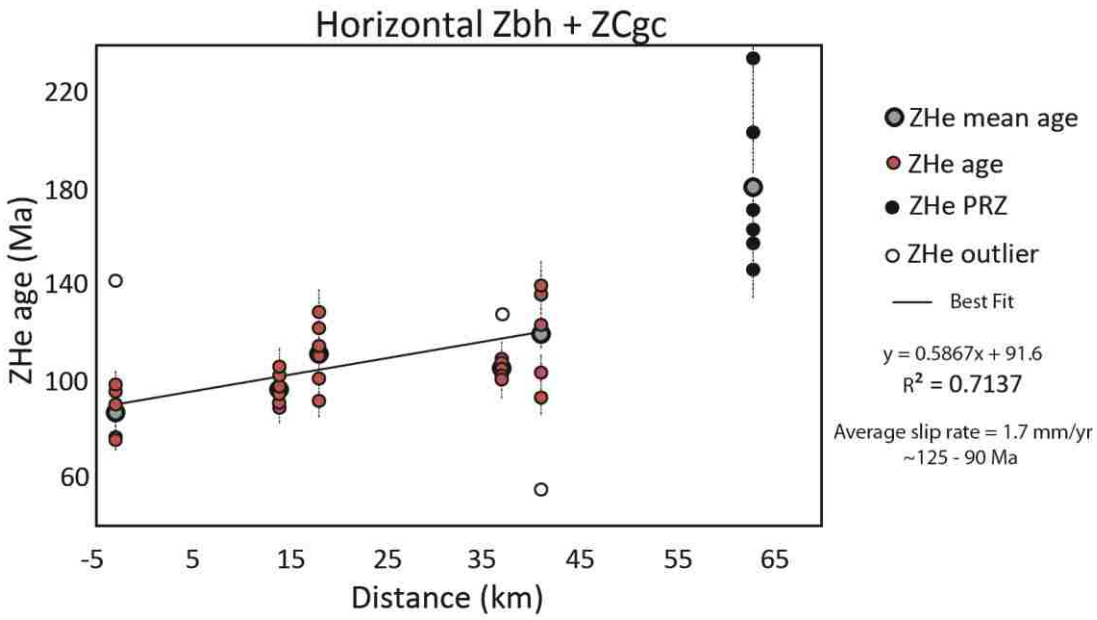

Figure 14. Geertsen Canyon Age vs. Distance Diagram

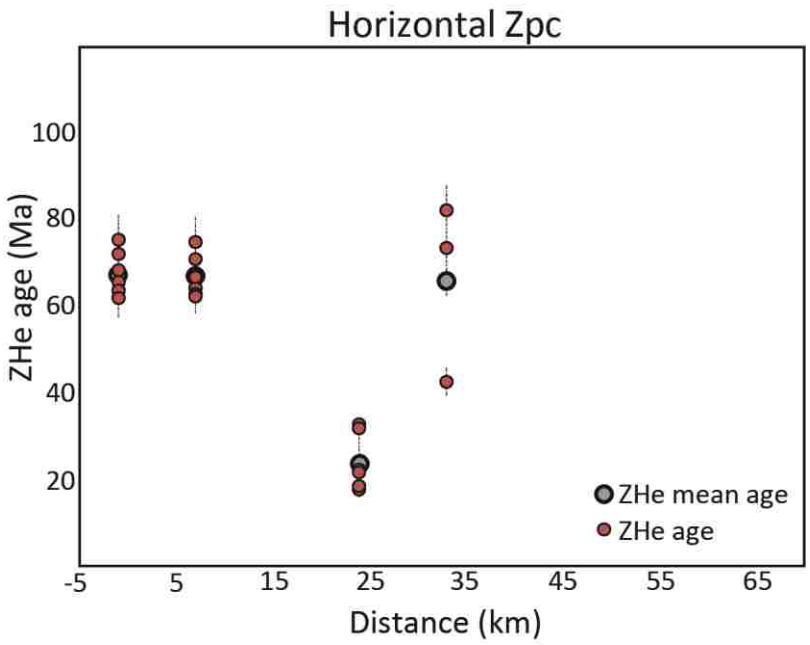

Figure 15. Perry Canyon Age vs. Distance Diagram

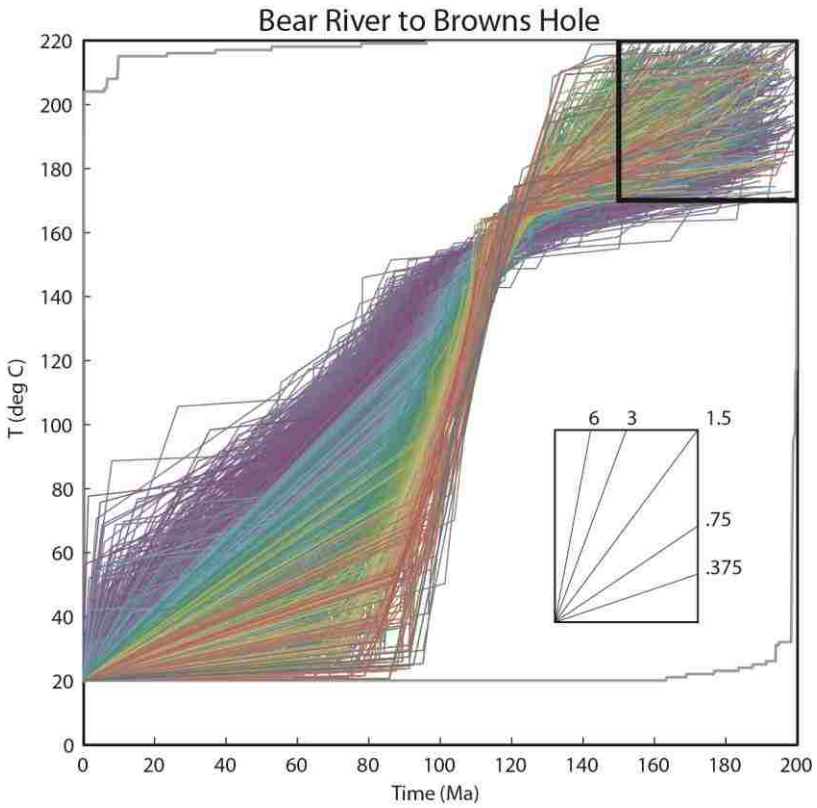

Figure 16. Bear River to Browns Hole t-T Diagram

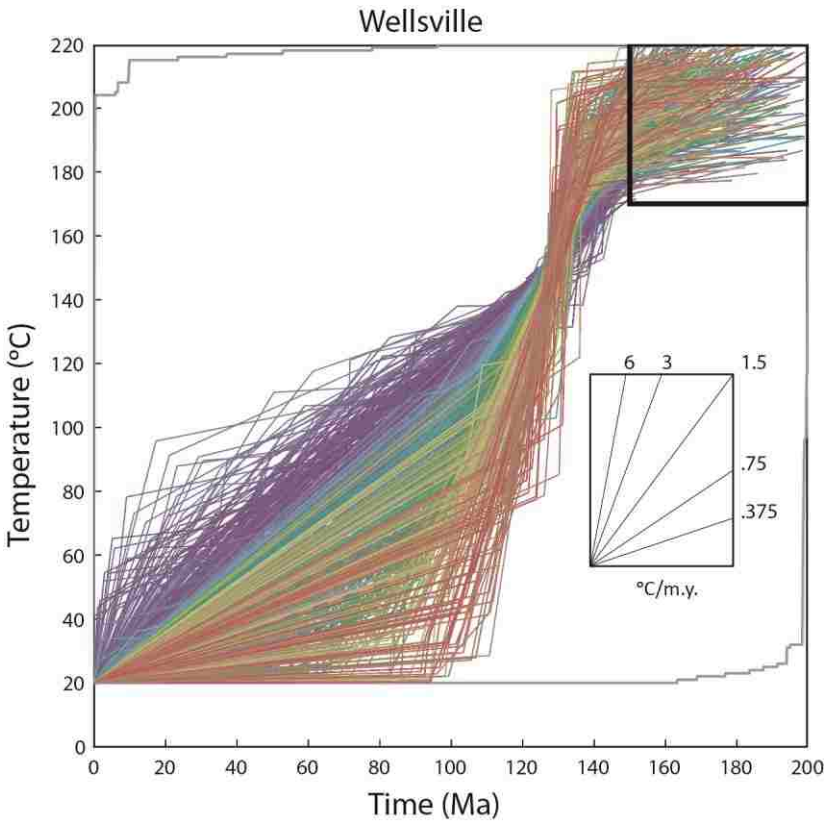

Figure 17. Wellsville t-T Diagram

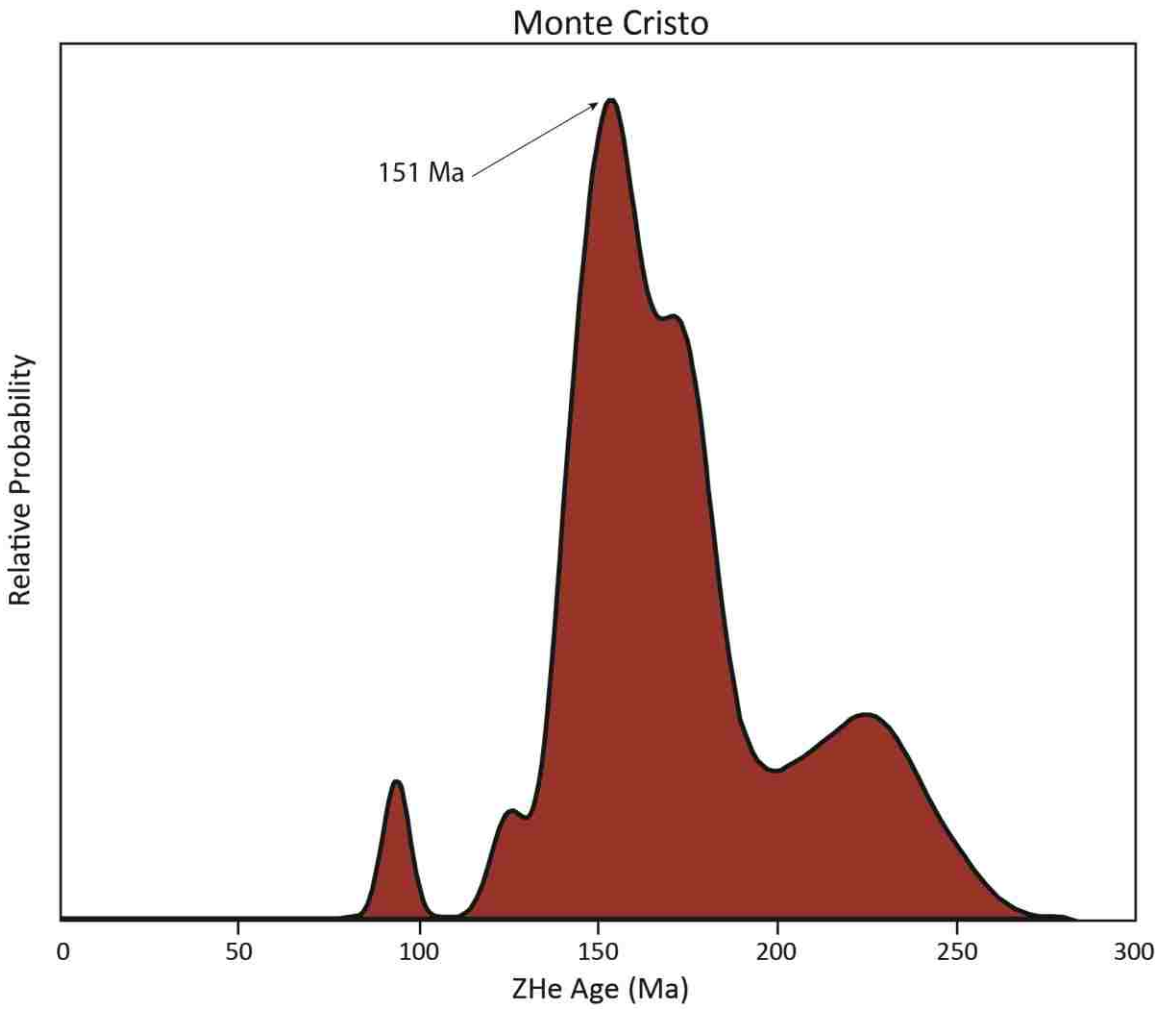

Figure 18. Monte Cristo Virticle Transect Age Probability Diagram

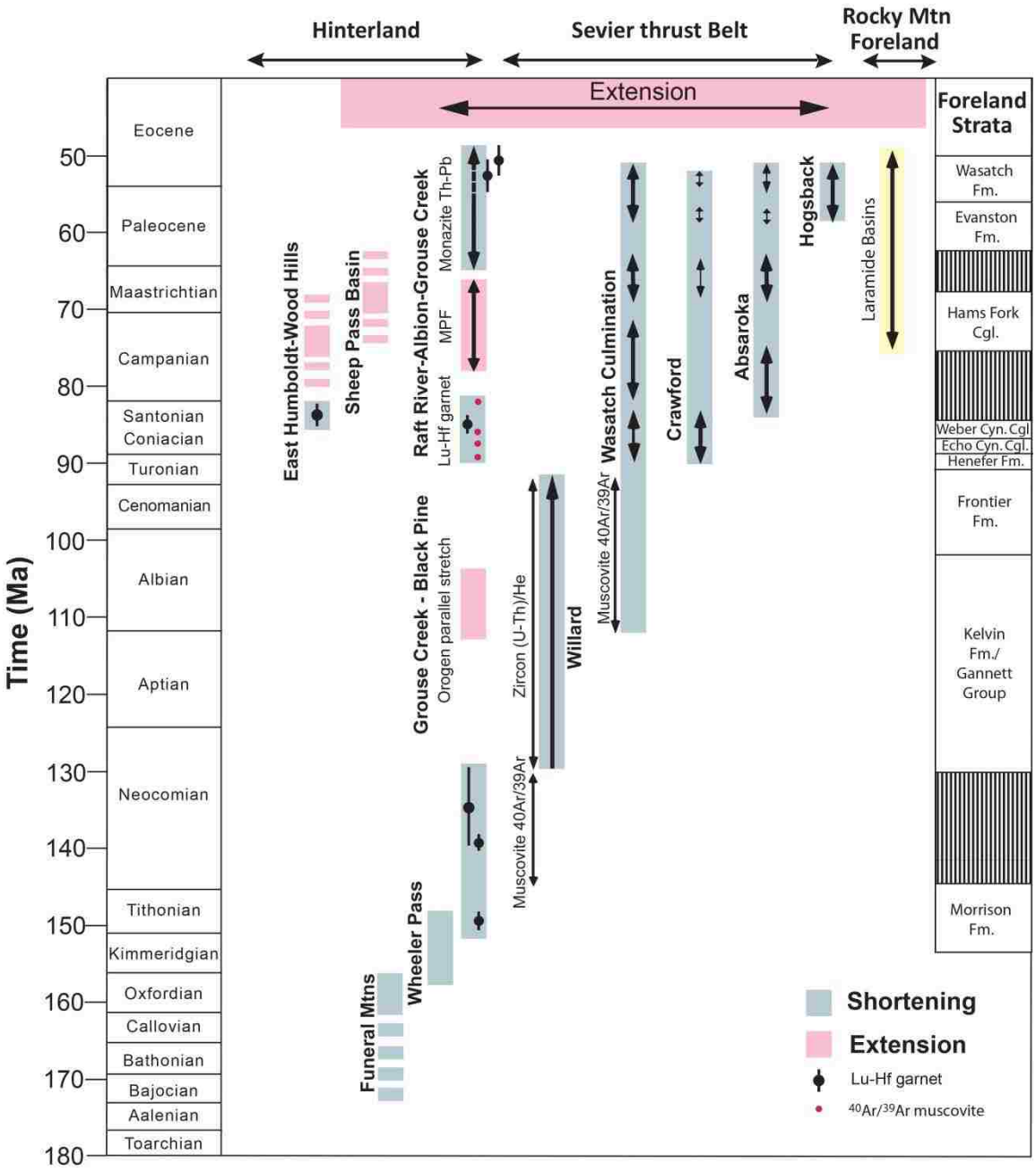

Figure 19. Sevier Orogeny Timing Relations Diagram

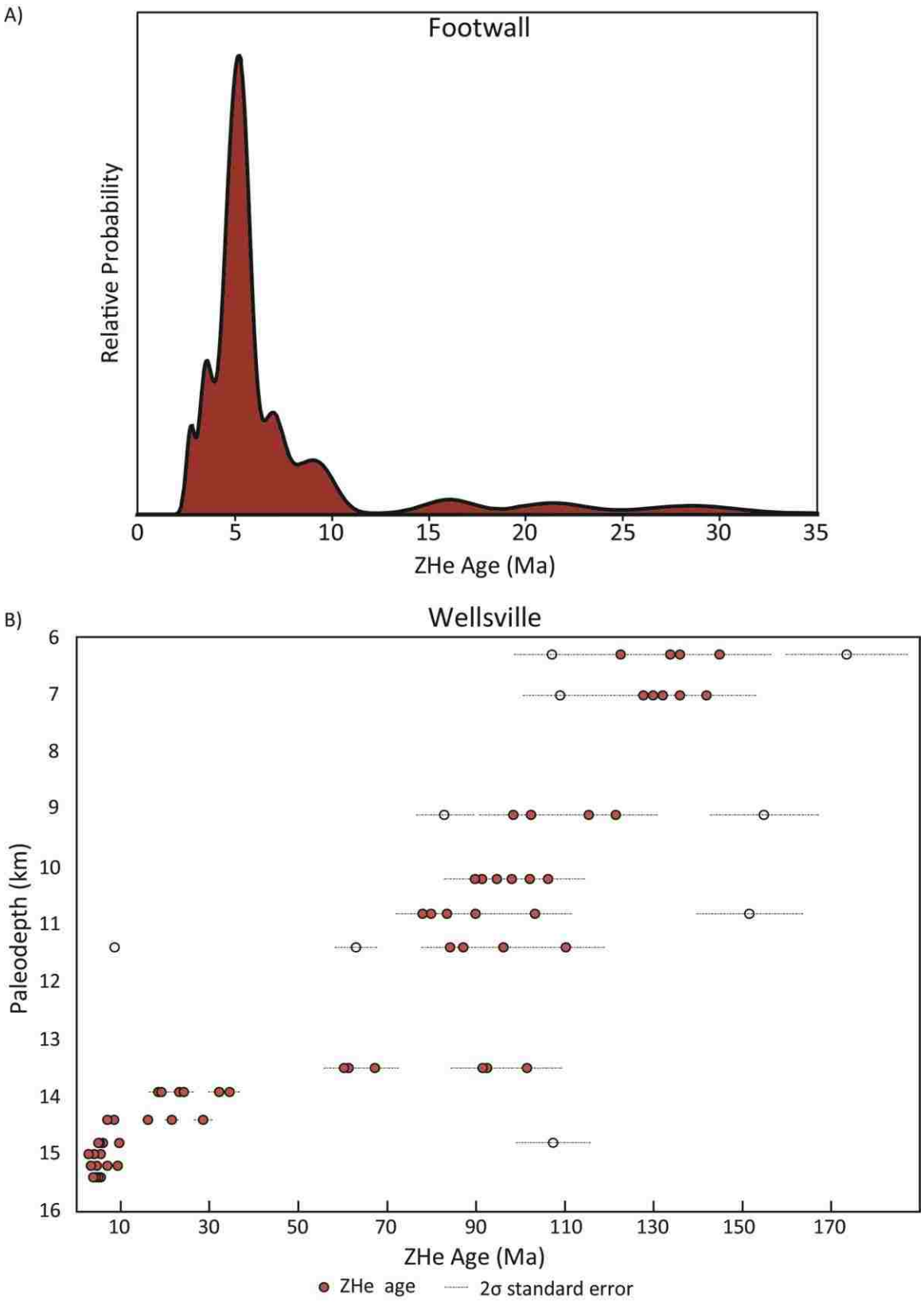

Figure 20. Wellsville and Footwall Vertical Transects Diagram

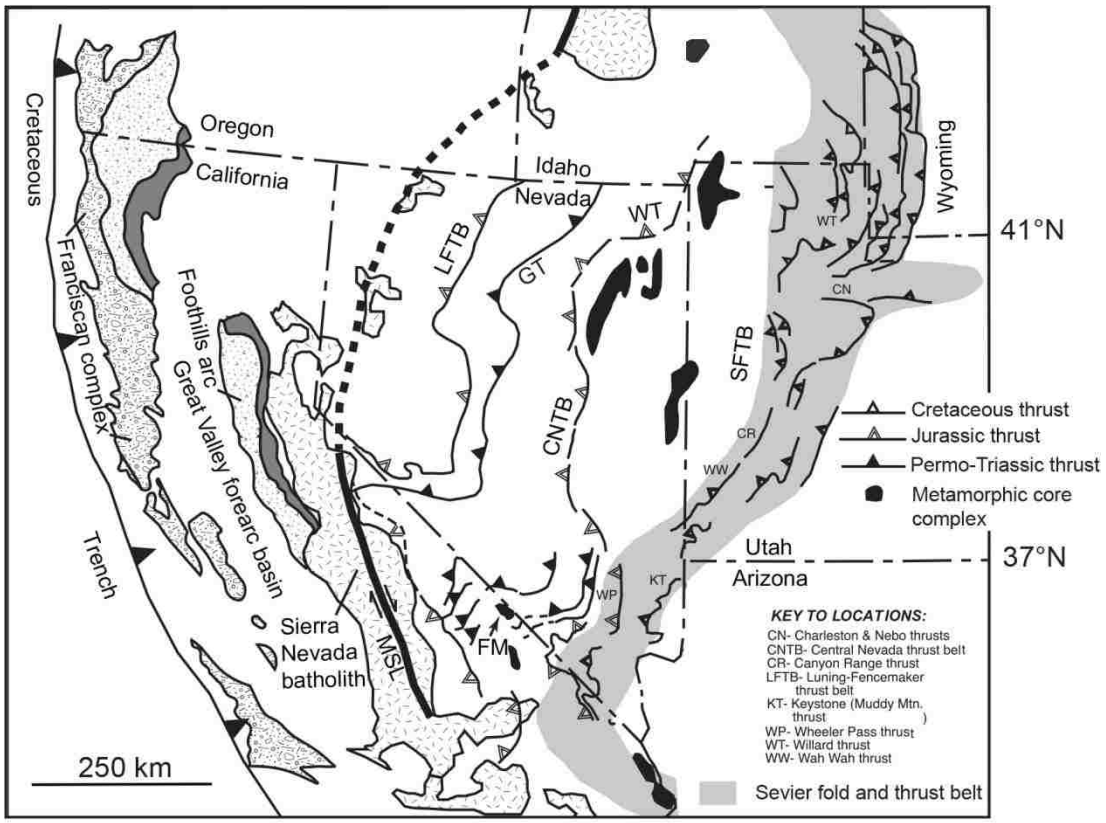

Figure 21. Map Showing Dominant Western Thrusts in the Sevier FTB

Appendix A: Sample Locations

Sample	Unit/Formation	Latitude	Longitude	Elevation (m)
WT12-3	Worm Creek	41.67238	-111.443498	5669
WT12-5	Water Canyon	41.62509	-111.734843	5258
WT12-6	Beirdneau	41.52421	-111741347	5517
WT12-8	Basal Tintic	41.41573	-112.014235	5184
WT12-9	Farmington Canyon	41.39934	-112.021863	4925
WT12-10	Farmington Canyon	41.40644	-112.021197	4941
WT12-11	Farmington Canyon	41.38015	-112.019446	4901
WT12-12	Farmington Canyon	41.39004	-112.022100	4963
WT12-14	lower Geertsen Canyon	41.49713	-111.958272	5094
WT12-15	middle Geertsen Canyon	41.49947	-111.952807	5247
WT12-16	upper Geertsen Canyon	41.50203	-111.948280	5344
WT12-17	Caddy Canyon	41.48320	-111.377796	7503
WT12-18	Perry Canyon	41.48301	-111.376776	7462
WT12-19	Mutual equivalent	41.48039	-111.387038	7518
WT12-20	middle Geertsen Canyon	41.48447	-111.401125	7655
WT12-21	upper Geertsen Canyon	41.48329	-111.414701	7756
WT12-24	Terra Cotta member	41.32881	-111.735794	7789
WT12-25	middle Geertsen Canyon	41.33653	-111.732164	8367
WT12-26	upper Geertsen Canyon	41.51197	-111.673629	5894
WT12-28	Mutual Formation	41.32562	-111.731647	7271
WT12-29	lower Caddy Canyon	41.32023	-111.731886	6687
WT12-30	Terra Cotta	41.45941	-111.980347	8122
WT12-31	Mutual	41.45909	-111.978247	8049
WT12-32	lower Caddy Canyon	41.45961	-111.989198	7469
WT12-35	middle Water Canyon	41.65046	-112.045769	6000
WT12-37	Facer Gneiss	41.44115	-111.987314	5342
WT12-38	Swan Peak	41.54483	-111.956099	5836
WT12-40	Worm Creek	41.46410	-111.879316	7212
WT12-41	Worm Creek	41.46385	-111.831570	5725
WT12-43	Perry Canyon	41.25964	-111.830848	5008
WT12-45	Kelly Canyon	41.37237	-111.871479	5601
WT12-46	Lower Geertsen Canyon	41.39788	-111.919119	6535
WT12-47	Perry Canyon	41.42076	-112.013319	6511
WT12-49	Perry Canyon	41.24489	-112.244833	4272
EAB10-11	Perry Canyon	41.153867	-112.328107	1421
CAT-23	Geertsen Canyon	41.299	-112.483	1415
CD10-59	Geertsen Canyon	41.333	-111.692	2027
CD10-55	Maple Canyon	41.308384	-111.73021	1721
CAT-9	Worm Creek	41.454984	-111.457240	2453
CAT-15	Geertsen Canyon	41.347	-111.805	2082

Appendix B: (U-Th)/He Data

Sample Number	Unit/Pdepth (km)	Mean (Ma)	Std (Ma)	Age (Ma)	err., (Ma)	U (ppm)	Th (ppm)	Sm (ppm)	[U]e (ppm)	αDamage (α/g)	He (nmol/g)	Mass (µg)	Ft	ESR
Monte Cristo Transect														
NCAT-9	Worm	159.23	8.19											
2	Creek			148.1	11.8	48.7	25.5	6.0	54.6	3.53E+17	33.7	5.38	0.76	49.45
*15**	5.3			*194.2*	*15.54*	*149.0*	*69.2*	*2.7*	*164.9*	*1.14E+17*	*124.2*	*2.60*	*0.71*	*39.44*
21				161.1	12.89	89.1	56.3	1.4	102.0	2.30E+17	68.0	5.28	0.76	48.47
25				156.8	12.55	93.4	41.6	1.8	103.0	2.27E+17	69.6	7.25	0.79	55.84
31				170.9	13.67	225.8	25.0	0.8	231.6	8.42E+17	154.8	3.04	0.72	39.70
WT12-21	Beirdneau	159.58	15.21											
19	6			154.3	12.34	272.6	164.9	16.8	310.7	1.14E+18	201.7	5.86	0.77	51.58
*22**				*398.8*	*31.90*	*99.5*	*86.0*	*1.3*	*119.3*	*4.33E+17*	*199.1*	*5.12*	*0.75*	*48.09*
29				183.6	14.69	101.6	47.7	3.2	112.6	4.22E+17	91.4	9.35	0.81	61.96
32				158.6	12.69	107.5	57.8	2.1	120.8	4.65E+17	83.8	8.86	0.80	59.67
33				141.8	11.34	204.4	44.8	1.5	214.7	6.22E+17	131.3	6.98	0.79	55.87
*36**				*93.6*	*7.49*	*53.1*	*19.2*	*0.4*	*57.5*	*2.18E+17*	*21.2*	*2.97*	*0.72*	*41.57*
WT12-20	middle	193.28	39.74											
11	Geertsen			173.8	13.90	59.9	24.0	1.0	65.4	1.34E+17	48.9	6.93	0.79	55.15
13	Canyon			219.8	17.59	79.2	38.9	1.5	88.2	1.84E+17	85.1	10.64	0.80	59.32
29	6			140.2	11.22	35.9	23.7	1.4	41.3	1.12E+17	26.2	14.91	0.83	70.45
30				224.3	17.94	74.7	37.3	1.7	83.3	3.26E+17	84.6	15.32	0.82	68.46
31				153.3	12.26	61.9	46.4	1.8	72.6	2.52E+17	49.2	10.10	0.81	62.89
32				248.2	19.86	57.6	43.1	1.1	67.5	1.45E+17	77.8	19.18	0.84	77.29
WT12-19	Mutual	168.53	19.31											
11	7.1			157.7	12.62	170.9	43.1	1.2	180.8	3.71E+17	128.9	13.72	0.83	68.83
17				171.3	13.71	81.8	66.6	0.4	97.2	2.06E+17	75.4	14.43	0.83	70.41
*20**				*234.2*	*18.74*	*84.4*	*27.1*	*0.7*	*90.6*	*1.78E+17*	*91.9*	*7.38*	*0.79*	*55.44*
24				203.7	16.30	108.7	39.6	1.0	117.8	2.47E+17	103.6	7.22	0.79	55.37
25				163.0	13.04	170.0	68.9	0.7	185.9	4.68E+17	129.2	6.46	0.78	53.51
33				146.8	11.75	78.1	39.2	0.7	87.2	1.83E+17	56.0	9.26	0.80	59.99
WT12-18	Perry	166.21	10.90											

Appendix B: (U-Th)/He Data

Sample Number	Unit/Pdepth (km)	Mean (Ma)	Std (Ma)	Age (Ma)	err., (Ma)	U (ppm)	Th (ppm)	Sm (ppm)	[U]e (ppm)	αDamage (α/g)	He (nmol/g)	Mass (µg)	Ft	ESR
13	Canyon			176.6	14.13	59.4	34.2	1.3	67.2	1.51E+17	50.0	5.38	0.77	51.35
17	7.35			176.4	14.11	33.8	26.6	2.4	39.9	8.84E+16	30.2	7.05	0.78	55.11
20				149.7	11.98	92.0	34.1	0.9	99.8	2.09E+17	66.1	9.68	0.81	62.45
27				168.3	13.47	137.2	56.8	1.1	150.2	3.29E+17	111.9	9.48	0.81	62.24
35				173.2	13.85	97.4	48.4	1.3	108.6	2.34E+17	82.8	9.36	0.81	61.10
38				153.0	12.24	88.0	120.6	2.7	115.8	2.60E+17	75.0	6.41	0.77	53.39
WT12-17	Caddy	174.29	37.90											
17	Canyon			211.6	16.93	43.7	40.0	1.3	52.9	1.05E+17	45.5	4.78	0.74	45.67
22	7.45			181.8	14.54	22.2	21.6	1.5	27.1	5.32E+16	20.3	5.05	0.75	47.45
23				125.1	10.01	19.3	15.6	0.5	22.9	5.24E+16	11.7	4.21	0.75	47.15
28				143.3	11.47	71.9	29.8	1.4	78.8	1.72E+17	45.4	3.70	0.74	44.20
31				231.8	18.54	72.2	35.4	1.3	80.4	1.90E+17	79.0	5.43	0.77	51.66
33				152.2	12.17	26.5	25.5	0.8	32.4	7.53E+16	20.1	4.21	0.75	46.77
Bear River to Browns Hole Transect														
WT12-5	Water	121.03	25.45											
5	Canyon			112.9	9.03	43.5	47.2	0.9	54.4	2.13E+17	25.7	5.49	0.77	51.12
18	5			102.2	8.17	37.0	14.1	0.5	40.2	9.23E+16	17.1	5.64	0.77	49.99
*20**				*482.3*	*38.59*	*28.7*	*22.2*	*0.6*	*33.8*	*1.33E+17*	*67.3*	*4.09*	*0.74*	*45.03*
24				119.8	9.59	28.3	17.6	0.7	32.4	1.33E+17	16.1	5.11	0.76	49.53
28				169.9	13.59	49.2	22.8	0.5	54.5	2.06E+17	40.3	8.03	0.80	58.39
33				100.3	8.03	25.1	17.7	0.5	29.1	1.17E+17	11.9	4.41	0.75	47.27
WT12-6	Beirdneau	171.67	25.40											
*6**	5.8			*493.7*	*39.49*	*88.0*	*68.5*	*0.8*	*103.8*	*4.13E+17*	*211.1*	*4.13*	*0.74*	*44.67*
8				192.7	15.42	104.6	115.3	2.7	131.1	5.31E+17	98.3	3.27	0.71	40.57
22				153.7	12.30	155.3	78.7	1.1	173.4	6.96E+17	101.6	2.35	0.70	38.03
28				140.0	11.20	94.4	56.6	1.7	107.5	4.23E+17	61.8	4.40	0.75	47.50
*34**				*307.0*	*24.56*	*102.4*	*87.4*	*2.9*	*122.6*	*5.07E+17*	*143.3*	*2.45*	*0.69*	*37.50*
37				200.2	16.02	121.6	67.2	2.3	137.1	5.37E+17	105.3	2.36	0.70	38.44
WT12-3	Worm	126.83	4.69											

Appendix B: (U-Th)/He Data

Sample Number	Unit/Pdepth (km)	Mean (Ma)	Std (Ma)	Age (Ma)	err., (Ma)	U (ppm)	Th (ppm)	Sm (ppm)	[U]e (ppm)	αDamage (α/g)	He (nmol/g)	Mass (µg)	Ft	ESR
3	Creek			133.8	10.71	46.8	52.1	0.7	58.8	5.28E+16	31.2	3.70	0.73	43.25
6	6.5			125.3	10.02	42.0	28.1	1.1	48.4	4.17E+16	25.8	7.19	0.78	54.00
9				128.4	10.19	34.4	19.0	0.6	38.8	3.46E+16	20.6	5.41	0.77	50.12
*10**				*207.6*	*16.61*	*126.1*	*109.9*	*1.9*	*151.4*	*4.28E+17*	*118.2*	*2.26*	*0.69*	*36.91*
13				120.8	9.67	95.2	85.2	1.3	114.8	3.11E+17	53.6	2.82	0.71	40.00
WT12-26	Upper	112.44	7.58											
7	Geertsen			119.9	9.59	47.9	36.2	1.8	56.3	1.47E+17	29.0	7.62	0.79	56.83
9	Canyon			122.5	9.80	65.6	42.8	1.8	75.4	2.85E+17	37.9	4.87	0.75	47.65
*13**	7.7			*150.4*	*12.03*	*119.3*	*77.6*	*1.9*	*137.2*	*3.79E+17*	*89.4*	*7.68*	*0.79*	*57.90*
22				107.0	8.56	57.1	41.7	3.3	66.7	1.73E+17	29.9	6.75	0.77	51.15
25				110.0	8.80	48.6	27.3	1.3	54.9	2.04E+17	24.2	3.48	0.74	44.07
36				102.7	8.22	156.6	65.9	4.9	171.8	6.26E+17	70.7	3.46	0.74	44.03
WT12-25	middle	150.76	73.82											
2	Geertsen			125.2	10.02	146.5	146.0	3.8	180.1	6.78E+17	101.1	12.40	0.82	68.09
12	Canyon			179.1	14.33	212.8	77.9	1.9	230.8	8.98E+17	183.9	10.10	0.81	63.67
18	8.4			250.2	20.02	99.7	78.9	1.7	117.8	4.47E+17	140.5	35.69	0.86	90.77
*25**				*575.9*	*46.07*	*21.9*	*13.9*	*0.2*	*25.1*	*9.45E+16*	*71.4*	*35.80*	*0.87*	*94.71*
28				48.5	3.88	255.2	97.5	1.9	277.7	1.03E+18	60.4	13.65	0.83	69.04
*33**				*1422.1*	*113.77*	*22.7*	*15.2*	*0.5*	*26.2*	*9.82E+16*	*201.4*	*27.14*	*0.86*	*85.10*
WT12-24	Brownshole	105.62	2.88											
2	Member			108.1	8.65	140.2	103.0	2.0	163.9	3.40E+17	71.4	5.36	0.74	45.13
3	9			106.6	8.52	78.3	55.5	0.8	91.0	1.87E+17	42.9	11.46	0.81	64.05
4				108.9	10.28	146.3	85.8	1.0	166.0	3.46E+17	95.1	11.83	0.82	65.81
*5**				*128.5*	*8.71*	*63.1*	*79.6*	*1.5*	*81.4*	*1.09E+17*	*39.5*	*13.43*	*0.82*	*66.68*
6				101.6	8.12	139.6	52.4	0.6	151.7	3.17E+17	69.7	15.44	0.83	70.98
10				103.0	8.24	132.1	75.2	1.2	149.4	2.97E+17	65.7	7.30	0.78	55.09
WT12-28	Mutual	96.24	8.91											
*1**	Formation			*34.3*	*2.74*	*321.5*	*283.9*	*4.7*	*386.9*	*8.11E+17*	*56.7*	*8.53*	*0.79*	*56.63*
6	9.5			93.6	7.49	63.2	23.6	0.6	68.6	1.42E+17	28.4	11.90	0.81	64.05

Appendix B: (U-Th)/He Data

Sample Number	Unit/Pdepth (km)	Mean (Ma)	Std (Ma)	Age (Ma)	err., (Ma)	U (ppm)	Th (ppm)	Sm (ppm)	[U]e (ppm)	αDamage (α/g)	He (nmol/g)	Mass (µg)	Ft	ESR
18				90.3	7.22	31.9	20.9	1.6	36.8	7.94E+16	14.7	11.94	0.82	65.32
29				109.6	8.77	33.3	15.9	0.7	37.0	7.72E+16	18.6	18.34	0.84	75.23
30				102.9	8.23	248.7	144.0	1.0	281.8	6.59E+17	119.7	6.58	0.76	48.81
31				84.8	6.78	57.6	55.6	1.3	70.5	1.38E+17	27.4	20.85	0.84	78.45
WT12-29	Lower	94.77	3.37											
3	Caddy			92.0	7.36	101.3	30.1	1.1	108.2	2.20E+17	40.9	4.39	0.76	47.43
11	Canyon			97.8	7.82	55.1	34.3	1.4	63.0	1.33E+17	26.1	7.03	0.78	53.78
26	10			98.4	7.87	66.5	25.1	1.1	72.3	1.65E+17	29.9	5.61	0.77	51.66
*29**				*1094.8*	*87.58*	*75.2*	*23.5*	*1.2*	*80.6*	*1.66E+17*	*391.2*	*3.79*	*0.75*	*45.86*
32				90.9	7.27	36.7	26.5	2.7	42.8	8.89E+16	16.5	6.56	0.78	54.29
*35**				*121.3*	*9.71*	*99.9*	*57.7*	*2.2*	*113.2*	*2.48E+17*	*53.4*	*2.84*	*0.71*	*40.39*
CD10-55	Maple Canyon	70.90	0											
5	5			70.9	5.67	210.8	166.2	2.3	249.1	1.62E+18	76.1	7.38	0.79	57.72
Wellsville Transect														
WT12-35	Beirdneau	134.24	7.98											
*1**	6.3			*107.2*	*8.58*	*186.5*	*120.1*	*1.0*	*214.2*	*4.59E+17*	*96.9*	*6.09*	*0.78*	*52.78*
15				122.6	9.81	33.4	46.7	0.6	44.2	1.64E+17	22.4	4.80	0.76	49.35
16				135.5	10.84	60.2	49.1	0.5	71.5	4.42E+17	41.3	6.57	0.78	54.78
*26**				*173.5*	*13.88*	*59.9*	*37.1*	*0.4*	*68.5*	*2.73E+17*	*48.2*	*3.70*	*0.74*	*45.24*
30				145.0	11.60	59.2	43.0	0.6	69.1	4.30E+17	41.9	5.16	0.77	50.87
36				133.8	10.70	60.7	51.9	0.9	72.6	4.64E+17	36.6	2.32	0.69	37.36
WT12-38	Swan Peak	133.58	4.92											
6	7			128/.1	10.25	21.8	24.4	1.2	27.4	1.04E+17	13.2	2.21	0.69	37.81
13				132.2	10.57	59.9	20.8	0.3	64.7	2.49E+17	30.7	1.38	0.66	32.96
*16**				*109.2*	*8.73*	*73.2*	*74.0*	*1.1*	*90.2*	*3.32E+17*	*35.2*	*1.55*	*0.66*	*33.41*
19				135.9	10.87	82.9	14.5	0.4	86.2	3.46E+17	45.8	2.69	0.72	40.20
25				141.9	11.35	111.0	64.3	1.4	125.8	3.83E+17	72.9	4.02	0.75	46.54
27				129.8	10.39	142.5	68.7	0.8	158.3	6.26E+17	72.8	1.42	0.65	32.16

Appendix B: (U-Th)/He Data

Sample Number	Unit/Pdepth (km)	Mean (Ma)	Std (Ma)	Age (Ma)	err., (Ma)	U (ppm)	Th (ppm)	Sm (ppm)	[U]e (ppm)	αDamage (α/g)	He (nmol/g)	Mass (µg)	Ft	ESR
WT12-16	Upper	109.46	9.40											
9	Geertsen			98.4	7.87	63.2	54.7	5.1	75.8	1.58E+17	31.4	7.16	0.77	52.94
*10**	Canyon			*155.0*	*12.40*	*69.9*	*81.1*	*1.2*	*88.6*	*2.33E+17*	*55.9*	*4.40*	*0.74*	*46.64*
14	9.1			121.5	9.72	88.9	489.2	5.2	201.5	4.18E+17	108.3	11.86	0.80	63.83
22				102.5	8.20	106.8	156.1	3.5	142.7	2.98E+17	64.6	11.14	0.81	64.05
33				115.4	9.24	42.4	52.2	1.1	54.4	9.97E+16	25.9	4.85	0.75	48.76
*34**				*83.0*	*6.64*	*75.1*	*61.1*	*0.5*	*89.2*	*2.22E+17*	*29.7*	*4.00*	*0.74*	*45.00*
WT12-15	Middle	115.05	37.51											
5	Geertsen			110.5	8.84	189.3	67.9	18.8	205.0	4.37E+17	93.2	5.47	0.76	47.60
12	Canyon			76.1	6.09	139.0	182.5	22.6	181.2	1.77E+17	55.2	3.94	0.73	44.94
15	9.6			176.4	14.11	41.9	20.4	1.3	46.6	9.69E+16	34.3	5.18	0.76	49.56
24				97.1	7.77	116.2	79.4	3.9	134.5	2.93E+17	58.0	10.87	0.82	65.19
WT12-30	Terra	97.03	5.78											
6	Cotta			89.9	7.19	29.8	17.8	0.4	33.9	9.75E+16	13.1	8.15	0.79	56.73
8	10			106.1	8.49	195.6	114.6	1.0	222.0	6.64E+17	101.2	7.14	0.79	56.28
11				91.4	7.31	225.4	83.0	1.0	244.5	9.30E+17	97.0	8.40	0.80	58.79
26				102.2	8.17	55.9	47.3	0.8	66.8	1.60E+17	30.2	11.21	0.81	64.53
27				98.0	7.84	82.1	69.5	2.2	98.1	1.32E+17	43.9	17.14	0.84	75.51
30				94.6	7.57	78.8	62.0	1.1	93.1	2.60E+17	36.9	5.44	0.77	51.76
WT12-31	Mutual	86.98	9.11											
12	Formation			89.9	7.19	86.7	55.3	1.7	99.4	2.07E+17	36.1	4.40	0.74	45.62
13	10.6			103.2	8.26	130.4	178.9	38.2	171.8	3.68E+17	70.7	3.88	0.73	44.23
*21**				*151.7*	*12.13*	*60.0*	*27.1*	*1.0*	*66.3*	*1.46E+17*	*42.5*	*6.68*	*0.78*	*52.36*
25				79.0	6.24	85.0	63.9	1.0	99.7	2.02E+17	30.8	3.29	0.73	42.98
32				89.5	6.68	212.4	86.1	2.6	232.2	4.80E+17	78.9	4.61	0.75	46.47
37				79.9	6.39	62.1	57.4	1.3	75.4	1.78E+17	24.2	3.80	0.74	45.30
WT12-32	Lower	94.49	10.16											
*5**	Caddy			*8.4*	*0.68*	*374.0*	*467.4*	*1.8*	*481.6*	*9.39E+17*	*15.8*	*3.10*	*0.72*	*41.83*

Appendix B: (U-Th)/He Data

Sample Number	Unit/Pdepth (km)	Mean (Ma)	Std (Ma)	Age (Ma)	err., (Ma)	U (ppm)	Th (ppm)	Sm (ppm)	[U]e (ppm)	αDamage (α/g)	He (nmol/g)	Mass (µg)	Ft	ESR
6	Canyon			84.2	6.73	49.6	34.3	0.9	57.5	1.26E+17	19.6	4.32	0.75	46.19
14	11.4			96.2	7.70	60.9	57.3	2.2	74.1	2.18E+17	26.4	2.66	0.68	36.11
27				110.3	8.83	138.9	65.8	2.6	154.1	3.27E+17	66.4	3.40	0.72	40.93
*28**				*63.0*	*5.04*	*86.7*	*45.4*	*1.5*	*97.2*	*2.46E+17*	*24.2*	*3.22*	*0.73*	*42.77*
41				87.2	6.98	82.1	35.4	1.0	90.2	2.45E+17	31.3	3.88	0.73	43.43
WT12-37	Facer	62.84	3.15											
	Gneiss	95.16	4.50											
2	13.5			60.3	4.82	163.6	51.1	2.2	175.4	9.08E+17	41.9	3.25	0.73	42.74
8				67.3	5.38	315.2	155.8	3.0	351.1	1.94E+18	98.1	6.45	0.77	49.97
9				91.7	7.34	153.2	78.7	6.1	171.4	6.66E+17	62.3	3.48	0.73	42.89
13				61.0	4.88	243.9	88.6	1.6	264.3	1.46E+18	62.6	2.85	0.72	40.43
41				92.3	7.38	161.2	45.7	1.1	171.7	9.65E+17	60.0	2.39	0.70	37.34
42				101.5	8.12	107.3	44.5	1.1	117.5	6.44E+17	46.8	2.81	0.72	41.40
Perry Canyon Traverse														
EAB10-11	Perry	67.81	4.57											
3	Canyon			72.0	5.76	43.4	25.8	0.8	49.3	6.79E+17	14.1	3.50	0.73	43.85
9	-1			75.4	6.03	55.6	53.0	2.0	67.8	3.04E+17	21.4	7.51	0.77	52.23
14				62.4	4.99	114.2	29.5	1.0	121.0	8.05E+16	31.5	5.28	0.77	50.66
17				65.9	5.27	64.4	48.9	2.5	75.7	3.41E+17	20.9	6.57	0.77	51.71
25				67.6	5.41	38.2	17.0	0.4	42.2	7.33E+16	12.2	7.44	0.79	55.70
30				63.6	5.09	110.3	64.0	1.4	125.0	2.56E+17	30.1	2.64	0.70	37.81
WT12-49	Perry	67.19	4.31											
7	Canyon			74.8	5.99	98.6	37.1	1.8	107.2	1.01E+17	33.8	5.88	0.78	52.50
16	7			66.7	5.33	103.8	30.7	0.6	110.8	1.45E+17	32.2	9.18	0.80	59.65
17				64.2	5.13	84.9	26.0	1.0	90.9	2.85E+17	24.9	7.63	0.79	55.25
30				63.2	5.05	100.8	17.1	0.7	104.7	1.77E+17	26.6	4.17	0.74	44.16
24				70.9	5.67	79.0	68.5	1.0	94.8	9.74E+16	28.9	8.05	0.79	57.43
34				63.4	5.07	62.2	27.3	1.0	68.5	2.75E+17	17.7	4.50	0.75	46.83
WT12-47	Perry	24.00	5.87											

Appendix B: (U-Th)/He Data

Sample Number	Unit/Pdepth (km)	Mean (Ma)	Std (Ma)	Age (Ma)	err., (Ma)	U (ppm)	Th (ppm)	Sm (ppm)	[U]e (ppm)	αDamage (α/g)	He (nmol/g)	Mass (µg)	Ft	ESR
4	Canyon			22.5	1.80	223.1	66.7	0.8	238.4	4.91E+17	23.1	7.50	0.80	57.31
5	24			17.7	1.42	79.5	29.7	1.0	86.4	1.82E+17	6.7	10.20	0.81	63.00
8				22.5	1.80	65.2	26.3	0.6	71.3	1.42E+17	7.0	10.30	0.81	60.95
10				17.7	1.41	118.6	26.8	0.5	124.8	2.03E+17	9.4	7.36	0.79	56.02
14				31.5	2.52	66.7	49.1	2.1	78.0	1.47E+17	10.5	8.37	0.79	56.64
16				32.1	2.57	60.3	31.4	1.2	67.6	1.65E+17	9.3	9.92	0.80	58.01
WT12-43	Perry	66.15	16.97											
5	Canyon			82.2	6.58	393.3	335.8	4.1	470.6	2.86E+18	146.7	2.63	0.70	38.39
15	33			76.6	5.89	77.3	78.0	1.3	95.3	5.36E+17	26.3	2.38	0.69	37.63
26				42.7	3.41	273.1	302.3	6.4	342.7	2.06E+18	56.0	2.56	0.70	39.81
Geertsen Canyon Traverse														
CAT-23	Geertsen	87.47	8.88											
6	Canyon			95.7	7.66	90.0	45.0	0.9	100.4	3.94E+17	42.3	9.98	0.81	62.85
*7**	-3			*142.1*	*11.37*	*66.7*	*24.7*	*1.3*	*72.4*	*2.21E+17*	*38.9*	*2.53*	*0.70*	*37.26*
8				97.3	7.79	349.6	163.8	2.2	387.4	1.43E+18	154.4	4.46	0.75	47.37
16				77.0	6.16	154.1	93.4	1.0	175.6	7.32E+17	56.1	5.55	0.76	50.06
17				90.4	7.23	240.7	88.1	0.6	260.9	1.60E+18	91.6	2.74	0.72	40.23
22				76.9	6.15	205.3	132.0	1.2	235.7	9.51E+17	77.8	7.79	0.79	56.82
WT12-30	Terra	97.03	5.78											
6	Cotta			89.9	7.19	29.8	17.8	0.4	33.9	9.75E+16	13.1	8.15	0.79	56.73
8	14			106.1	8.49	195.6	114.6	1.0	222.0	6.64E+17	101.2	7.14	0.79	56.28
11				91.4	7.31	225.4	83.0	1.0	244.5	9.30E+17	97.0	8.40	0.80	58.79
26				102.2	8.17	55.9	47.3	0.8	66.8	1.60E+17	30.2	11.21	0.81	64.53
27				98.0	7.84	82.1	69.5	2.2	98.1	1.32E+17	43.9	17.14	0.84	75.51
30				94.6	7.57	78.8	62.0	1.1	93.1	2.60E+17	36.9	5.44	0.77	51.76
WT12-46	Lower	111.72	12.25											
2	Geertsen			101.4	8.11	230.8	139.5	2.6	263.0	9.92E+17	111.2	6.14	0.77	50.51
5	Canyon			129.0	10.32	163.2	110.0	5.5	188.6	7.02E+17	103.4	7.07	0.78	53.89
6	18			122.5	9.80	103.4	141.1	8.5	136.0	5.15E+17	67.4	4.66	0.74	46.19

Appendix B: (U-Th)/He Data

Sample Number	Unit/Pdepth (km)	Mean (Ma)	Std (Ma)	Age (Ma)	err., (Ma)	U (ppm)	Th (ppm)	Sm (ppm)	[U]e (ppm)	αDamage (α/g)	He (nmol/g)	Mass (µg)	Ft	ESR
10				111.4	8.91	284.7	85.7	1.5	304.4	1.18E+18	140.1	5.14	0.76	48.31
21				92.3	7.39	243.0	165.1	4.3	281.1	1.07E+18	112.6	9.08	0.80	59.06
29				113.8	9.10	249.7	101.5	1.3	273.0	5.41E+17	135.6	8.96	0.80	59.74
CAT-15	Geertsen	120.72	2.73											
13	Canyon			122.6	9.81	44.3	21.4	0.97	49.3	6.04E+17	26.8	12.94	0.8	64.3
31	27			118.8	9.50	43.1	38.3	0.79	51.9	6.73E+17	27.5	12.51	0.8	66.8
WT12-24	37	105.62	8.92											
2				108.1	8.65	140.2	103.0	2.0	163.9	3.40E+17	71.4	5.36	0.74	45.13
3				106.6	8.52	78.3	55.5	0.8	91.0	1.87E+17	42.9	11.46	0.81	64.05
4				108.9	10.28	146.3	85.8	1.0	166.0	3.46E+17	95.1	11.83	0.82	65.81
*5**				*128.5*	*8.71*	*63.1*	*79.6*	*1.5*	*81.4*	*1.09E+17*	*39.5*	*13.43*	*0.82*	*66.68*
6				101.6	8.12	139.6	52.4	0.6	151.7	3.17E+17	69.7	15.44	0.83	70.98
10				103.0	8.24	132.1	75.2	1.2	149.4	2.97E+17	65.7	7.30	0.78	55.09
CD10-59	Brownshole	119.43	18.13											
3	Member			123.3	9.87	96.0	60.6	1.2	109.9	2.59E+17	59.9	10.18	0.81	63.46
5	41			136.7	10.93	45.5	45.6	0.4	56.0	1.55E+17	34.9	16.92	0.83	74.19
7				93.5	7.48	38.2	25.2	0.6	44.0	1.26E+17	17.2	5.77	0.77	51.24
*11**				*54.9*	*4.40*	*108.5*	*75.1*	*1.2*	*125.8*	*3.21E+17*	*29.5*	*7.20*	*0.79*	*55.59*
17				139.8	11.19	59.0	41.5	0.6	68.6	1.33E+17	41.7	8.34	0.80	58.98
24				103.9	8.31	53.9	48.9	1.2	65.1	1.40E+17	28.9	8.89	0.78	55.66
WT12-19	Geertsen	179.47	30.17											
11	Canyon			157.7	12.62	170.9	43.1	1.2	180.8	3.71E+17	128.9	13.72	0.83	68.83
17	63			171.3	13.71	81.8	66.6	0.4	97.2	2.06E+17	75.4	14.43	0.83	70.41
*20**				*234.2*	*18.74*	*84.4*	*27.1*	*0.7*	*90.6*	*1.78E+17*	*91.9*	*7.38*	*0.79*	*55.44*
*24**				*203.7*	*16.30*	*108.7*	*39.6*	*1.0*	*117.8*	*2.47E+17*	*103.6*	*7.22*	*0.79*	*55.37*
25				163.0	13.04	170.0	68.9	0.7	185.9	4.68E+17	129.2	6.46	0.78	53.51
33				146.8	11.75	78.1	39.2	0.7	87.2	1.83E+17	56.0	9.26	0.80	59.99

Swan Peak Traverse

Appendix B: (U-Th)/He Data

Sample Number	Unit/Pdepth (km)	Mean (Ma)	Std (Ma)	Age (Ma)	err., (Ma)	U (ppm)	Th (ppm)	Sm (ppm)	[U]e (ppm)	αDamage (α/g)	He (nmol/g)	Mass (µg)	Ft	ESR
WT12-40	Swan Peak	111.27	13.69											
4	22			121.3	9.70	37.4	60.8	1.0	51.4	4.58E+16	25.2	4.40	0.74	46.01
6				99.2	7.94	23.3	14.6	0.4	26.6	2.46E+16	11.4	7.49	0.79	57.59
9				100.4	8.04	30.2	36.3	0.7	38.6	3.53E+16	15.9	4.86	0.75	47.93
11				101.2	8.10	25.1	18.9	0.5	29.4	2.65E+16	12.2	4.44	0.75	47.99
14				136.8	10.95	36.1	21.4	0.8	41.1	3.72E+16	24.1	7.67	0.79	55.54
15				108.6	8.69	34.2	39.5	0.6	43.3	3.73E+16	19.2	4.60	0.75	47.65
WT12-41	Swan Peak	149.41	17.52											
1	26			167.5	13.40	44.9	32.5	0.6	52.4	4.54E+16	36.4	4.65	0.76	49.06
*2**				*82.9*	*6.64*	*153.9*	*54.6*	*0.7*	*166.5*	*1.47E+17*	*53.4*	*2.84*	*0.71*	*39.76*
6				137.8	11.02	46.1	57.8	2.7	59.5	5.20E+16	32.5	3.56	0.73	43.39
12				165.5	13.24	60.6	48.1	1.3	71.6	6.36E+16	47.5	3.97	0.73	44.17
14				129.9	10.15	33.4	27.9	0.8	39.8	3.74E+16	19.4	2.72	0.70	39.20
WT12-3	Swan Peak	126.83	4.69											
3	36			133.8	10.71	46.8	52.1	0.7	58.8	6.14E+16	31.2	3.70	0.73	43.25
6				125.3	10.02	42.0	28.1	1.1	48.4	5.85E+16	25.8	7.19	0.78	54.00
9				127.4	10.19	34.4	19.0	0.6	38.8	6.75E+16	20.6	5.41	0.77	50.12
*10**				*207.6*	*16.61*	*126.1*	*109.9*	*1.9*	*151.4*	*2.80E+17*	*118.2*	*2.26*	*0.69*	*36.91*
13				120.8	9.67	95.2	85.2	1.3	114.8	5.78E+17	53.6	2.82	0.71	40.00
NCat-9	Swan Peak	166.23	15.79											
2	57			148.1	11.85	48.7	25.5	6.0	54.6	3.53E+17	33.7	5.38	0.76	49.45
15				194.2	15.54	149.0	69.2	2.7	164.9	1.14E+17	124.2	2.60	0.71	39.44
21				161.1	12.89	89.1	56.3	1.4	102.0	2.30E+17	68.0	5.28	0.76	48.47
25				156.8	12.55	93.4	41.6	1.8	103.0	2.27E+17	69.6	7.25	0.79	55.84
31				170.9	13.67	225.8	25.0	0.8	231.6	8.42E+17	154.8	3.04	0.72	39.70
Footwall														
WT12-8	Tintic	14.68	8.14											
5	14.4			8.3	0.66	291.8	210.7	4.5	340.3	1.28E+18	11.9	6.64	0.78	54.66
15				7.0	0.56	404.3	355.4	4.8	486.2	1.78E+18	14.0	5.02	0.76	48.62

Appendix B: (U-Th)/He Data

Sample Number	Unit/Pdepth (km)	Mean (Ma)	Std (Ma)	Age (Ma)	err., (Ma)	U (ppm)	Th (ppm)	Sm (ppm)	[U]e (ppm)	αDamage (α/g)	He (nmol/g)	Mass (µg)	Ft	ESR
17				6.9	0.55	402.3	468.0	18.6	510.2	1.91E+18	14.5	5.51	0.76	49.50
23				16.0	1.28	161.3	224.5	3.2	213.0	8.11E+17	14.6	8.11	0.79	57.72
28				21.4	1.71	215.8	264.0	6.6	276.6	1.04E+18	24.4	5.28	0.76	50.44
32				28.5	2.28	187.1	201.3	5.2	233.4	8.70E+17	28.6	8.75	0.79	58.32
WT12-10	Farmington	6.36	1.68											
1	Canyon			5.4	0.43	441.4	176.5	1.9	482.0	N/A	11.3	7.76	0.80	58.65
2	14.8			5.7	0.45	13.6	2.7	15.2	14.3	N/A	0.3	4.87	0.77	49.40
3				5.3	0.43	7.9	2.3	9.3	8.5	N/A	0.2	4.77	0.77	49.93
4				9.7	0.78	6.2	1.7	9.2	6.6	N/A	0.3	3.30	0.74	43.41
5				5.7	0.45	6.5	1.5	10.2	6.9	N/A	0.2	9.86	0.81	61.99
*6**				*107.5*	*8.60*	*254.3*	*112.6*	*6.8*	*280.2*	*N/A*	*113.8*	*2.12*	*0.70*	*37.42*
WT12-9	Farmington	4.68	1.03											
1	Canyon			5.5	0.44	5.7	1.3	10.8	6.1	N/A	0.1	4.07	0.75	46.87
2	15			5.4	0.43	395.1	35.5	0.5	403.3	N/A	7.9	1.92	0.68	34.17
3				2.7	0.22	10.1	2.7	9.7	10.7	N/A	0.1	5.98	0.77	51.63
4				5.2	0.42	279.1	18.1	1.3	283.2	N/A	6.1	4.30	0.76	47.39
5				3.9	0.31	370.5	17.5	0.5	374.6	N/A	5.5	2.23	0.70	37.30
6				5.4	0.43	20.5	1.4	7.8	20.8	N/A	0.5	3.59	0.74	43.69
WT12-11	Farmington	5.53	2.23											
1	Canyon			7.0	0.56	85.8	26.5	75.4	92.3	3.09E+17	2.8	6.90	0.79	55.48
14	15.2			3.6	0.29	8.8	2.2	15.1	9.4	3.89E+16	0.1	5.84	0.78	52.80
19				4.6	0.36	370.3	103.8	1.1	394.2	1.63E+18	6.8	2.24	0.70	37.25
25				3.4	0.27	7.6	1.7	10.1	8.1	2.92E+16	0.1	5.50	0.78	52.51
26				9.2	0.73	61.7	23.7	61.1	67.5	2.68E+17	2.8	12.71	0.83	69.09
WT12-12	Farmington	4.88	0.26											
1	Canyon			5.0	0.40	499.0	17.5	1.4	503.0	N/A	9.0	1.47	0.66	32.10
2	15.4			4.5	0.36	340.7	11.3	1.0	343.3	N/A	6.0	2.69	0.73	40.73
3				5.0	0.40	387.1	76.2	0.8	404.7	N/A	7.8	2.90	0.72	39.96
4				4.6	0.37	401.5	10.6	0.8	403.9	N/A	7.1	2.11	0.70	36.91

Appendix B: (U-Th)/He Data

Sample Number	Unit/Pdepth (km)	Mean (Ma)	Std (Ma)	Age (Ma)	err., (Ma)	U (ppm)	Th (ppm)	Sm (ppm)	[U]e (ppm)	αDamage (α/g)	He (nmol/g)	Mass (µg)	Ft	ESR
5				4.9	0.39	1061.3	11.2	0.4	1063.9	N/A	18.7	1.71	0.67	32.82
6				5.3	0.42	513.7	14.2	0.3	517.0	N/A	10.3	1.97	0.69	36.10

*Analysis from grains excluded

Note: Latitude and Longitude for samples are listed in Appendix A

Appendix C: U/Pb Data

Sample	206/207 (Ma)	2σ (Ma)	207/235 (Ma)	2σ (Ma)	208/232 (Ma)	2σ (Ma)	U (ppm)	Th (ppm)	207/206 (Ma)	2σ (Ma)	Disc. (%)
WT12-3-1	1603	13	1647.8	6.8	1589	24	106.6	93.9	1702.6	8.7	3.09
WT12-3-2	1619	16	1661.9	7.9	1640	13	174.6	126	1713.5	8.9	3.2
WT12-3-3	482	6.9	487	6.5	509	13	59.4	38.5	519	24	3.81
WT12-3-4	1646	14	1673.5	6.3	1624	10	288	105.6	1711.6	5.9	2.5
WT12-3-5	1603	24	1651	13	2017	48	214	43.2	1710	13	4.4
WT12-3-6	462.5	5.5	473.3	5.8	487	10	56.9	48.2	509	22	2.76
WT12-3-7	1668	17	1688.4	8.6	1658	25	198	42.4	1712.9	9.1	2.25
WT12-3-8	478.5	6.3	477.6	5.8	475.9	9.1	64.2	50.1	493	25	3.16
WT12-3-9	1391	13	1404.6	7.6	1381	13	64.6	156	1427.9	9.9	2
WT12-3-10	1696	13	1684.5	5.4	1671	31	99.6	32	1679	7.3	2.09
WT12-3-11	1675	12	1697.5	5.2	1642	17	276	57.4	1725.3	5.3	2
WT12-3-12	1340	11	1349.4	7.3	1338	10	147	300	1367	10	1.94
WT12-3-13	453.1	6.5	470	10	484	13	24.6	27.9	564	31	5.14
WT12-3-14	1646	20	1657	10	1693	21	71.5	64.6	1671.7	9.1	2.83
WT12-3-15	1684	17	1689.8	8.4	1714	18	135	90.4	1692.3	7	2.37
WT12-3-16	1722	13	1704.7	7.2	1703	18	172	100	1696.4	7.8	2.37
WT12-3-17	1018	19	1034.9	9.9	980	13	140	100.5	1063	21	4.06
WT12-3-18	1403	27	1436	15	1378	19	80.3	61.3	1482	23	4.89
WT12-3-19	993	11	1005.7	7.3	980	11	246	119	1041	8.9	2.07
WT12-3-20	1722	27	1733	13	1641	14	116.5	92.6	1756	18	4.15
WT12-3-21	1032.9	8.5	1040.7	6.3	1013	13	92	74	1068	12	2.16
WT12-3-22	1099	9.1	1091.7	6.4	1034	13	131.3	102.6	1085.2	8.6	1.78
WT12-3-23	1009.2	7	1016.3	5	986	15	139.9	55.6	1041.6	7.1	1.55
WT12-3-24	1070.2	8.8	1064.9	5.7	1054.2	9.8	294	192.3	1065.4	6.8	1.49
WT12-3-25	2418	34	2612	15	2273	82	97.7	129	2780	17	11
WT12-3-26	1747	12	1753.1	4.8	1669	14	249	269.1	1764.2	4.3	1.9
WT12-3-27	1372	18	1373	11	1327	18	217	159	1379	12	2.49

Appendix C: U/Pb Data

Sample	206/207 (Ma)	2σ (Ma)	207/235 (Ma)	2σ (Ma)	208/232 (Ma)	2σ (Ma)	U (ppm)	Th (ppm)	207/206 (Ma)	2σ (Ma)	Disc. (%)
WT12-3-28	1054.8	9	1063	7	1094	17	53	33.8	1085	14	2.42
WT12-3-29	1093	12	1087.2	7.4	1097	14	109.4	65.6	1088.8	9.5	2.32
WT12-3-30	1048	16	1071	12	1045	27	77.9	50	1120	12	3.24
WT12-3-31	1023.4	7.6	1025.6	5.4	1041	17	122.3	56.6	1020.2	8.1	1.78
WT12-3-32	1015	12	1036	10	1080	22	108	55.3	1087	14	2.81
WT12-3-33	1347	11	1351.5	6.6	1379	13	96.1	64	1361.2	8.5	2.25
WT12-3-34	1400	12	1385.9	7.4	1347	24	98.3	74.5	1367.7	8.2	2.3
WT12-3-35	1086.7	7.6	1085.2	6.5	1070	15	106.7	55.1	1076	11	2
WT12-3-36	1096	10	1096.3	6.2	1089	10	283	140.9	1103.3	7.1	1.73
WT12-3-37	1095	17	1096	11	1158	21	77.8	39.8	1118	18	3.24
WT12-3-38	1038.4	9.6	1040.1	6.7	1085	14	98	53	1044.2	9.3	2.01
WT12-3-39	1351	11	1342.5	6	1352	15	74.3	88.4	1344	10	2.35
WT12-3-40	1399	14	1399.2	8.2	1402	19	74.3	95.5	1402	11	2.49
WT12-3-41	1034	9.8	1038.9	7	828	30	56	30.6	1055	11	2.37
WT12-3-42	1207	11	1209.9	6.2	1220	12	170	137.8	1215	8	1.94
WT12-3-43	2673	27	2675	11	2804	38	47.3	32.2	2679	7.4	3.8
WT12-3-44	1104	11	1108.8	6.7	1094	12	111.8	108.5	1121	10	2.18
WT12-3-45	1187	12	1202.1	8.9	1198	20	23.61	29.95	1234	16	2.95
WT12-3-46	1256.1	9.9	1252.3	6.9	1269	24	97	41.72	1246	11	2.25
WT12-3-47	1506	16	1530.9	9.6	1617	13	178	196	1565	11	2.76
WT12-3-48	1048.6	8.3	1040.8	7	1029	17	72.1	48.8	1030	14	2.15
WT12-3-49	1216	13	1198.8	8.3	1232	12	95	151	1174	12	2.63
WT12-3-50	1296	14	1326	10	1160	52	297	391	1381.6	7.1	2.39
WT12-3-51	1077.8	8.7	1087.3	7	1034	12	166	192	1108.6	9.8	1.92
WT12-3-52	1754	26	1779	15	1363	98	124	91	1809	8.9	3.16
WT12-3-53	1187.5	9.4	1185.5	5.7	1180	12	94.9	138.1	1181.4	9.1	1.67
WT12-3-54	1338	11	1343.7	7.7	1349	18	88	61	1342	11	2.22

Appendix C: U/Pb Data

Sample	206/207 (Ma)	2σ (Ma)	207/235 (Ma)	2σ (Ma)	208/232 (Ma)	2σ (Ma)	U (ppm)	Th (ppm)	207/206 (Ma)	2σ (Ma)	Disc. (%)
WT12-5-1	1511	13	1469	7.7	1446	27	55.4	28	1417	11	2.68
WT12-5-2	2714	34	2779	15	2622	39	110.2	88.3	2824.4	6.6	4.42
WT12-5-3	1959	12	1940	5.8	1911	19	113.4	83.7	1918.2	7.2	2.35
WT12-5-4	1167	10	1179	10	1220	22	62.5	37.1	1212	16	2.44
WT12-5-5	1842	16	1842.4	9.5	1835	28	46.8	76.8	1830.3	9.4	2.6
WT12-5-6	1553	28	1668	15	1513	23	52.5	57.4	1815	10	7.2
WT12-5-7	1772	18	1806	11	1768	21	64.9	54.2	1837	11	3.07
WT12-5-8	1821	16	1849.4	6.9	1877	21	79.4	57.8	1872.8	8	2.38
WT12-5-9	1940	15	1934.8	8.4	1933	17	46.4	152	1926.2	9.3	2.93
WT12-5-10	1855	18	1853.1	8.9	1840	27	28.65	63.8	1852	11	2.58
WT12-5-11	1399	15	1395	11	1369	30	45.9	39.9	1384	13	2.95
WT12-5-12	1838	22	1860	15	1884	40	21.5	19.3	1895	14	3.93
WT12-5-13	1762	14	1734.9	8.1	1728	23	157	97	1697.4	6.1	2.29
WT12-5-14	1973	15	1954.4	6.6	1951	18	66.7	64.5	1931.3	8	2.75
WT12-5-15	2098	20	2103	11	2073	35	20.49	23.56	2108	11	3.22
WT12-5-16	1882	16	1846.1	8.7	1860	22	43.2	54.6	1820.3	9.7	2.35
WT12-5-17	1851	12	1841	7.4	1838	22	75.6	63.5	1824	7.3	2.29
WT12-5-18	1150	14	1152	11	1160	33	25.3	8.93	1162	19	3.73
WT12-5-19	2898	25	2855	11	2954	39	31.25	65.39	2821.7	8	4.3
WT12-5-20	1835	20	1833	11	1873	30	31.3	36.2	1820	12	3.21
WT12-5-21	2476	31	2565	12	2486	45	37.6	31.7	2639.1	8	5.6
WT12-5-22	1975	14	1979.1	7.7	2066	56	133.7	15.1	1977.8	8.2	2.06
WT12-5-23	1436.2	8.7	1442	6	1379	33	109.5	26.2	1443.3	8.7	1.91
WT12-5-24	1899	17	1899	10	1921	30	16.52	22.22	1901	12	3.55
WT12-5-25	1893	14	1873.3	8.4	1869	20	34.2	78.6	1844.7	9.2	2.49
WT12-5-26	2688	23	2674	8.5	2683	25	46.5	90.9	2659.6	4.8	3.39
WT12-5-27	1824	33	1817	16	1905	21	181	75	1815	10	3.85
WT12-5-28	1772	15	1775.2	6.9	1642	36	62.9	45.3	1775.4	7.6	2.4

Appendix C: U/Pb Data

Sample	206/207 (Ma)	2σ (Ma)	207/235 (Ma)	2σ (Ma)	208/232 (Ma)	2σ (Ma)	U (ppm)	Th (ppm)	207/206 (Ma)	2σ (Ma)	Disc. (%)
WT12-5-29	1910	14	1877.2	7.5	1910	30	90.3	51.4	1836.9	6.6	2.43
WT12-5-30	1436	11	1439.4	7.3	1423	16	91.3	72.8	1444	10	2.07
WT12-5-31	2072	17	2079.2	7.3	2087	23	66.5	94.4	2076.1	7	2.35
WT12-5-32	1508	10	1487.6	8.2	1503	17	102.3	84.3	1456	11	2.17
WT12-5-33	1864	16	1854	11	1869	29	25.8	33.9	1856	12	2.81
WT12-5-34	1865	18	1853.4	9.5	1925	20	84	73.4	1848	8.1	2.9
WT12-5-35	1433	11	1430.2	7	1446	15	77	85.9	1429	11	2.33
WT12-5-36	2621	30	2645	13	2673	42	14.58	21.03	2687	11	4.75
WT12-5-37	2186	30	2137	15	2269	38	43.1	86.1	2068	11	3.99
WT12-5-38	2564	16	2563.3	6.6	2564	23	121	84.1	2556.4	5.9	2.22
WT12-5-39	1927	15	1894.1	6.4	1899	20	89.7	62.9	1861.5	7.8	2.75
WT12-5-40	2660	22	2604	10	2659	28	50	75.8	2554.7	7	3.91
WT12-6-12	1842	16	1833.9	8.3	1684	26	40.8	59.7	1825	12	2.6
WT12-6-22	1665	15	1674.1	8.3	1550	29	64.2	48.5	1691.1	8.4	2.51
WT12-6-42	2073	22	2075	12	1957	25	25.1	86.7	2068	14	3.2
WT12-6-52	1855	20	1847	10	1758	30	73.9	73.7	1845.4	8.7	2.38
WT12-6-62	1808	12	1812.4	6.7	1656	17	132.3	208.1	1821.9	6.5	1.97
WT12-6-72	1974	21	1958	13	1895	38	48	83.2	1931	13	3.32
WT12-6-82	1894	16	1892.1	6.6	1740	21	66.3	140.2	1904.1	9.8	2.84
WT12-6-102	1892	24	1871	15	1850	26	47.9	145.5	1850	16	3.35
WT12-6-112	1818	23	1830.9	9.8	1734	29	100.3	120.6	1853	11	2.89
WT12-6-122	1889	21	1909	11	1861	27	31.4	84.3	1926	15	3.44
WT12-6-132	2213	40	2264	17	1739	88	61	64.2	2320.5	8.9	5.65
WT12-6-142	1783	15	1808.3	7.8	1717	30	62.6	24.4	1844	10	2.72
WT12-6-152	2474	37	2524	16	2389	40	59.8	141.7	2573.3	9.5	4.39
WT12-6-162	2060	27	2061	10	1926	28	48	72	2061.3	9.2	3.44
WT12-6-172	1755	25	1800	13	1639	28	28	43.9	1847	16	4.73

Appendix C: U/Pb Data

Sample	206/207 (Ma)	2σ (Ma)	207/235 (Ma)	2σ (Ma)	208/232 (Ma)	2σ (Ma)	U (ppm)	Th (ppm)	207/206 (Ma)	2σ (Ma)	Disc. (%)
WT12-6-182	2035	18	2042	8.1	1960	24	105.4	236.5	2051.3	7.1	2.55
WT12-6-212	2047	17	2067.2	7.9	1911	28	75.6	76.3	2083.9	8	2.29
WT12-6-222	1861	14	1850.8	6.3	1875	21	163.1	108	1840.6	7.3	2.53
WT12-6-202	1802	19	1816.7	7.6	1752	27	79.7	114	1841	11	3.63
WT12-6-232	1845	13	1851	7.3	1757	21	111	143.1	1850.2	8.5	2.27
WT12-6-242	1906	19	1872.7	7.9	1818	30	158	212	1843.8	7.6	3.44
WT12-6-252	1348	22	1393	12	1357	20	109.2	193	1455	12	3.83
WT12-6-262	1744	14	1785.6	7	1709	21	85.8	66.3	1831.4	7.6	3.2
WT12-6-272	2325	20	2314.5	9.2	2315	28	120.3	91.1	2310.6	6.9	2.61
WT12-6-282	1834	17	1834.7	8.6	1771	28	130	76.2	1846.4	8.7	2.51
WT12-6-292	1719	19	1764	10	1699	18	61.9	140.2	1822	12	3.38
WT12-6-302	1844	20	1844.9	8.9	1899	22	63.8	96	1849	13	3.14
WT12-6-312	1814	13	1833.3	6	1792	14	153.6	236	1849.8	7.4	2.56
WT12-6-322	1864	35	1848	13	1857	32	90.5	73.5	1820	15	3.95
WT12-6-332	1798	26	1780	13	1732	37	45.2	61.7	1770.8	9.1	3.7
WT12-6-342	1921	15	1919.4	8.2	1858	24	76.9	96.7	1910	10	2.44
WT12-6-352	1892	14	1889.7	6.4	1813	23	128.8	114.7	1893.6	6.4	2.38
WT12-6-362	1796	21	1812	12	1789	35	32.8	42.2	1829	11	3.32
WT12-6-372	1825	15	1830.3	6.3	1801	21	79.9	72.7	1836.9	9.8	2.71
WT12-6-382	1747	20	1795.2	9.4	1772	22	39.6	92	1853	12	4.04
WT12-6-392	1997	25	1950	11	1982	32	108	97.5	1895.5	8.2	3.96
WT12-6-402	1808	16	1823.3	7.2	1794	19	139	169	1837.3	9.6	2.73
WT12-6-412	2527	28	2530	13	2543	46	81	40.3	2535.9	6.9	3.66
WT12-6-422	1793	17	1817.5	9.6	1801	22	58.9	74.9	1840.5	9.1	2.89
WT12-8-1	864	24	1203	21	318	10	790	957	1891	5.7	28.18
WT12-8-2	1134	16	1240	13	1199	31	29.2	19.23	1429	21	7.2
WT12-8-3	1383	16	1503.8	9.8	1598	18	82.9	112.8	1693.7	8.4	8

Appendix C: U/Pb Data

Sample	206/207 (Ma)	2σ (Ma)	207/235 (Ma)	2σ (Ma)	208/232 (Ma)	2σ (Ma)	U (ppm)	Th (ppm)	207/206 (Ma)	2σ (Ma)	Disc. (%)
WT12-8-4	1855	14	1848.9	8.2	1774	26	93.1	70.6	1844.3	6.5	2.21
WT12-8-5	1767	24	1768	12	1556	48	218.8	188	1777.7	6.6	2.44
WT12-8-6	1757	13	1770.4	6.4	1673	15	333.6	358	1786.5	4.8	1.85
WT12-8-7	1020	11	1042.6	9.2	1059	12	38.8	73.3	1106	14	3.2
WT12-8-8	1486	18	1619.4	9.9	1610	22	744	225.4	1796.6	5.2	8.76
WT12-8-9	1735	15	1757.1	5.8	1725	16	247	105.3	1783.1	6	2.77
WT12-8-10	1736	15	1751.4	9.2	1455	48	233	124	1771.6	5.4	1.79
WT12-8-11	1346	27	1521	20	534	39	414	346	1779.2	7.4	11.69
WT12-8-12	1776	12	1785.3	5.6	1713	31	301	179	1794.9	5.1	1.68
WT12-8-13	1460	29	1594	18	1454	37	248	105.1	1774.2	7.1	8.5
WT12-8-14	1521	16	1651.3	9.9	1170	67	397	373	1822.4	5.7	8.12
WT12-8-15	1539	26	1657	18	527	25	494	135.4	1790	13	7.06
WT12-8-16	2574	19	2631.9	7.1	2553	50	36.7	24.17	2683.9	7.6	3.95
WT12-8-17	1718	17	1740.4	8	1805	21	54.6	59.8	1763	10	2.74
WT12-8-18	1808	18	1797.7	8.6	1780	34	219	362	1780.9	5.4	2.37
WT12-8-19	1767	25	1795	15	1251	95	150	53.5	1834	11	2.4
WT12-8-20	1508	17	1480.4	8.8	1512	34	52.6	56.3	1449.5	9.9	2.64
WT12-8-21	1783	12	1790.6	8.1	1709	41	168.5	93.8	1802.5	9.8	1.88
WT12-8-22	428	11	688	15	61.4	1.3	1256	3.27E+04	1659	11	31.55
WT12-8-23	1454	39	1589	25	775	65	413	182	1779.6	6.8	8.8
WT12-8-24	1431	38	1786	32	459	66	329	1160	2257	25	24.7
WT12-8-25	1767	11	1773.7	6.5	1764	14	156.9	165.7	1786.7	5.2	1.87
WT12-8-26	1584	47	1663	27	1367	80	540	110	1774.3	6.1	5.8
WT12-8-27	1802	11	1796.8	5	1803	21	365	124	1785.9	4.3	1.61
WT12-8-28	1600	19	1699	11	1261	17	239	185	1823	12	6.57
WT12-8-29	1031	11	1053.9	7	998	21	387	311	1094.9	9.6	2.01
WT12-8-30	2660	14	2684.7	5.6	2620	24	79	100.2	2701	4.3	2.39
WT12-8-31	1626	28	1695	16	1914	58	426	58.5	1789.6	7.3	4.58

Appendix C: U/Pb Data

Sample	206/207 (Ma)	2σ (Ma)	207/235 (Ma)	2σ (Ma)	208/232 (Ma)	2σ (Ma)	U (ppm)	Th (ppm)	207/206 (Ma)	2σ (Ma)	Disc. (%)
WT12-11-1	1601	11	1699.7	5.9	2192	37	144.6	75.3	1830.1	9.2	6.17
WT12-11-2	1997	28	2912	17	10760	260	12.24	6.75	3648	18	63.2
WT12-11-3	1396	13	1509.4	7.6	1991	95	803	24.28	1676.2	9.7	7.46
WT12-11-4	876.1	9	1130	10	5640	230	734	13.28	1641	11	20.43
WT12-11-5	731	12	1101	23	3540	290	509	49.6	1938	43	33.8
WT12-11-6	1980	33	2949	27	13260	390	10.82	4.78	3709	27	67.5
WT12-11-7	799	13	1040	12	2284	54	766	21.53	1599	13	21.08
WT12-11-8	1700	110	1861	92	3060	130	303	37	2084	67	10.4
WT12-11-9	2228	37	3134	27	11990	300	9.95	6.25	3790	26	59.9
WT12-11-10	1909	31	2823	20	12300	330	9.78	4.05	3562	24	62.8
WT12-11-11	1392	13	1582	11	2549	48	394	33.26	1835	13	12.18
WT12-11-12	937.9	9.5	1227.3	8	2563	73	377	28.2	1787	13	23.08
WT12-11-13	1911	19	2719.3	9.4	11320	190	13.74	5.72	3392	14	54.5
WT12-11-14	1574	31	2486	30	8540	300	10.61	6.01	3356	31	65.7
WT12-11-15	1532	23	1623.3	9.7	2890	150	246	6.85	1755	15	5.9
WT12-11-16	3636	88	4310	31	2.02E+04	1.10E+03	1.128	1.3	4664	21	40
WT12-11-17	1707	26	1993	21	1524	57	288	417	2312	11	18.51
WT12-11-18	1897	67	2145	36	2391	92	66	53	2395	11	15
WT12-11-19	2359	68	3423	67	1.77E+04	1.30E+03	5.61	2.8	4121	62	71.3
WT12-11-20	1778	15	2008	13	2287	30	260	178.7	2259	12	14.43
WT12-11-21	1868	43	2837	46	12680	710	10.52	4.4	3627	40	67.3
WT12-11-22	2880	54	3754	30	21670	520	4.15	2.21	4258	25	55.5
WT12-11-23	2569	19	2579	12	3168	87	244	332	2586	16	2.95
WT12-11-24	1707	20	2503	11	10460	220	15	5.35	3247.2	9	55.2
WT12-11-25	1485	10	1645.2	6.6	2034	31	107.9	61.1	1858.9	5.6	10.26
WT12-11-26	1078	41	1304	40	1895	87	555	51.7	1712	35	17.5
WT12-11-27	2343	32	2404	13	2407	31	247.9	344.4	2445.5	5.5	3.75

Appendix C: U/Pb Data

Sample	206/207 (Ma)	2σ (Ma)	207/235 (Ma)	2σ (Ma)	208/232 (Ma)	2σ (Ma)	U (ppm)	Th (ppm)	207/206 (Ma)	2σ (Ma)	Disc. (%)
WT12-11-28	2340	25	2363	14	2511	37	52.1	49	2371	13	2.37
WT12-11-29	1516	18	1595	14	1574	80	392	20.6	1703	17	5.25
WT12-11-30	1527	24	1885	18	1702	51	253	248	2318	16	23
WT12-11-31	2096	30	2982	17	11710	270	8.81	4.87	3669	13	60.5
WT12-11-32	1896	24	2885	25	12260	300	6.18	2.91	3666	30	68.9
WT12-11-33	1525	12	1682.9	6.9	2080	38	111.4	80.7	1893	11	10.21
WT12-11-35	1782	49	2021	29	1944	81	281	257	2271.5	7.2	14.7
WT12-11-36	993	73	1317	85	2954	80	714	51.3	1887	68	24.17
WT12-15-1	1396.2	8	1428	13	1479	17	187	404	1486	29	3.39
WT12-15-2	1035	19	1048	20	1129	49	6.39	4.09	1084	48	6.9
WT12-15-3	1122.9	7.7	1121.4	5.8	1140	11	127	163.8	1122	10	1.89
WT12-15-4	996	26	1288	21	73.4	5.3	427	4330	1822.5	9.9	22.51
WT12-15-5	1077	10	1085.7	7.7	1102	16	90.2	69.5	1096.9	9.1	2.47
WT12-15-6	1793	18	1783.7	9.3	1844	33	193.5	101.1	1780	8.1	2.3
WT12-15-7	1103.8	8.3	1097.2	6.4	1123	14	104.4	226.4	1076	12	2.21
WT12-15-8	254.2	3.6	381.8	3.9	265.2	4	1090	968	1252.6	9.8	23.33
WT12-15-9	1129	10	1109.8	8.1	1106	19	108.4	76.4	1083	10	2.22
WT12-15-10	521.3	7.3	522	10	529	16	40.5	40.7	545	27	3.47
WT12-15-11	1081.5	7.1	1081.8	5	1074	13	209	78.2	1090.4	6.7	1.67
WT12-15-12	524.7	5.5	531.8	6.7	529	10	47	42.3	574	20	3.47
WT12-15-13	1747	10	1759.2	5	1713	29	261	74.5	1778.5	5.8	1.78
WT12-15-14	2681	21	2674.5	7.7	2656	54	69.4	40.3	2669.8	5.6	2.91
WT12-15-15	1055.4	8.6	1065.1	8.5	1042	20	39	31.1	1090	17	2.88
WT12-15-16	1555	30	1610	18	1763	24	95.4	119	1674	13	3.88
WT12-15-17	1143.7	9.4	1129.6	6.1	1111	22	76.7	32.3	1129	12	2.53
WT12-15-18	1343	11	1354.5	8.4	1364	17	64.6	100.8	1365	9	1.84
WT12-15-19	1436	12	1427.8	6.7	1418	12	108.5	214	1422.3	7.7	1.89

Appendix C: U/Pb Data

Sample	206/207 (Ma)	2σ (Ma)	207/235 (Ma)	2σ (Ma)	208/232 (Ma)	2σ (Ma)	U (ppm)	Th (ppm)	207/206 (Ma)	2σ (Ma)	Disc. (%)
WT12-15-20	1119	12	1115.4	9.3	1125	22	79	51.6	1102.9	9.7	2.13
WT12-15-21	566	24	550	22	585	24	43.7	52.9	526	51	3.74
WT12-15-22	1065.2	8.1	1071.6	6.3	1080	16	125	95.4	1092	10	1.89
WT12-15-23	1103.5	9.7	1107.2	6.4	1038	14	119.8	104.7	1124.1	6.6	1.95
WT12-15-24	1739	14	1755.9	5.9	1453	22	263.4	189.4	1779.3	5.4	2.58
WT12-15-25	2835	51	2758	19	2842	93	35.3	35.5	2707	11	5.2
WT12-16-32	1020	18	1142	14	1000	21	70.7	50.8	1385	15	9.61
WT12-16-52	789	23	1099	19	758	32	146	39.8	1789	14	27.2
WT12-16-62	971	22	1116	18	1055	27	205	92.9	1369	18	9.9
WT12-16-72	2115	31	2378	14	965	53	38.6	42.2	2613	11	15.8
WT12-16-82	1527	24	1586	16	1282	37	35.8	33	1655	19	4.64
WT12-16-92	1059	15	1078	14	962	35	17.7	10.8	1118	28	5.01
WT12-16-102	1310	13	1339.7	8.8	1312	19	85.2	86.9	1378	12	3.19
WT12-16-112	1590	25	1674	13	1601	28	134.4	75	1777	12	5.57
WT12-16-122	1577	16	1651.4	7.4	1646	15	101.5	171.4	1748	11	4.99
WT12-16-132	827	21	1007	17	541	30	35	25.5	1414	18	14.8
WT12-16-142	1079	14	1088	13	1064	23	45.5	48.4	1103	19	3.64
WT12-16-152	983	23	1118	21	1051	36	28.5	21	1416	19	10.8
WT12-16-162	1395	18	1382.8	9.5	1380	26	135.7	106.4	1369	10	2.48
WT12-16-172	2233	31	2455	17	2469	68	57	14.1	2657	14	12.9
WT12-16-182	1764	22	1807.4	9.6	1557	45	172	45.6	1851	11	3.23
WT12-16-192	1363	13	1390.4	8.1	1314	34	48.9	15.65	1432	13	3.35
WT12-16-202	2683	55	2907	27	2802	41	62	60	3059.4	8.7	11.6
WT12-16-212	1364	15	1394.8	7.2	1255	31	57.4	22.82	1427	13	3.2
WT12-16-222	1066	12	1075.5	7.2	997	17	156.9	71.9	1097	12	2.63
WT12-16-232	2205	41	2327	23	2469	57	118.5	46.6	2421	11	6.94
WT12-16-242	1446	41	1568	28	1250	29	348	127	1727	11	7.38

Appendix C: U/Pb Data

Sample	206/207 (Ma)	2σ (Ma)	207/235 (Ma)	2σ (Ma)	208/232 (Ma)	2σ (Ma)	U (ppm)	Th (ppm)	207/206 (Ma)	2σ (Ma)	Disc. (%)
WT12-16-252	2595	21	2622.6	7.6	2487	42	67.7	44.4	2639.1	8	3.41
WT12-16-262	1747	22	1748	12	1693	28	59.2	40	1751	12	3.12
WT12-16-272	1884	29	1946	14	2170	39	140.4	86.4	2009.3	8.5	4.26
WT12-16-282	899	16	943	10	846	24	43.6	31.3	1057	24	4.3
WT12-16-292	1260	18	1295	12	1356	18	103.3	161.9	1348	14	3.57
WT12-16-302	1554	22	1707	13	1288	40	44.4	17.7	1889	13	9.05
WT12-16-312	1164	40	1375	27	1135	58	110	33.1	1732	15	14.5
WT12-16-322	2808	30	2874	12	2692	39	107.5	126.7	2922	12	5.59
WT12-16-332	944	16	977	13	830	24	24.9	30.7	1036	29	4.88
WT12-16-342	1242	14	1273	9.4	1188	29	63.2	26.3	1327	11	3.14
WT12-16-352	1111	14	1153	9.4	1078	18	44.2	56.5	1236	14	4.12
WT12-16-362	1887	34	2160	20	2051	53	93	46.3	2430	13	15.8
WT12-16-372	2365	20	2390.2	8.9	2187	24	109	77	2406.9	9.4	3.33
WT12-16-382	2854	22	2866	9.2	2781	32	62.4	75.6	2869.8	7.3	3.41
WT12-17-1	1479	29	1547	18	999	44	96.3	87.8	1641.2	8.8	4.68
WT12-17-2	1891	18	1841	11	1985	35	135.8	87.8	1780.3	6.8	3.17
WT12-17-3	1195.9	9.8	1162.2	7	1198	20	97	46.3	1099.2	9.8	2.68
WT12-17-4	1182.2	9.4	1162.3	6.7	1178	12	82.4	96.5	1121	12	2.6
WT12-17-5	1153.9	6.9	1133.3	6.7	1182	12	96	143.9	1100	11	2.22
WT12-17-6	1139.7	9.8	1125	10	1174	36	36.22	13.44	1113	17	3.05
WT12-17-7	1125.7	6.8	1115.9	5.1	1127.5	9.3	172	137.9	1092.2	9.8	1.81
WT12-17-8	1217.7	8.3	1191.5	8.6	1226	20	50.3	40.28	1138	15	2.92
WT12-17-9	1173	15	1168.1	9.1	1163	19	186	140.5	1143.9	8.3	2.24
WT12-17-10	1331	10	1357.2	8.8	1399	35	94.5	68.2	1402	17	2.75
WT12-17-11	1157.3	9.7	1144.5	7.3	1174	16	58.5	67.7	1113	12	2.87
WT12-17-12	1518	28	1643	24	1700	22	248	228.1	1822	15	9.02
WT12-17-13	1753	20	1754	11	1716	82	122.4	45.9	1750.5	7.6	2.1

Appendix C: U/Pb Data

Sample	206/207 (Ma)	2σ (Ma)	207/235 (Ma)	2σ (Ma)	208/232 (Ma)	2σ (Ma)	U (ppm)	Th (ppm)	207/206 (Ma)	2σ (Ma)	Disc. (%)
WT12-17-14	1034	9.2	1050.6	8.8	1061	15	57	69.4	1081	13	2.52
WT12-17-15	1469	13	1458.7	7.3	1528	18	45.1	76.5	1447.1	9.6	2.46
WT12-17-16	1015.3	8.6	1010.7	8.7	1052	15	43.8	57.1	1012	18	3.14
WT12-17-17	1125.7	7.6	1135.4	5.5	1102	30	182.7	20.18	1154.5	7.1	1.68
WT12-17-18	1133	12	1113.7	8.2	1096	14	60.3	61.6	1075	13	2.96
WT12-17-19	1463	10	1435	7.2	1426	14	59.7	105.8	1397.3	9.5	2.94
WT12-17-20	1004	10	1004.2	9	994	13	33.5	42.3	1001	18	2.95
WT12-17-21	1155	14	1152	13	1101	32	19.77	15.35	1151	18	3.86
WT12-17-22	1033	20	1679	19	487	33	265.5	523	2608.3	9.6	49.9
WT12-17-23	1670	11	1664.7	6.3	1711	21	155.3	169.3	1651.7	6.7	1.75
WT12-17-24	1593	17	1584.2	8.4	1597	13	78.8	142.3	1584	12	3.05
WT12-17-25	1113	10	1087.8	5.6	1109	15	217	96	1041.7	9.9	2.47
WT12-17-26	1100.1	8.7	1096.4	6.7	1082	17	93.9	48.5	1093	14	2.28
WT12-17-27	1054.1	8.4	1037.4	6.7	1036	18	123	57.2	1014	11	2.17
WT12-17-28	1301	14	1268	15	1257	23	26	37	1221	28	5.1
WT12-17-29	1180.6	9.1	1172.7	5.6	1141	16	110.9	67.6	1172.7	9	2.07
WT12-17-30	1272	16	1291.7	9.8	1163	22	38	49.4	1324	13	3.27
WT12-17-31	1172	17	1157	10	1160	21	31.2	40.9	1160	18	3.95
WT12-17-32	2011	17	1934	13	2029	34	46	67.6	1852	15	4.52
WT12-17-33	2767	28	2716	13	2751	83	8.96	4.62	2676	14	4.78
WT12-17-34	1564	16	1606	11	1486	16	127.5	147.5	1661	11	3.28
WT12-17-35	2008	27	1984	12	1939	25	67.3	55.8	1951.7	9.4	4.06
WT12-17-36	1220	19	1202	12	1209	24	45.1	31.6	1159	18	3.84
WT12-17-37	1450	17	1466	12	1487	19	30.9	85.3	1478	14	3.11
WT12-18-1	2541	26	2600.4	7.4	2432	18	83.6	162.8	2643.9	8.7	4.38
WT12-18-2	1403	17	1428	10	1367	15	67.5	63.6	1466.9	9.6	2.46
WT12-18-3	1434	17	1446.8	9.1	1446	21	55.8	26.9	1469	10	2.53

Appendix C: U/Pb Data

Sample	206/207 (Ma)	2σ (Ma)	207/235 (Ma)	2σ (Ma)	208/232 (Ma)	2σ (Ma)	U (ppm)	Th (ppm)	207/206 (Ma)	2σ (Ma)	Disc. (%)
WT12-18-4	1221	25	1309	14	1344	33	24.2	24.1	1447	22	6.5
WT12-18-5	1173	15	1217.4	9	1180	25	23.7	15.15	1299	16	4.26
WT12-18-6	1404	12	1420.2	8.3	1346.7	9.2	94.5	196.5	1446.6	9	2.23
WT12-18-7	1062	15	1073.8	9.5	1112	14	152	59.9	1087	11	2.09
WT12-18-8	2705	24	2726	12	2583	22	30.1	67.4	2741.8	8.4	3.75
WT12-18-9	904	23	947	16	692	39	192	194	1055	10	3.76
WT12-18-10	1228	14	1232	11	1168	18	38.4	33.8	1248	13	2.95
WT12-18-11	1233	12	1245.4	7.4	1156	14	127.9	65	1261.2	8.9	2.02
WT12-18-12	1083	15	1108	13	1116	28	16.91	13.53	1155	23	3.7
WT12-18-13	1134	12	1135.7	5.2	1088	14	67.7	64.5	1150	10	2.36
WT12-18-14	1128.2	9.9	1156.1	8.5	1151	19	82.4	49.1	1210	14	2.55
WT12-18-15	1114	11	1112.8	7.6	1051	14	49.3	51.5	1116	15	3.06
WT12-18-16	1327	13	1337.1	7.8	1336	13	68.6	181	1353.9	9.9	2.29
WT12-18-17	1119	18	1114	12	1116	27	30.8	33.5	1110	16	3.07
WT12-18-18	1079	11	1091.1	6.9	1062	16	65.1	57.2	1118	12	2.71
WT12-18-19	1096	13	1090.1	7.8	1040	17	73.8	63.1	1094	11	2.61
WT12-18-20	1057.6	9.5	1060.7	6.2	1056	14	98	56.3	1071	11	2.09
WT12-18-21	1649	11	1707.3	8.2	1682	22	68	51.1	1780.8	5.6	3.65
WT12-18-22	1415	17	1431.5	8.8	1443	17	128	121	1462	11	2.86
WT12-18-23	1028	10	1042.6	6.9	998	11	89.4	71.7	1080	13	2.46
WT12-18-24	1252	11	1245.6	7.7	1238	18	66.2	61.7	1237	13	2.34
WT12-18-25	1835	18	1852	8.3	1852	21	68.5	111	1878	11	2.95
WT12-18-26	1015.8	9.2	1026	5.8	1002	12	138.3	79.5	1032	11	2.15
WT12-18-27	1103	13	1100.3	6.8	1032	10	197	115	1099.8	8	2.22
WT12-18-28	1081.6	8.8	1087.9	5	1051.8	9.5	277	172.7	1093.5	6.9	1.89
WT12-18-29	2508	29	2606.9	9.4	2520	52	22	9.21	2688.3	8.2	6.2
WT12-18-30	2465	30	2548	12	2539	31	60.1	69.1	2617.3	9.3	5.76
WT12-18-31	1111	20	1127	12	1133	17	25.56	36.26	1179	22	4.53

Appendix C: U/Pb Data

Sample	206/207 (Ma)	2σ (Ma)	207/235 (Ma)	2σ (Ma)	208/232 (Ma)	2σ (Ma)	U (ppm)	Th (ppm)	207/206 (Ma)	2σ (Ma)	Disc. (%)
WT12-18-32	1039.2	7.7	1030	5.4	988	10	211	213	1015.4	8.4	1.48
WT12-18-33	1355	14	1369	8	1422	21	144	56.9	1384.5	6.7	2.15
WT12-18-34	1089.6	8.4	1094.2	5.9	1043	13	129	95.4	1115.6	8.1	1.91
WT12-18-35	1306	10	1315.9	6.1	1282	14	90.5	129.4	1329.4	7.2	2.36
WT12-18-36	1202	10	1197	6.9	1181	15	123.8	84.3	1167	12	2.09
WT12-18-37	1138	19	1135	13	1100	9.4	81.5	154.7	1135	17	3.16
WT12-18-38	1736	14	1747.4	7.1	1719	15	88.3	101.7	1772.9	7.3	2.55
WT12-18-39	1664	13	1657.2	7.1	1620	14	118.9	158.4	1651	7.8	2.15
WT12-19-12	1012.2	8.5	1015.9	6.2	954	12	148.5	155.7	1036	10	1.9
WT12-19-22	1468	37	1594	21	1599	21	80	78	1755.9	9.8	7.7
WT12-19-32	933	13	994	12	1066	20	80.3	85.9	1127	13	4.48
WT12-19-42	1049	23	1100	17	1011	26	171	96	1197	10	4.06
WT12-19-52	1021	11	1037.2	7.6	969	15	108.8	66	1073	12	2.95
WT12-19-62	1080	10	1061.4	7.5	1005	18	112.1	64.8	1020.9	9.7	2.12
WT12-19-92	983.4	9.7	992.4	9.2	974	25	58.4	29.3	1012	17	2.47
WT12-19-102	997	10	1015.7	6.7	974	16	119.2	82.7	1044.1	8.5	2.5
WT12-19-112	1038.8	9.3	1049.7	5.9	1000	15	141.9	66.6	1062.4	9.6	2.12
WT12-19-122	887	20	1025	13	1223	19	289	65.6	1331	11	11.14
WT12-19-132	1030	13	1095	12	1164	21	34.2	48.3	1227	19	5.51
WT12-19-142	1009	19	1073	15	1143	23	63.3	35.5	1194	14	4.98
WT12-19-152	953	14	994.6	9.2	990	23	27.4	26.27	1079	23	4.88
WT12-19-162	995.9	8.9	1034.7	7	1091	16	95.6	50.2	1120	12	3.08
WT12-19-172	1074.8	8.8	1077.6	6.6	1007	15	112.7	157.2	1088	12	2.39
WT12-19-182	1116	15	1121	10	1074	18	244	154	1128.6	8.6	2.15
WT12-19-202	1001.5	9.8	1008.6	9.1	1003	25	58.6	29.92	1015	19	2.74
WT12-19-212	1012	17	1056	10	1059	25	44.7	41	1144	19	4.17
WT12-19-222	1644	20	1716	14	1866	59	23.7	7.63	1795	19	4.65

Appendix C: U/Pb Data

Sample	206/207 (Ma)	2σ (Ma)	207/235 (Ma)	2σ (Ma)	208/232 (Ma)	2σ (Ma)	U (ppm)	Th (ppm)	207/206 (Ma)	2σ (Ma)	Disc. (%)
WT12-19-232	1013	20	1029	13	1017	18	99	53.7	1045	16	3.23
WT12-19-242	1061	10	1069	11	1066	20	26.1	23.82	1073	21	3.5
WT12-19-252	1250	13	1253	8.1	1174	16	95.2	65.3	1255	12	2.64
WT12-19-262	1099.6	9.4	1098	5.8	1039	12	222	284	1088	10	2.17
WT12-19-272	996	10	1034.7	7.8	1098	15	166.9	131.1	1107	14	3.09
WT12-19-282	940	23	969	15	1032	18	121	65	1042	15	3.71
WT12-19-292	997	15	1006.2	9.9	1028	17	52.1	90.5	1030	17	2.88
WT12-19-302	1683	20	1723.6	9.8	1796	34	48	35.1	1761	11	3.72
WT12-19-312	856	15	952	12	1071	31	24.4	11.46	1187	22	8.5
WT12-19-322	1340	12	1357.1	7.2	1316	14	125.7	125.4	1386.2	8.7	2.54
WT12-19-332	1061	14	1071.4	8.7	1057	16	49.4	55.8	1090	19	3.4
WT12-19-342	948	12	970	13	967	29	18.3	15.81	1034	21	4.04
WT12-19-352	1219	16	1206	12	1171	29	36.6	27.5	1196	16	3.32
WT12-19-362	1145	11	1152.3	6.9	1117	17	134	67.9	1172	10	2.49
WT12-19-372	1123	12	1113.1	6.4	1138	25	114	37.7	1089	13	2.84
WT12-19-382	1278	16	1304	10	1435	30	213.4	157.4	1340	10	2.66
WT12-19-392	1280	13	1326.6	8.2	1382	18	77.7	84.9	1406	12	3.95
WT12-19-402	986	12	1037.5	8.2	1069	15	82.8	89.1	1162	16	4.82
WT12-20-1	1823	23	1808	10	1975	25	240	143.3	1786.7	8.8	2.68
WT12-20-2	1750	13	1764	7	1823	25	116.8	77.4	1778	5.7	1.99
WT12-20-3	1114	12	1107	13	1152	28	19.7	15.74	1091	24	3.96
WT12-20-4	1036	10	1050.4	9.1	1145	17	46.8	49.8	1077	17	2.68
WT12-20-5	1452	19	1447	11	1474	31	27.3	45.6	1456	18	3.15
WT12-20-6	1811	13	1800.5	5.9	1851	29	274	41.3	1793.8	7.9	2.14
WT12-20-7	1116	12	1114.9	7	1095	20	153.1	89.5	1107	12	2.57
WT12-20-8	1828	12	1825.8	6.1	1794	23	146.9	131.3	1824.4	5.5	1.83
WT12-20-9	1852	14	1844.2	7.2	1850	25	69.5	36.4	1832.7	8	2.22

Appendix C: U/Pb Data

Sample	206/207 (Ma)	2σ (Ma)	207/235 (Ma)	2σ (Ma)	208/232 (Ma)	2σ (Ma)	U (ppm)	Th (ppm)	207/206 (Ma)	2σ (Ma)	Disc. (%)
WT12-20-10	1038	12	1047	11	1088	28	20.7	13.66	1079	20	3.15
WT12-20-11	1058.6	8.7	1069.6	5.4	1081	13	110.7	77.3	1089	12	2.43
WT12-20-12	1091	10	1101.6	9.1	1140	22	27.4	23.62	1111	16	2.59
WT12-20-13	1760	15	1762.8	6.9	1767	23	68.2	48.9	1769.3	8.4	2.48
WT12-20-14	1768	11	1769.7	6.2	1734	18	92.1	115.7	1772.2	6.3	1.84
WT12-20-15	795	12	875	15	1021	26	21.8	12.62	1084	28	6.59
WT12-20-16	1066.1	7.5	1066.8	5.9	1073	11	98.5	103.8	1068.8	9.8	2.04
WT12-20-17	1702	19	1730	12	1634	25	226	161	1769.4	7.1	2.48
WT12-20-18	1070	16	1090.6	9.4	1154	20	102	36.2	1100	13	2.15
WT12-20-19	1442	13	1430.5	8	1468	24	72	52.2	1424	12	2.74
WT12-20-20	1353	11	1358.7	6.2	1376	19	53.4	73.4	1380	12	2.65
WT12-20-21	1681	12	1674.4	5.6	1647	18	84.4	88	1672	11	2.02
WT12-20-22	1014	18	1119	15	1282	32	16.07	11.53	1333	23	7.9
WT12-20-23	1348	21	1382	17	1178	37	99.3	35.6	1421	14	2.65
WT12-20-24	1087.7	9.1	1091.4	6.9	1123	18	77.6	73.5	1084	13	2.29
WT12-20-25	1651	19	1693.4	8	1788	32	30.3	30.4	1763	8.8	3.99
WT12-20-26	739	16	823	14	1029	23	39.1	21.99	1068	21	7.92
WT12-20-27	1337	18	1502.8	8.9	1746	36	211.9	58.3	1741.3	9.7	10.83
WT12-20-28	1822	18	1806.1	8.9	1820	27	156.2	316	1787.1	5.4	2.44
WT12-20-29	1655.3	9.6	1671.4	4.7	1657	14	234	287	1688.6	5.1	1.84
WT12-20-30	1089	11	1103.6	9.5	1127	17	45	49.3	1144	15	2.5
WT12-20-31	898	34	1147	30	823	21	721	344	1680.4	9.7	21
WT12-20-32	261	16	313	24	203.6	8.6	1850	4190	672	67	9.2
WT12-20-33	514.9	5.5	520.9	4.8	526.7	6.2	185	157.6	543	14	2.12
WT12-20-34	1721	27	1751	12	1901	23	157	82.7	1784.7	8.4	3.35
WT12-20-35	1027	25	1276	23	985	21	880	129.7	1727	12	18.56
WT12-20-36	1185	12	1248.1	9.2	1268	17	139.4	106.2	1355.7	9.7	4.4

Appendix C: U/Pb Data

Sample	206/207 (Ma)	2σ (Ma)	207/235 (Ma)	2σ (Ma)	208/232 (Ma)	2σ (Ma)	U (ppm)	Th (ppm)	207/206 (Ma)	2σ (Ma)	Disc. (%)
WT12-21-1	1645	11	1697.5	6.4	1599	12	81	60	1759.2	6.7	3.18
WT12-21-2	992	14	1029	10	997	29	22.3	13.72	1135	16	3.9
WT12-21-3	1320	11	1344.8	6.8	1281	14	56.9	52.9	1374.9	8.1	2.21
WT12-21-4	1061	10	1068.6	7.2	1008	13	79	78.6	1092	11	2.19
WT12-21-5	931	16	990	14	994	23	21.81	20.96	1123	15	5.05
WT12-21-6	1582	12	1617.8	6.6	1512	13	112.8	126.5	1674.8	6.2	2.83
WT12-21-7	1600	10	1639.1	5.6	1624	17	124.5	99.7	1689.6	6.4	2.73
WT12-21-8	1357	11	1391.1	5.8	1329	18	205.3	142	1440.9	7.4	2.68
WT12-21-9	1718	13	1750	5.6	1735	21	269	71.5	1785.6	5.2	2.64
WT12-21-10	1272	11	1326.1	8.5	1339	25	38.2	19.9	1421	12	3.9
WT12-21-11	1715	14	1782.4	7.4	1599	25	72.1	28.89	1860.1	7.5	4.01
WT12-21-12	1671	16	1714	7.5	1767	24	45.7	27.5	1776.2	9.4	3.32
WT12-21-13	1689	15	1738.6	7.3	1685	18	182	86.2	1799.2	5.8	3.28
WT12-21-14	1732	12	1753.5	5.2	1674	15	179.1	148	1781.4	6.5	2.29
WT12-21-15	1780	25	1867	16	2107	72	120.7	121	1974	19	5.82
WT12-21-16	1716	12	1745.5	6.3	1671	14	212	107.9	1788.4	6.6	2.47
WT12-21-17	1722	13	1738.6	6.7	1705	27	70.5	82.5	1764.6	8.2	2.38
WT12-21-18	1345	15	1384.7	8.6	1198	63	180	93.9	1442	10	3.15
WT12-21-19	1726	10	1759.4	5.5	1670	13	246	214	1797.1	5.6	2.36
WT12-21-20	1458	19	1593	13	1197	32	118.4	64.4	1775.1	9.7	8.63
WT12-21-21	1695	12	1753	17	1702	44	56.6	89.5	1825	32	4.94
WT12-21-22	1258	25	1331	15	1147	26	115.3	72.7	1437	12	4.54
WT12-21-23	1758	15	1779.6	7.2	1728	21	85.6	42.5	1794.8	6.3	2.43
WT12-21-24	1557	13	1593.6	7.9	1577	17	52	61.4	1649	10	3.21
WT12-21-25	1800	14	1793.7	6.9	1857	14	160	118	1782	6.9	2.22
WT12-21-26	1409	11	1421.3	5.9	1383	22	178	48.7	1439.3	7.6	2.14
WT12-21-27	1768	13	1773.3	7.1	1749	28	199	60.9	1775.9	6.3	2.12
WT12-21-28	1364	13	1383.8	7.4	1463	28	47.9	14.33	1422	12	2.53

Appendix C: U/Pb Data

Sample	206/207 (Ma)	2σ (Ma)	207/235 (Ma)	2σ (Ma)	208/232 (Ma)	2σ (Ma)	U (ppm)	Th (ppm)	207/206 (Ma)	2σ (Ma)	Disc. (%)
WT12-21-29	989	23	1030	17	903	27	137	83.6	1129	10	3.37
WT12-21-30	1370	14	1397	8.6	1348	22	81	40.7	1435.1	9.4	2.81
WT12-24-12	2656	31	2680	13	2443	81	11.63	9.47	2691	12	4.85
WT12-24-22	1053	13	1063	12	1070	25	34.5	25.3	1074	19	3.49
WT12-24-32	1044	11	1047.2	7	1074	15	194	85.6	1059	11	2.39
WT12-24-42	1057	14	1068	11	1094	19	44.3	77.2	1088	19	3.4
WT12-24-52	702.8	7.9	703.3	6.1	703	11	191.1	146.8	700	14	2.26
WT12-24-62	1059	12	1052.6	6.8	1042	19	138.8	54.1	1049	11	2.1
WT12-24-72	675.8	7.6	673.2	6.3	666	11	83.8	100.1	671	15	2.87
WT12-24-82	2526	45	2595	22	1910	180	79.5	29.9	2657	14	5.9
WT12-24-92	2540	47	2622	19	2841	64	54.9	48.3	2686	12	7.3
WT12-24-102	1013	14	1019	14	1058	34	22.1	16.5	1027	29	4.37
WT12-24-112	1690	15	1700.4	5.9	1607	30	176	51.2	1706	10	3.03
WT12-24-122	1181	59	1783	48	780	110	17.1	31.1	2595	24	43.5
WT12-24-132	1260	45	1878	32	934	45	33.9	43.4	2652	13	44.4
WT12-24-142	2609	39	2620	15	2743	58	33.6	53.6	2614	11	5.35
WT12-24-162	2530	23	2579.8	8.3	2450	25	78.6	119.3	2632.5	7.2	4.18
WT12-24-172	1279	15	1304	11	1267	26	29.3	33.9	1348	15	3.56
WT12-24-182	1377	28	1409	16	1583	46	111	96.2	1437	11	3.86
WT12-24-192	1754	16	1717	11	1776	29	189	68.7	1672	11	2.86
WT12-24-202	1231	21	1431	13	563	27	210	104.7	1744	11	14
WT12-24-212	453.6	6.5	472.3	7.9	492	21	47.13	39.31	557	43	4.65
WT12-24-222	2549	34	2624	13	2525	65	15.2	9.8	2674	11	5.9
WT12-24-232	1051	11	1041.7	6	1005	15	295	79.7	1027	11	2.26
WT12-24-242	966	16	1005	12	971	25	37.2	32.1	1079	18	3.59
WT12-24-252	2656	33	2674	14	2673	45	100.1	68.3	2679.7	9	4.1
WT12-24-262	1426	10	1423.6	6.6	1359	21	141	144	1423	11	2.39

Appendix C: U/Pb Data

Sample	206/207 (Ma)	2σ (Ma)	207/235 (Ma)	2σ (Ma)	208/232 (Ma)	2σ (Ma)	U (ppm)	Th (ppm)	207/206 (Ma)	2σ (Ma)	Disc. (%)
WT12-24-272	2079	77	2335	36	1912	91	57	55.1	2604	14	17.3
WT12-24-282	2817	25	2806	13	2706	37	105.5	126.3	2792	11	2.88
WT12-24-292	1327	15	1336.3	9.5	1235	35	38.3	24.76	1360	12	3.42
WT12-24-302	1595	18	1638	9.5	1599	23	48.4	41	1691	11	3.72
WT12-24-312	1396	13	1403.4	7.9	1356	22	71.1	56.9	1424	13	2.89
WT12-24-322	1084	10	1085.4	6.6	1023	21	109	103	1096	12	2.73
WT12-24-332	2602	26	2644	9.2	2640	31	68	129.4	2675.4	9.2	4.41
WT12-24-342	716.7	8.5	706	6.3	660.4	7.7	197.2	296	676	19	2.53
WT12-24-352	2296	18	2290.4	8.4	2285	27	85.3	85.8	2292.5	7	2.84
WT12-24-362	675.1	8.6	689.2	9.6	682	13	51.1	61.7	737	21	3.55
WT12-24-372	2027	55	2351	32	2092	86	13.51	9.14	2651	15	20
WT12-24-382	1721	25	1737	12	1568	33	43.9	37.4	1754	13	3.9
WT12-24-392	669	11	659	11	707	14	38	60.5	635	36	5.17
WT12-24-412	721	8	721	7	695	15	115.7	101.6	712	19	2.85
WT12-24-422	2531	37	2630	16	2257	79	11.61	6.95	2691	11	6.8
WT12-24-432	1673	16	1683	10	1698	26	87	44	1677	11	2.8
WT12-25-1	1781	19	1776	11	1847	23	44.5	86.4	1766	11	2.19
WT12-25-2	1834	14	1822.1	6.2	1795	21	64.1	55.8	1808	10	2.62
WT12-25-3	1810	14	1803.5	8.1	1782	21	261	98.3	1787.8	4.3	1.68
WT12-25-4	1025	18	1278	14	1337	34	951	59.9	1735.3	9.1	19.5
WT12-25-5	1855	16	1839.2	8.8	1830	17	159	168	1821	6.9	2.16
WT12-25-6	1731	19	1767.9	9.6	1747	25	307	97.1	1805.3	5.9	2.88
WT12-25-7	1529	16	1622.3	9.5	1386	26	560	91	1759.4	5.7	6.42
WT12-25-8	1799	11	1781.6	8	1796	26	42.7	28.2	1763	10	2.68
WT12-25-9	1833	12	1809.2	5.7	1813	26	383.6	152.6	1784.5	4.3	2.13
WT12-25-10	1746	10	1763.2	5.8	1752	15	103.5	186.2	1781.9	6.3	2.01
WT12-25-11	1809	14	1799.2	6.9	1805	38	366	42.25	1786.5	6.4	1.92

Appendix C: U/Pb Data

Sample	206/207 (Ma)	2σ (Ma)	207/235 (Ma)	2σ (Ma)	208/232 (Ma)	2σ (Ma)	U (ppm)	Th (ppm)	207/206 (Ma)	2σ (Ma)	Disc. (%)
WT12-25-12	1061.8	6.7	1056.6	4.9	1049	15	225	121.7	1044	9.8	1.62
WT12-25-13	1463	10	1452	5.9	1464.5	9.8	162.8	324	1444.7	6.1	1.84
WT12-25-14	1747	10	1763.3	5.4	1774	21	274.6	120.4	1782.4	4.3	1.68
WT12-25-15	1067.7	8.8	1087.4	6.9	1101	14	82.2	79.3	1124	8.8	1.99
WT12-25-16	1786	10	1777.9	5.9	1765	18	160.1	204.2	1774.9	6	1.79
WT12-25-17	1623	15	1739.5	9.7	1742	21	239	276	1888.9	9.3	7.27
WT12-25-18	1655	15	1703.1	9.2	1747	24	61.9	55	1761	10	3.45
WT12-25-19	1427	38	1573	23	1709	35	781	169	1774.8	6.1	9.3
WT12-25-20	1530	23	1631	15	1513	33	498	119.3	1770.5	8.6	5.96
WT12-25-21	1719	12	1747.3	6.3	1701	17	281	322	1785.8	6	2.3
WT12-25-22	1610	11	1649.4	7	1688	18	68.5	47.5	1698.9	8.3	2.62
WT12-25-23	1771	11	1769.1	5.5	1735	16	76.2	162.5	1773.4	7.9	2.09
WT12-25-24	1135	29	1328	21	1475	35	392	376	1662.7	9.6	14.33
WT12-25-25	1844	15	1819	10	1845	35	41.3	61.3	1781	13	2.97
WT12-25-26	1741	17	1747.1	7	1701	28	43.5	44.8	1757	10	3.25
WT12-25-27	1676	12	1720.9	7.8	1704	18	69.9	72.5	1774.8	7.3	3.14
WT12-25-28	1789	13	1785.6	6.3	1767	15	94.6	207	1776	7.8	2.51
WT12-25-29	1839	14	1815.1	8.5	1830	25	352	74.6	1784.3	6.3	1.73
WT12-25-30	1763	14	1768.7	5.6	1684	21	137.1	75.5	1774.2	6.2	2.14
WT12-26-12	1263	16	1359	12	892	21	109	198	1500	17	5.79
WT12-26-22	1273	42	1352	28	1418	66	110.8	93.7	1469	20	6.5
WT12-26-52	1786	19	1807.5	8.4	1791	28	238	41.2	1822.2	9.3	2.97
WT12-26-62	2480	40	2598	18	2546	49	32.92	31.4	2679.1	7.8	6.7
WT12-26-72	1297	16	1346	11	1334	23	101	115	1425	14	3.54
WT12-26-92	1774	20	1779.4	9.9	1775	28	90.8	55.6	1771	12	2.8
WT12-26-102	818	21	893	17	902	32	38.2	29.5	1083	22	6.72
WT12-26-122	944	18	1021	20	1135	36	26.4	37.1	1166	36	6.4

Appendix C: U/Pb Data

Sample	206/207 (Ma)	2σ (Ma)	207/235 (Ma)	2σ (Ma)	208/232 (Ma)	2σ (Ma)	U (ppm)	Th (ppm)	207/206 (Ma)	2σ (Ma)	Disc. (%)
WT12-26-132	1360	15	1384	10	1429	32	44	40.1	1418	14	2.8
WT12-26-152	925	22	1241	20	1367	46	16.8	15.72	1824	27	25.2
WT12-26-162	1359	21	1567	16	1586	30	24.8	23.8	1867	15	14.5
WT12-26-172	2349	25	2528	13	2414	36	37.2	36.3	2671	11	9.8
WT12-26-182	488.1	8.8	508	11	525	18	37.1	33.02	611	38	5.34
WT12-26-192	1625	25	1727	16	1722	50	96	44.1	1854.7	9.6	6.5
WT12-26-202	1669	25	1732	13	1789	37	33.8	33.7	1787	21	4.94
WT12-26-212	1638	15	1654.6	8.4	1562	22	142	93.1	1666.4	8.6	2.47
WT12-26-222	1284	19	1276	12	1267	24	33.2	46.2	1260	16	3.8
WT12-26-232	1837	62	2358	35	1007	69	71.5	90.5	2858	14	33.6
WT12-26-242	2212	28	2465	14	2396	39	32	41.2	2672	11	14
WT12-26-252	1746	22	1785	13	1798	34	35.3	23.9	1826	14	4.04
WT12-26-262	2667	33	2664	14	2754	70	94	51.1	2655	11	4.4
WT12-26-282	1156	16	1266.2	9	1310	19	52.3	50.4	1470	13	7.59
WT12-26-292	2013	82	2479	41	840	31	85.2	86.5	2902	15	29.1
WT12-26-312	2356	29	2542	11	2700	40	62.3	86.5	2696.2	9.1	10.2
WT12-26-322	804	16	912	16	1016	37	31.6	28.2	1191	25	9.9
WT12-26-332	1337	39	1369	23	1343	49	110	105	1371	13	4.13
WT12-26-342	1820	22	1798	10	1754	29	82.3	46.5	1765	11	3.2
WT12-26-352	1174	44	1816	35	1360	130	39.2	24.5	2627	15	45.9
WT12-26-362	1715	26	1730	14	1659	57	86.5	30	1747	11	2.88
WT12-26-372	1106	29	1321	23	539	21	34	47.1	1673	19	14.7
WT12-26-382	1057	18	1183	15	1113	40	36	23.92	1416	17	9.1
WT12-26-392	1433	26	1574	15	1752	30	127	120	1758	13	8.56
WT12-28-1	1066	15	1064.5	9.1	1073	15	63.3	53.9	1050	20	3.66
WT12-28-2	1424	18	1437.7	8.9	1384	12	141.9	152.8	1460	11	2.66
WT12-28-3	1012	13	1015.5	8.7	996	13	111	91.7	1042	13	2.45

Appendix C: U/Pb Data

Sample	206/207 (Ma)	2σ (Ma)	207/235 (Ma)	2σ (Ma)	208/232 (Ma)	2σ (Ma)	U (ppm)	Th (ppm)	207/206 (Ma)	2σ (Ma)	Disc. (%)
WT12-28-4	1128.1	8.6	1138.1	5.1	1101.9	9.6	121.8	153.6	1163.4	8	1.88
WT12-28-5	1017	17	1032	11	1046	14	118.1	73.9	1061	15	2.95
WT12-28-6	1052	16	1053	11	1029	17	50.2	50	1062	22	3.62
WT12-28-7	1078	7	1078.4	5.8	1066	14	90.2	63.9	1083	11	1.96
WT12-28-8	1091.9	8.1	1092.2	6.8	1062	13	75.3	57.4	1104	11	2.09
WT12-28-9	1044.1	9.2	1055.8	5.7	1049	11	135.2	113.1	1079.6	9.1	1.99
WT12-28-10	1306	9.7	1308.2	7.1	1293	14	79.3	73.9	1325.6	8	1.93
WT12-28-11	1092.5	6.2	1087.8	5.3	1053	18	142	77.6	1088.6	7.6	1.47
WT12-28-12	1086	12	1083.9	8.3	1139	20	176	40.6	1089	11	2.21
WT12-28-13	1034.5	7.7	1033.1	5.7	1000.9	9.8	137.4	110.9	1044.6	8.2	1.81
WT12-28-14	1109.8	9.6	1110.6	6.1	1094	16	87.8	73.4	1127	11	2.2
WT12-28-15	1002	11	1005.6	6.4	1040	10	269	119	1022.1	7.7	1.98
WT12-28-16	1111	10	1102.1	6.4	1092	16	95.2	101	1094	13	2.69
WT12-28-17	1082.7	8.5	1078.2	8	1102	12	78.9	83.3	1074	11	1.95
WT12-28-18	1092	12	1096.9	8.4	1146	23	28.9	22.23	1128	17	3.32
WT12-28-19	1351	14	1356.2	8.7	1411	15	77	115	1370	11	2.44
WT12-28-20	1020.3	9.2	1022.8	7	1002	22	41	27.9	1021	16	2.9
WT12-28-21	2490	21	2504	8.1	2492	20	90.8	105.1	2523.5	7.5	3.27
WT12-28-22	1078	14	1073	10	1094	20	43.3	41.6	1075	16	3.05
WT12-28-23	1656	18	1663	11	1757	30	94.8	67.4	1667.4	9.2	2.16
WT12-28-24	1243	11	1274.3	7.6	1324	26	54.1	33.03	1329	11	2.8
WT12-28-25	1057	13	1068	14	1062	21	14.28	16.72	1087	28	4.7
WT12-28-26	1642	15	1653.6	7	1620	19	86	58.6	1675.7	9.6	2.64
WT12-28-27	1448	14	1453	10	1471	19	50	52.5	1459	13	2.39
WT12-28-28	992	16	1084	12	703	15	57.2	50	1280	14	6.59
WT12-28-29	1057	11	1065	7.4	1068	20	47	31.64	1089	13	2.55
WT12-28-30	1171.9	9.3	1175.4	5.4	1158	10	178	179.8	1192.1	6.4	1.72
WT12-28-31	1003	10	1002.4	7.1	1015.5	9.8	85.3	145.5	1008	14	2.78

Appendix C: U/Pb Data

Sample	206/207 (Ma)	2σ (Ma)	207/235 (Ma)	2σ (Ma)	208/232 (Ma)	2σ (Ma)	U (ppm)	Th (ppm)	207/206 (Ma)	2σ (Ma)	Disc. (%)
WT12-28-32	1071	13	1069.4	7.7	1100	15	113	75.9	1088	11	2.43
WT12-28-33	947	27	1129	23	1336	30	82.8	113.4	1495	56	14.5
WT12-28-34	1354	14	1360	7.7	1378	14	167	153	1369.3	8.5	2.39
WT12-28-35	1346.3	9.3	1343.9	6.2	1360	29	112	74	1347.6	9.3	2.3
WT12-28-36	1087	10	1082.8	6.5	1086	16	98.9	60.7	1086	13	2.42
WT12-28-37	1503	11	1489.6	6.2	1492	13	250	272	1475.4	6	1.67
WT12-28-38	1228.8	9.4	1224.3	6.8	1267	22	78.7	31.9	1216.7	9.5	2.11
WT12-28-39	1215	12	1227.8	7.7	1209	24	93.3	53.6	1271	11	2.43
WT12-28-40	1190	13	1197.9	9.8	1194	15	296	161	1229	11	2.28
WT12-28-41	1008	10	1012.7	5.9	1003	14	186	98	1028.2	9.5	2.06
[redacted]											
WT12-29-12	1429	14	1441.3	7.2	1287	19	124.7	181.2	1455.7	8.3	2.37
WT12-29-22	1319	11	1313.8	7	1196	21	88.9	127	1308	10	2.32
WT12-29-32	1029.8	7.9	1027	5.2	953	17	111.8	36.42	1030	11	1.94
WT12-29-42	1361	35	1354	23	1247	65	29	55.1	1327	16	4.42
WT12-29-52	1149	11	1155.5	7.4	1115	19	62.8	43.3	1179	11	2.51
WT12-29-62	1018	8.9	1019.3	5	960.4	9.6	177	228	1029.3	9.8	1.9
WT12-29-72	1347	13	1367.4	8.1	1244	16	77.6	76.9	1401	13	3.05
WT12-29-82	1353	24	1354	15	1249	25	119	100	1360	13	3.35
WT12-29-92	972.1	7.9	1030.2	7.8	1026	14	125.6	136	1114	12	4.46
WT12-29-102	1379	12	1371.9	6.4	1299	14	152	166	1364.5	8.6	2.51
WT12-29-112	1067	12	1061	10	1006	18	59.8	61.6	1049	22	2.65
WT12-29-122	1729	15	1694.9	8.3	1651	21	202	278	1657.6	8.7	2.66
WT12-29-132	1371	12	1373.4	7.3	1290	16	97.9	107.9	1375.3	9.7	2.32
WT12-29-142	1448	12	1471.8	6	1387	19	134	123.9	1496.9	9.2	2.53
WT12-29-152	1667	13	1659.5	5.6	1530	16	271	487	1649.1	8.1	2.09
WT12-29-162	1753	10	1761.2	6.7	1656	22	111.1	91	1780	7.8	2
WT12-29-172	938.4	9.8	944.6	8.9	968	19	126.2	64.6	971	17	2.7

Appendix C: U/Pb Data

Sample	206/207 (Ma)	2σ (Ma)	207/235 (Ma)	2σ (Ma)	208/232 (Ma)	2σ (Ma)	U (ppm)	Th (ppm)	207/206 (Ma)	2σ (Ma)	Disc. (%)
WT12-29-182	1445	15	1457.4	8.5	1419	22	96.8	70.2	1474.5	9.8	2.52
WT12-29-202	1071	7.7	1077.1	5.1	1001	13	154	168	1085	10	1.87
WT12-29-212	1155	10	1156	7.1	1107	15	95.9	59.2	1163	14	2.36
WT12-29-222	1095.8	9.4	1088.8	7.4	1080	19	179.5	124.1	1069	10	2.02
WT12-29-232	1485	13	1475.8	9	1418	22	147.9	107.6	1474.3	8.5	1.8
WT12-29-242	962	18	999	19	947	22	15.78	27.7	1074	33	5.44
WT12-29-252	1155.6	8.6	1159.1	4.6	1122	13	165	116.5	1162.2	8.3	1.86
WT12-29-262	1147.8	8.7	1152	6	1075	17	87.9	43.4	1155	10	2.14
WT12-29-272	1035	31	1291	26	785	36	204.6	140.3	1767	12	19.71
WT12-29-282	1349	14	1347.8	7.5	1289	23	46.8	53.9	1357	12	3.19
WT12-29-292	1041	11	1041.3	7.8	1003	21	48.3	35.8	1040	18	3.05
WT12-29-302	2541	33	2624	13	2349	49	51.8	48	2684.5	5.9	5.12
WT12-29-322	1056.2	7.9	1067.2	6.9	1016	14	62.8	68.2	1104	14	2.61
WT12-29-342	1349.7	9.4	1351.3	5.3	1265	14	151.9	177.2	1354.1	9.9	2.06
WT12-29-352	1107	13	1097.5	7.4	1052	17	85.5	78.6	1091	11	2.59
WT12-29-362	1274.6	9.6	1275.6	5.7	1165	13	203	152.7	1273.8	7.2	1.81
WT12-29-372	1175	14	1174.7	7.8	1129	16	109.9	94	1171	12	2.35
WT12-29-382	1066	10	1083.7	8.4	1065	18	75.3	57.7	1126	15	2.64
WT12-29-392	2533	20	2538.2	9	2509	27	69.3	125.3	2543.8	6.7	2.71
WT12-29-402	1458	12	1466.5	6.5	1373	21	114	96	1482.4	8.7	2.3
WT12-30-12	1669	19	1711	11	1682	20	92	70.5	1769	11	3.56
WT12-30-22	1606	24	1687	14	1661	45	208	93.2	1789	7.4	4.96
WT12-30-32	1655	21	1712	11	1434	31	177	61.6	1787.9	7.2	3.98
WT12-30-42	2547	32	2626	16	2383	59	97.8	62.5	2702.1	5.7	5.11
WT12-30-52	1036.7	8.3	1033.6	5.4	1006	14	235	110.1	1034	11	1.92
WT12-30-62	1406	14	1413.5	8.7	1341	34	33.6	16.91	1432	15	3.08
WT12-30-72	1722	25	1765	12	975	58	290	179.9	1817.6	8.9	3.72

Appendix C: U/Pb Data

Sample	206/207 (Ma)	2σ (Ma)	207/235 (Ma)	2σ (Ma)	208/232 (Ma)	2σ (Ma)	U (ppm)	Th (ppm)	207/206 (Ma)	2σ (Ma)	Disc. (%)
WT12-30-82	1455	14	1465	7.9	1471	18	195	200	1483	7.2	2.24
WT12-30-92	1270	19	1446	13	1155	22	529	48.8	1715.6	9	12.23
WT12-30-102	1720	14	1749.6	7.4	1612	23	103.1	54	1793.9	9.5	2.89
WT12-30-112	1776	13	1782.4	6.2	1675	27	275.1	63.6	1794.2	6.3	2.18
WT12-30-132	1454	12	1457.7	7.2	1346	23	130.5	103.3	1466.8	9	2.31
WT12-30-142	1800	32	1803	16	895	63	370	52	1815	12	3.68
WT12-30-152	1015	16	1021.6	9.6	1210	110	257	5.8	1048	17	2.34
WT12-30-152	1214	16	1214.4	8	1127	23	76.5	51.1	1209	14	2.53
WT12-30-162	2621	19	2642.2	7.6	2377	38	252	500	2658.3	6	2.29
WT12-30-172	1799	28	1795	12	1754	31	373	186.2	1795.2	7.6	3.33
WT12-30-182	1369	30	1545	19	1249	61	59.8	74	1790	11	11.4
WT12-30-192	2535	19	2580	10	2343	24	178.3	206.2	2614.9	7	3.18
WT12-30-202	1769	27	1791	15	1587	42	228	150	1815.4	9.4	2.94
WT12-30-212	1728	23	1742	12	1538	44	364	145.2	1761	6.3	2.41
WT12-30-222	1685	36	1773	19	1461	76	138.4	73.4	1865	12	5
WT12-30-232	1160	28	1151	17	855	80	113.6	101.7	1144	21	3.24
WT12-30-242	1500	11	1470.3	7.6	1381	19	157.7	142.9	1432.7	7.6	2.3
WT12-30-252	1812	28	1805	11	1749	44	114.7	84.3	1801	16	2.83
WT12-30-262	1202	15	1190	12	1107	21	30.5	48.9	1193	16	3.62
WT12-30-272	707.4	9.5	704.2	6.6	656	11	63.2	98.7	699	23	3.16
WT12-30-282	2358	38	2554	18	2492	38	44.6	60.6	2704.6	7.6	10.6
WT12-30-302	1373	12	1368.3	7.6	1299	13	142.4	224.1	1364.4	8.7	2.08
WT12-30-312	2225	36	2485	20	2470	100	304	187.6	2710	14	15.2
WT12-30-322	1561	36	1679	15	749	54	585	217	1818	11	7.2
WT12-30-322	1785	38	2058	16	1201	37	223.9	174	2357	14	18.1
WT12-30-332	1764	22	1772	13	1624	36	257	144	1780.5	7.8	2.73
WT12-31-1	1018	19	1034.9	9.9	980	13	140	100.5	1063	21	4.06

Appendix C: U/Pb Data

Sample	206/207 (Ma)	2σ (Ma)	207/235 (Ma)	2σ (Ma)	208/232 (Ma)	2σ (Ma)	U (ppm)	Th (ppm)	207/206 (Ma)	2σ (Ma)	Disc. (%)
WT12-31-2	1403	27	1436	15	1378	19	80.3	61.3	1482	23	4.89
WT12-31-3	993	11	1005.7	7.3	980	11	246	119	1041	8.9	2.07
WT12-31-4	1722	27	1733	13	1641	14	116.5	92.6	1756	18	4.15
WT12-31-5	1032.9	8.5	1040.7	6.3	1013	13	92	74	1068	12	2.16
WT12-31-6	1092.2	8.5	1089.6	5.9	1044	14	129.6	103.4	1088.8	9.7	1.61
WT12-31-7	1009.2	7	1016.3	5	986	15	139.9	55.6	1041.6	7.1	1.55
WT12-31-8	1070.2	8.8	1064.9	5.7	1054.2	9.8	294	192.3	1065.4	6.8	1.49
WT12-31-9	2418	34	2612	15	2273	82	97.7	129	2780	17	11
WT12-31-10	1747	12	1753.1	4.8	1669	14	249	269.1	1764.2	4.3	1.9
WT12-31-11	1393	15	1384	10	1336	17	176	150	1381	13	2.24
WT12-31-12	1054.8	9	1063	7	1094	17	53	33.8	1085	14	2.42
WT12-31-13	1093	12	1087.2	7.4	1097	14	109.4	65.6	1088.8	9.5	2.32
WT12-31-14	1072	16	1086	11	1080	26	67.2	44.3	1125	13	3.22
WT12-31-15	1023.4	7.6	1025.6	5.4	1041	17	122.3	56.6	1020.2	8.1	1.78
WT12-31-16	1014	12	1036.5	9.4	1098	26	85.1	52	1094	16	2.77
WT12-31-17	1347	11	1351.5	6.6	1379	13	96.1	64	1361.2	8.5	2.25
WT12-31-18	1400	12	1385.9	7.4	1347	24	98.3	74.5	1367.7	8.2	2.3
WT12-31-19	1086.7	7.6	1085.2	6.5	1070	15	106.7	55.1	1076	11	2
WT12-31-20	1096	10	1096.3	6.2	1089	10	283	140.9	1103.3	7.1	1.73
WT12-31-21	1107	14	1108.1	9.6	1155	23	61.2	37.42	1111	17	2.68
WT12-31-22	1038.4	9.6	1040.1	6.7	1085	14	98	53	1044.2	9.3	2.01
WT12-31-23	1351	11	1342.5	6	1352	15	74.3	88.4	1344	10	2.35
WT12-31-24	1399	14	1399.2	8.2	1402	19	74.3	95.5	1402	11	2.49
WT12-31-25	1034	9.8	1038.9	7	828	30	56	30.6	1055	11	2.37
WT12-31-26	1207	11	1209.9	6.2	1220	12	170	137.8	1215	8	1.94
WT12-31-27	2676	27	2676	11	2817	40	44.6	31.3	2678	7.6	3.8
WT12-31-28	1104	11	1108.8	6.7	1094	12	111.8	108.5	1121	10	2.18
WT12-31-29	1187	12	1202.1	8.9	1198	20	23.61	29.95	1234	16	2.95

Appendix C: U/Pb Data

Sample	206/207 (Ma)	2σ (Ma)	207/235 (Ma)	2σ (Ma)	208/232 (Ma)	2σ (Ma)	U (ppm)	Th (ppm)	207/206 (Ma)	2σ (Ma)	Disc. (%)
WT12-31-30	1256.1	9.9	1252.3	6.9	1269	24	97	41.72	1246	11	2.25
WT12-31-31	1503	14	1530.2	9	1617	14	172.1	193.2	1563.2	9.9	2.59
WT12-31-32	1048.6	8.3	1040.8	7	1029	17	72.1	48.8	1030	14	2.15
WT12-31-33	1216	13	1198.8	8.3	1232	12	95	151	1174	12	2.63
WT12-31-34	1296	14	1326	10	1160	52	297	391	1381.6	7.1	2.39
WT12-31-35	1077.8	8.7	1087.3	7	1034	12	166	192	1108.6	9.8	1.92
WT12-31-36	1769	23	1791	11	1454	84	110.5	75	1815.2	8	2.79
WT12-31-37	1190.4	9.1	1183.5	4.8	1182	10	97.1	143.5	1178.3	9.8	1.66
WT12-31-38	1338	11	1343.7	7.7	1349	18	88	61	1342	11	2.22
WT12-32-1	1074	12	1071.3	9.4	1069	28	73	43.9	1055	13	3.02
WT12-32-2	1514	12	1492.3	5.9	1466	18	112.6	102.4	1468	10	2.55
WT12-32-3	1028	11	1023.6	8.3	1020	22	38.9	25.98	1001	17	3.17
WT12-32-4	1097.3	6.7	1099	4.2	1070	10	287	174.3	1093.4	7.4	1.56
WT12-32-5	1000	13	991	13	987	26	23.2	16.9	993	22	4.07
WT12-32-6	1105	11	1111	10	1121	21	44.8	53.9	1092	16	2.98
WT12-32-7	1400	16	1373.4	7.2	1399	30	49.27	27.32	1327	13	3.58
WT12-32-8	1349.7	9.3	1340.9	5.4	1359	12	198.4	253.4	1326	7.4	1.66
WT12-32-9	1137	12	1147.1	9.9	1167	24	29.5	34.66	1169	16	3.27
WT12-32-10	1129	14	1118.9	8.3	1086	24	114.3	63.7	1082	15	2.01
WT12-32-11	1393	12	1383.5	5.5	1376	12	150.3	182.7	1366.3	7.8	2.15
WT12-32-12	1323	17	1335	11	1067	35	102	110.1	1361	11	2.66
WT12-32-13	1041	14	1075	15	1009	26	19.7	17	1133	28	4.46
WT12-32-14	1444	15	1448.7	9.1	1426	21	25.2	46.8	1444	15	3.36
WT12-32-15	1360	12	1402.4	7.6	1241	17	88.3	90.2	1462	10	3.27
WT12-32-16	1087.8	7.3	1092.4	5.7	1087	14	148	106	1101	10	1.79
WT12-32-17	1100.1	9.3	1094	10	1096	19	33.6	29.68	1078	20	3.16
WT12-32-18	2605	32	2651	13	2382	49	51.2	55.4	2678.2	9.3	4.8

Appendix C: U/Pb Data

Sample	206/207 (Ma)	2σ (Ma)	207/235 (Ma)	2σ (Ma)	208/232 (Ma)	2σ (Ma)	U (ppm)	Th (ppm)	207/206 (Ma)	2σ (Ma)	Disc. (%)
WT12-32-19	1456	13	1455.2	8.8	1435	25	52.2	53.3	1461	11	2.5
WT12-32-20	1438	11	1450.9	7	1423	18	72.2	56.3	1468	11	2.6
WT12-32-21	1075.9	8.9	1085.5	8.8	1082	19	67.3	29.4	1113	13	2.71
WT12-32-22	1038	18	1056	12	1001	17	118	90.4	1092	12	2.64
WT12-32-23	1433	15	1453	11	1457	24	32.7	28.8	1470	19	3.8
WT12-32-24	1471.8	9.9	1475.6	6.7	1458	20	67.7	84.5	1465	12	2.4
WT12-32-25	1094	11	1069.5	7.2	1034	16	137.4	76.6	1025	10	2.43
WT12-32-26	2701	21	2686.9	8	2665	36	49.3	64.7	2665.3	6.6	3.22
WT12-32-27	1072.5	9.9	1072.7	9.9	1049	21	43.7	42.5	1067	18	2.98
WT12-32-28	1258	12	1256.7	8.4	1220	16	49.2	44.5	1259	13	2.78
WT12-32-29	992	10	987.3	6.2	984	14	79.7	60.3	981	13	2.5
WT12-32-30	1096	14	1075	11	1077	23	34.5	20.98	1030	16	3.57
WT12-32-31	1067.2	9.6	1072.4	6.5	1038	13	84.2	71.4	1068	13	2.51
WT12-32-32	1059	9.6	1061.6	7.6	1037.5	9.5	66	116.4	1062	13	2.55
WT12-32-33	1093.1	8.5	1103.8	9.1	1089	17	54.9	52.7	1118	15	2.93
WT12-32-34	1170.1	9	1165.7	7	1146	21	58.8	39.6	1142	13	2.62
WT12-32-35	1344.1	9.2	1332.2	6.8	1330	18	61.8	79	1318	12	2.18
WT12-32-36	1059.9	7.3	1046.4	4.5	1058	11	250	153.5	1020.9	9.5	1.83
WT12-32-37	1321.2	8.7	1315.8	6.6	1306	13	66.4	73.6	1307.1	9.8	1.98
WT12-32-38	1443	11	1455.9	6	1376	17	96.2	120.2	1469	7.6	2.11
WT12-32-39	1186	11	1180	7.3	1130	15	62	55.9	1164	11	2.53
WT12-32-40	1143.3	7.2	1138.4	4.8	1102.9	9.2	221	292	1128.4	6.4	1.37
WT12-32-41	1335	12	1318.4	9.7	1332	21	52.4	47	1295	12	2.78
WT12-35-12	1085	11	1097.9	8.6	1067	12	147.3	151.6	1115	13	2.14
WT12-35-22	2426	28	2575	12	2695	33	32.1	67	2694	12	8.1
WT12-35-32	2586	28	2648	13	2415	47	49.4	69	2700.9	8.3	4.68
WT12-35-42	1490	17	1599	11	1562	36	128.4	121.9	1755	11	6.96

Appendix C: U/Pb Data

Sample	206/207 (Ma)	2σ (Ma)	207/235 (Ma)	2σ (Ma)	208/232 (Ma)	2σ (Ma)	U (ppm)	Th (ppm)	207/206 (Ma)	2σ (Ma)	Disc. (%)
WT12-35-52	2694	27	2777	11	2779	49	29.1	25.9	2842.6	9.6	5.81
WT12-35-62	2673	25	2778	12	2821	49	31.9	18.81	2844.9	8.7	6
WT12-35-72	2545	32	2647	12	2437	60	18.6	15.9	2710	11	5.86
WT12-35-82	2606	23	2673	11	2414	50	43.7	21.4	2729	11	4.91
WT12-35-92	2145	25	2415	12	2588	33	40.3	62.6	2655	10	15.8
WT12-35-102	2433	36	2588	12	2758	53	55.9	35.9	2710	11	9
WT12-35-112	2532	24	2626.4	9.6	2680	50	110.4	28.14	2691.4	9.4	5.4
WT12-35-122	2198	97	2589	46	2920	230	29.4	26.4	2925	16	23.5
WT12-35-132	2088	40	2402	15	2352	32	39.8	130.1	2685	14	19.1
WT12-35-142	2576	35	2660	14	2642	34	30.8	57.4	2721.3	9.1	5.3
WT12-35-152	1766	23	1794	11	1855	30	44.1	123.4	1829	14	4.29
WT12-35-162	2616	25	2664	11	2809	31	59.4	81.1	2698	11	4.95
WT12-35-172	1544	33	1671	16	1682	43	30.6	15.77	1839	16	8.3
WT12-35-182	1781	22	1803	12	1757	26	74.1	71.2	1835	11	3.02
WT12-35-192	2642	26	2683.7	9.7	2681	27	76.8	165	2718	8.6	4.33
WT12-35-202	2627	23	2812.5	9.4	2673	37	68.9	38.6	2952.3	6.7	10.8
WT12-35-212	1637	44	2165	27	1240	51	131	205	2675	14	34.3
WT12-35-222	2391	22	2561.8	9.8	2545	30	51.1	88.6	2698.2	6.1	9.5
WT12-35-232	2788	23	2815.8	9.1	2904	42	107	38.3	2835	8	3.55
WT12-35-242	2443	32	2592	14	2476	47	34.8	44.6	2724	12	8.8
WT12-35-262	1856	21	1866.8	9.4	1673	40	73.5	66.1	1885	12	3.53
WT12-35-272	2654	28	2702	12	2760	50	69.4	95.4	2732.6	7.7	4.04
WT12-35-282	1600	22	1664	12	1696	41	20.29	15.64	1756	18	5.7
WT12-35-292	2514	39	2627	15	2446	61	21.9	16.41	2711	12	7.2
WT12-35-302	2621	23	2626.1	8.7	2622	29	121.4	81.9	2633.7	7.8	3.54
WT12-35-312	2722	20	2707	8.4	2744	29	78.1	153.3	2688	9.3	3.24
WT12-35-322	2519	27	2623	12	2763	36	82.5	121.8	2699	9.8	6.39
WT12-35-332	2697	37	2689	15	2784	46	55.6	170	2690.3	7.8	4.75

Appendix C: U/Pb Data

Sample	206/207 (Ma)	2σ (Ma)	207/235 (Ma)	2σ (Ma)	208/232 (Ma)	2σ (Ma)	U (ppm)	Th (ppm)	207/206 (Ma)	2σ (Ma)	Disc. (%)
WT12-35-342	3334	34	3358	19	3290	110	40.7	17.77	3374	17	4.35
WT12-35-352	2699	33	2721	11	1790	140	28.7	64.8	2728	11	5.25
WT12-35-362	2680	23	2687	7.9	2718	26	100.4	123.8	2700.9	5.5	3.24
WT12-35-372	2533	34	2632	15	2746	44	66.2	65.3	2715.9	9.2	6.5
WT12-37-22	1717	36	1718	22	1270	100	567	24.4	1726	10	1.58
WT12-37-22	2263	48	2333	26	2481	48	107	119	2410	10	5.2
WT12-37-32	1309	17	1463.4	8.9	2590	120	294	12.81	1692	12	10.29
WT12-37-42	2368	26	2388.8	8.5	2323	30	127.1	156.6	2413.9	6.9	3.45
WT12-37-52	1879	37	2077	21	1973	55	63.1	47.1	2284	13	11.6
WT12-37-72	1103	30	1455	24	2136	89	88.4	28.6	2036	19	26.9
WT12-37-82	2390	21	2422.3	7.7	2335	25	257	358	2455.1	6.7	3.13
WT12-37-92	1812	35	1821	16	2482	83	346	35	1814	29	3.33
WT12-37-92	2186	26	2281	11	2396	41	89	76.3	2369	15	5.47
WT12-37-102	2163	40	2256	19	2537	68	51.3	39.4	2323	14	5.7
WT12-37-112	1862	47	2071	27	2259	43	146.9	127.2	2299	14	12.2
WT12-37-122	2434	33	2431	13	2576	49	83.2	109.3	2433	13	4.28
WT12-37-132	2382	28	2403.8	9.8	2338	23	132.1	200.4	2428	10	4.22
WT12-37-142	1953	29	2156	16	2021	29	86.7	95.8	2349.8	8	11.6
WT12-37-152	1448	44	1806	29	2027	72	34.6	26.1	2301	18	24.5
WT12-37-162	1878	51	2113	34	2448	47	107.7	93	2348	20	13
WT12-37-172	2240	22	2325	11	2311	29	57.9	62	2406	12	5.13
WT12-37-182	1599	31	1659	11	2030	110	587	23.9	1773	41	4.7
WT12-37-182	2388	25	2415	10	2399	40	91	114	2447.2	8.9	3.17
WT12-37-192	1580	28	1624	14	1790	110	444	24	1699	11	3.73
WT12-37-202	2361	25	2396.4	9.6	2036	40	73.6	81.2	2426.7	7.1	3.67
WT12-37-212	1828	32	2077	17	2139	58	81.2	49	2328	16	15.3
WT12-37-232	2364	24	2409.8	9.4	2362	25	232	288	2449	12	3.64

Appendix C: U/Pb Data

Sample	206/207 (Ma)	2σ (Ma)	207/235 (Ma)	2σ (Ma)	208/232 (Ma)	2σ (Ma)	U (ppm)	Th (ppm)	207/206 (Ma)	2σ (Ma)	Disc. (%)
WT12-37-252	2373	46	2414	17	2580	67	37.2	38.5	2454	16	5.2
WT12-37-262	2049	61	2211	32	2757	80	105.1	96	2377	15	9.8
WT12-37-272	2011	35	2125	18	2426	43	89	49.2	2250.7	9.7	7.4
WT12-37-282	2067	80	2201	43	2108	96	60.2	58.8	2347	19	9
WT12-37-292	2136	47	2251	23	2150	42	67.7	65.2	2376.3	9.8	7.2
WT12-37-302	2195	27	2291	13	2014	48	235	241	2380	11	5.79
WT12-37-322	1526	31	1577	20	1650	110	633	9.18	1653	16	3.36
WT12-37-342	2422	32	2421	14	2402	42	50.6	44	2420.6	9.5	3.38
WT12-37-352	2280	34	2351	13	2322	41	131.4	148.2	2426	10	4.9
WT12-37-362	1775	46	2046	24	912	37	31.6	59.4	2363	14	16.8
WT12-37-372	2155	43	2274	21	2387	50	53.6	45.2	2392	13	7.5
WT12-37-382	1797	63	2055	37	2616	98	44.9	21.2	2358	18	17.2
WT12-37-392	2314	35	2382	16	2512	53	105	125	2441.8	9.6	4.7
WT12-37-402	2240	26	2328	14	2350	41	74	58.9	2410	11	4.48
WT12-37-412	1654	38	1698	16	2210	160	574	28.1	1751	12	2.7
WT12-37-412	2405	28	2398	13	2506	31	70.6	72.2	2398	12	3.37
WT12-37-422	1758	26	1741	16	2000	120	486	9.7	1731.5	8.7	1.9
WT12-37-422	2370	27	2404.6	8.9	2299	24	141.9	202.9	2443.7	9.3	3.56
WT12-38-12	2588	28	2618.4	9.4	2752	47	47.3	25.92	2651.9	8.5	4.25
WT12-38-22	2714	28	2692.7	8.1	2797	30	88	198	2673	12	4.74
WT12-38-32	388	8.5	422	10	451	16	27.6	22.43	616	39	7.5
WT12-38-42	2664	27	2729	8.5	2602	45	75.5	70.5	2774.8	8	4.83
WT12-38-52	2330	34	2517	12	2720	59	25.1	22.2	2673.2	9.8	10.5
WT12-38-62	1802	26	1856	12	1911	31	35.9	52.6	1913	13	4.45
WT12-38-72	1367	36	1977	27	2668	42	59.9	54	2689	13	42.8
WT12-38-82	2453	48	2643	22	2010	110	142	161	2800	10	11
WT12-38-92	2627	24	2653.6	8.5	2601	50	141.1	66.7	2675.4	7.5	3.7

Appendix C: U/Pb Data

Sample	206/207 (Ma)	2σ (Ma)	207/235 (Ma)	2σ (Ma)	208/232 (Ma)	2σ (Ma)	U (ppm)	Th (ppm)	207/206 (Ma)	2σ (Ma)	Disc. (%)
WT12-38-102	2619	24	2720	11	2618	40	71.3	84.1	2804.5	8.4	6.16
WT12-38-112	2735	33	2722	10	3039	62	40.3	53	2717	12	4.58
WT12-38-122	2717	47	2711	15	2976	63	40.4	34.5	2703	14	7.2
WT12-38-132	1794	22	1813.3	9.6	2001	41	45.7	21.3	1833	13	3.79
WT12-38-142	2640	31	2684	10	2543	45	79.2	43.5	2717	9.9	5.25
WT12-38-152	2586	26	2649.6	8	2643	28	59.4	111.8	2701.1	8	5.21
WT12-38-162	1747	21	1787	11	1840	35	58.5	50.8	1829	14	4.17
WT12-38-172	2572	32	2654	12	2851	37	31.8	34.2	2713	12	6.1
WT12-38-182	2707	57	2737	23	2812	58	59.8	31	2764	11	6.4
WT12-38-192	1849	31	1831	12	1984	44	111.3	25.6	1827	15	3.93
WT12-38-202	2710	37	2703	14	2996	58	29.4	35.9	2710	9.4	5.14
WT12-38-212	2312	29	2529	13	2645	37	73.5	132.1	2720.3	8.6	12.8
WT12-38-222	2530	33	2588	11	2718	46	56.9	88.3	2647	10	5.6
WT12-38-232	2520	34	2626	11	2785	40	40.7	99.6	2700.9	9.9	6.2
WT12-38-242	2583	31	2656	11	2718	37	27.4	35.2	2718	15	6
WT12-38-252	1478	16	1474.6	8.7	1561	22	80.4	48.4	1476	12	3.07
WT12-38-262	2584	23	2673.8	9.5	2595	35	53.4	38.8	2744	9.9	5.38
WT12-38-272	1838	26	1838	13	1866	35	203	150	1850	12	3.48
WT12-38-282	2695	26	2708.7	9.9	2826	36	57.7	45.1	2728	11	4.48
WT12-38-292	2665	27	2664.5	9.6	2756	26	73.1	155.1	2658.6	8.7	4.42
WT12-38-302	2684	27	2690.8	9.4	2817	31	75.3	155	2699.6	8.1	3.98
WT12-38-312	2641	32	2678	12	2795	44	84.1	81.5	2706	11	5.37
WT12-38-322	2697	25	2710.4	8.9	2779	37	74.6	110.6	2729.7	8	3.97
WT12-40-1	1649	15	1674.5	7.1	1605	20	66.4	56.7	1704.8	9.8	2.92
WT12-40-2	1612	16	1638.7	9.9	1654	19	44.9	70.3	1679	12	3.07
WT12-40-3	1690	16	1701	8.8	1700	21	136	53.4	1720	8.8	2.57
WT12-40-4	478.7	6.2	491	11	494.8	7.8	34.41	89.41	581	36	4.62

Appendix C: U/Pb Data

Sample	206/207 (Ma)	2σ (Ma)	207/235 (Ma)	2σ (Ma)	208/232 (Ma)	2σ (Ma)	U (ppm)	Th (ppm)	207/206 (Ma)	2σ (Ma)	Disc. (%)
WT12-40-5	1683	23	1707	12	1656	73	13.96	5.13	1748	16	4.66
WT12-40-6	494.3	6.1	500.1	5.6	507.4	5	85.5	172.5	540	18	2.55
WT12-40-7	1681	15	1664.6	7.3	1686	20	83	77	1670.1	8.9	2.65
WT12-40-8	1688	16	1693.7	7.5	1697	23	67.7	82.7	1701	10	2.52
WT12-40-9	490.4	5.6	495.5	5.4	492.5	9	61.1	61.9	543	18	2.8
WT12-40-10	1711	20	1703	10	1781	19	320	74.5	1709	7.2	2.77
WT12-40-11	483.8	7.4	493	10	548	18	22.3	17	583	42	5.17
WT12-40-12	1163	15	1336	8	1384	23	988	229	1625.8	6.7	12.14
WT12-40-13	490.5	6.5	495.8	6.3	515.8	7.8	81.1	181	498	25	3.32
WT12-40-14	485.4	6.6	495.4	8.5	526	11	52.2	38.5	533	26	3.33
WT12-40-15	463.2	7.8	471.9	8.8	529	15	32	27.1	496	32	4.16
WT12-40-16	507.1	6.6	502.4	5.6	511.2	5.6	77.7	205	505	21	2.73
WT12-40-17	1733	17	1718.4	8.2	1783	19	159.8	104.4	1710.1	7.7	2.6
WT12-41-12	465.1	8.1	479	11	492	13	44.2	34.21	536	32	5.05
WT12-41-22	472.4	5.8	491.6	6.8	453	12	97	78.9	582	32	4.31
WT12-41-32	459.6	8.1	488	11	500	15	43.9	78.7	624	36	6.5
WT12-41-42	473.2	6.3	495.6	7.8	505	10	78	67.7	587	23	4.39
WT12-41-52	1417	12	1418.2	7.3	1431	17	177	163	1421	12	2.45
WT12-41-62	469.8	6.2	479.5	9.3	473.3	7.4	47.1	91.2	521	40	4.67
WT12-41-72	1683	26	1696	14	1754	34	82	42.8	1708.4	9.5	3.79
WT12-41-82	492.7	7.6	517.2	8.2	522.1	7.2	116.2	330	625	22	4.34
WT12-41-92	517.5	5.6	520.3	4.3	486.9	7.5	299	248	535	22	2.55
WT12-41-102	477.6	6.2	483.9	6	468	9.3	108.4	155.6	497	22	2.61
WT12-41-112	2673	25	2701.1	9	2664	47	97	33.5	2724.9	8.2	3.86
WT12-41-122	476.5	9	496	12	487	18	35.8	38.1	558	35	4.84
WT12-41-132	1715	15	1703.4	9.3	1597	30	44.1	36.72	1678	12	3.22
WT12-41-142	503	11	518	14	527	22	27.2	24.3	592	33	4.78

Appendix C: U/Pb Data

Sample	206/207 (Ma)	2σ (Ma)	207/235 (Ma)	2σ (Ma)	208/232 (Ma)	2σ (Ma)	U (ppm)	Th (ppm)	207/206 (Ma)	2σ (Ma)	Disc. (%)
WT12-41-152	1663	17	1686	11	1606	17	90	152	1710.8	9.1	3.05
WT12-41-162	1698	16	1714.7	9.2	1605	21	94.4	119.9	1727	11	2.84
WT12-41-172	1391	11	1418	7.4	1343	22	65.8	43.6	1459	11	3.15
WT12-41-182	1366	15	1393.1	8.5	1339	15	144	197	1423.3	9.7	2.96
WT12-41-192	1642	14	1659.5	7.5	1586	20	154	180	1678.8	9.6	2.41
WT12-41-202	1644	21	1665	11	1278	39	73.9	21.65	1688	12	3.28
WT12-41-212	481.4	7.8	493.6	9.2	462	10	71.5	67.3	563	35	3.81
WT12-41-222	486.7	9.1	497	7.7	473	12	87.3	71.9	549	30	3.83
WT12-41-232	1662	22	1673	13	1630	23	82.7	74.9	1698	15	3.35
WT12-41-242	458.7	9.7	457	16	466	18	39	43.3	474	42	5.6
WT12-41-252	1536	26	1617	14	840	51	66.8	56.8	1718	13	5.72
WT12-41-262	496	19	522	11	477	20	108.4	111	603	39	3.2
WT12-41-272	467.9	9.7	475.3	8.7	491	13	50.5	51.1	549	34	4.48
WT12-41-282	472.6	8.3	481.3	8.8	487	11	141	136	544	32	4.31
WT12-41-292	485	7.1	507	10	470	10	64.5	94	614	30	4.57
WT12-41-302	493	12	504	11	460	11	130	152	540	19	3.02
WT12-41-312	1695	28	1697	13	1639	33	92.7	82.6	1709	16	4.14
WT12-41-332	463.6	8.6	464.8	7.3	454.2	9.6	62.8	100.9	469	27	3.19
WT12-41-342	509	11	508	11	486	14	76.7	68.2	481	24	3.86
WT12-41-352	480.8	6	479.9	7.2	456.9	7.8	76.3	136.1	495	27	3.25
WT12-41-362	1444	16	1550.9	9.5	1592	26	80.9	69.3	1709	11	6.82
WT12-41-372	535	11	532.4	9.2	519.4	8.8	215	179	525	20	2.52
WT12-41-382	495.2	6.1	503.1	6.6	487.4	7.2	96.9	163.1	547	25	3.14
WT12-41-392	1704	26	1702	14	1755	21	215	82.3	1705.3	8.3	3.38
WT12-43-1	2336	35	2395	15	2279	40	213	185	2444.4	6.2	4.74
WT12-43-2	2311	22	2389.7	8.4	1784	35	111	153	2452.2	7.1	4.54
WT12-43-3	1199	23	1787	18	1184	31	170	419	2571.2	9.3	43.4

Appendix C: U/Pb Data

Sample	206/207 (Ma)	2σ (Ma)	207/235 (Ma)	2σ (Ma)	208/232 (Ma)	2σ (Ma)	U (ppm)	Th (ppm)	207/206 (Ma)	2σ (Ma)	Disc. (%)
WT12-43-4	2586	18	2611.9	7.5	2518	25	287	669	2631.1	4	2.74
WT12-43-5	2364	27	2496	10	2180	100	173	260	2600.5	8.4	7.3
WT12-43-6	2396	19	2515.2	8.3	2257	24	207.5	438	2609.3	5.3	6.23
WT12-43-7	1910	29	2242	19	1675	51	414	254.4	2561.1	8.1	20.01
WT12-43-8	2580	25	2651	11	2398	29	368	299	2695.6	6.2	4.15
WT12-43-9	1631	25	2084	15	1534	31	522	904	2554	14	28.9
WT12-43-10	1342	21	1817	14	1217	38	483	1069	2399.6	6.4	32.94
WT12-43-11	858	14	1073	11	211	13	1001	1004	1553	12	18.25
WT12-43-12	2398	19	2418	10	2362	20	98.5	131.4	2435.7	8.6	2.61
WT12-43-13	2567	27	2580	11	2332	66	225	129.8	2605.5	6.8	3.15
WT12-43-14	2451	16	2450.3	6.1	2319	21	68.6	88.6	2455.7	5.2	2.48
WT12-43-15	2566	18	2595.7	7.1	1505	57	318	207.3	2616.3	5.3	2.49
WT12-43-16	2607	14	2610.3	6.2	2547	36	219.1	357	2610.8	3.8	2.05
WT12-43-17	2383	24	2495	11	2445	34	200	363	2582.7	8.5	5.91
WT12-43-18	2578	23	2592.9	8.3	2495	25	114.4	291	2606.8	4.5	3.21
WT12-43-19	2518	22	2512.6	9.4	2272	74	80.5	114.7	2504.7	8.1	2.74
WT12-43-20	1925	33	2172	20	1888	23	361	890	2406.9	9	15.11
WT12-43-21	1283	20	1432	12	1014	34	557	49.1	1663	11	10.56
WT12-45-1	1126	22	1233	37	1450	100	30.9	19.4	1479	64	10.4
WT12-45-2	1095	14	1103.1	7.2	1072.3	9.9	137	180	1118.7	8.7	2.68
WT12-45-3	1051	11	1049.8	7.7	1030	14	48.2	51.5	1059	12	2.6
WT12-45-4	1156	11	1180.2	7.5	977	20	100.7	71.8	1222.7	8.2	2.36
WT12-45-5	1375	12	1396.7	5.7	1410	11	126.6	145.3	1433.1	8.1	2.43
WT12-45-6	1428	15	1444.9	8.2	1367	15	83.9	69.7	1461	8.9	2.35
WT12-45-7	1290	12	1312.3	7.6	1258	13	73.6	60.8	1345	10	2.78
WT12-45-8	1041.3	9.5	1057	7.6	1089	19	56.8	27.4	1096	16	2.49
WT12-45-9	1187	21	1272	14	758	64	138.4	269	1421.4	9.1	6.12

Appendix C: U/Pb Data

Sample	206/207 (Ma)	2σ (Ma)	207/235 (Ma)	2σ (Ma)	208/232 (Ma)	2σ (Ma)	U (ppm)	Th (ppm)	207/206 (Ma)	2σ (Ma)	Disc. (%)
WT12-45-10	992	27	1024	21	943	36	254	129	1101	10	3.5
WT12-45-11	1010.5	8.7	1028.7	6.3	927	41	275	149	1073	14	2.1
WT12-45-12	1334	13	1392.3	8	1330	16	67.2	70.6	1481	10	3.83
WT12-45-13	1367	16	1415.4	8.3	1386	18	34.5	35.91	1491	13	3.86
WT12-45-14	1384	10	1387.1	7.2	1344	17	65.2	73.5	1400	11	2.28
WT12-45-15	1730	23	1748	13	1696	15	108.3	87.8	1770	9.6	3.41
WT12-45-16	1051.3	7.2	1061.2	5.3	1018	11	168	138	1083.5	9.6	1.83
WT12-45-17	956.7	6.4	976.3	7.1	962	13	117	81.6	1022	16	2.43
WT12-45-18	1365	11	1367.5	5.7	1337	10	85.7	211	1375	11	2.37
WT12-45-19	1386	12	1424.5	9.1	1408	15	65.2	71.7	1486	12	3.48
WT12-45-20	1597	15	1664.9	7.3	1494	31	121.5	109.9	1749.4	9.3	4.24
WT12-45-21	1288	13	1347	7.4	1096	35	263	369	1453.6	6.2	3.97
WT12-45-22	1059	8	1098.1	6.5	1157	18	74.8	34.3	1177.3	8.3	3.01
WT12-45-23	1080	11	1087.2	6.5	1136	14	134.1	88.4	1107	10	2.18
WT12-45-24	1089	11	1088.7	8.1	1071	18	49	43.1	1079	15	2.69
WT12-45-25	1068.7	9.5	1094.3	7	1083	16	67.3	38.3	1138	12	2.37
WT12-45-26	996.5	9.6	1012.2	6	1015	12	65.2	59.2	1039	10	2.7
WT12-45-27	1639	14	1724.6	8.1	1717	32	69.8	19.59	1821.8	8.4	4.88
WT12-45-28	1479	12	1481.5	6.8	1528	19	339	59.6	1483.1	8	2.21
WT12-45-29	1001.8	8.4	1014.6	4.2	970.3	9.5	228	92.7	1046.3	9.2	2.01
WT12-45-30	1036	11	1054.4	6.1	1084	10	119	91	1092.2	8.6	2.2
WT12-45-31	1061	10	1084.3	7.1	1080	18	81.1	33.1	1127	10	2.75
WT12-45-32	1223	14	1287.4	9.6	924	32	298	424	1390.1	9.6	4.32
WT12-45-33	1164	15	1144.6	7.2	1214	20	166	74	1100	11	3.3
WT12-45-34	1375	23	1415	10	1459	22	109	74.7	1483	12	4.41
WT12-45-35	1408.4	9.3	1433.5	6.5	1424	15	75.7	48.4	1466.5	9.8	1.87
WT12-45-36	1225	11	1259.3	6.9	1282	16	43.2	30.83	1318	11	2.86
WT12-45-37	1533	19	1586	11	1607	30	201	152	1673	12	3.96

Appendix C: U/Pb Data

Sample	206/207 (Ma)	2σ (Ma)	207/235 (Ma)	2σ (Ma)	208/232 (Ma)	2σ (Ma)	U (ppm)	Th (ppm)	207/206 (Ma)	2σ (Ma)	Disc. (%)
WT12-45-38	1138	10	1137.6	6.2	1135	20	77.6	37.9	1132	12	2.34
WT12-46-1	1743	13	1761.8	5	1826	18	166	159	1787.7	6.8	2.28
WT12-46-2	1772	12	1782.4	5.9	1833	17	283	87.9	1786.3	6.2	1.98
WT12-46-3	2481	29	2563	14	1924	96	180	130.1	2634	4.7	5.33
WT12-46-4	2647	18	2629.4	6.9	2717	41	221.9	314	2610.6	5.1	2.81
WT12-46-5	1754	12	1763.6	6	1798	17	111.5	111	1769.5	8.3	2.38
WT12-46-6	1798	13	1781.6	7.1	1810	27	60.6	67.4	1763.7	7.5	2.65
WT12-46-7	1718	17	1740.9	8.6	1935	24	69.7	77.6	1764.6	9.1	2.86
WT12-46-8	1832	14	1810.2	8	1897	18	102.3	76.9	1784.3	5.5	2.19
WT12-46-9	1801	20	1794	10	1930	24	266	198	1781	11	2.56
WT12-46-10	1731	13	1752.4	9	1652	37	77.3	53.3	1771.9	7.8	2.39
WT12-46-11	1646.6	9.6	1710.9	5.4	870	33	305.5	342.8	1786.3	6.5	3.9
WT12-46-12	2698	24	2764	12	1800	230	252	250	2808	11	4.54
WT12-46-13	1058	26	1383	23	727	35	930	419	1906	31	23.6
WT12-46-14	1533	23	1638	13	823	27	137.9	185.5	1779.8	8.6	6.67
WT12-46-15	1598	19	1672	11	808	33	424	138.2	1767	11	4.57
WT12-46-16	1943	18	1969.7	7	1746	35	195.3	127.8	1997	10	2.73
WT12-46-17	1897	20	1855.7	8.2	1982	42	287	147.6	1806.4	8.8	3.41
WT12-46-18	1787	16	1782.5	8	1287	49	249.3	58.3	1785.4	5	1.9
WT12-46-19	2790	20	2873	10	2676	41	303	91	2929.1	7.7	4.2
WT12-46-20	1727	13	1756.6	6.1	1623	18	328	118.4	1781.3	4.8	2.31
WT12-46-21	1759	12	1773.5	6.4	1768	37	402	18.95	1787.1	6.9	1.85
WT12-46-22	1718	13	1743	7.5	1842	20	61.4	95.4	1767.8	5.9	2.15
WT12-46-23	1719	12	1751.4	6.4	1787	15	202	249	1783	7.5	2.48
WT12-46-24	2599	22	2626.9	9.3	2505	54	206	177	2647.9	4.4	3
WT12-46-25	1009	13	1022	11	1080	18	35.8	57.2	1040	15	2.49
WT12-46-26	1804	13	1793	6.2	1478	28	346	102	1788.9	6.4	1.86

Appendix C: U/Pb Data

Sample	206/207 (Ma)	2σ (Ma)	207/235 (Ma)	2σ (Ma)	208/232 (Ma)	2σ (Ma)	U (ppm)	Th (ppm)	207/206 (Ma)	2σ (Ma)	Disc. (%)
WT12-47-1	1297	14	1317	11	1227	28	20.8	21	1348	15	2.77
WT12-47-2	1026	14	1026.3	9.9	994	18	341	116	1039	12	2.27
WT12-47-3	1725	20	1771	12	1737	26	112.7	99.6	1837.6	6.3	3.46
WT12-47-4	1043	6.8	1044.6	4.8	1009.9	8.9	305	131.9	1054.3	5.5	1.21
WT12-47-5	1067.2	9.5	1069.3	7.4	1006	18	111.8	30.9	1067.6	8.5	2.08
WT12-47-6	1295	18	1319	12	1243	28	27.1	15.4	1361	15	3.72
WT12-47-7	1090.7	9.4	1076.9	6	1057	19	167	94.2	1049.4	8.3	1.9
WT12-47-8	1013.3	9.3	1017.2	7.1	1003	13	61.1	51	1034	11	2.22
WT12-47-9	1002.6	9.8	1012.1	7.4	1007.4	7.2	159.1	293	1030	10	1.85
WT12-47-10	1018.3	7.8	1019.7	5.9	990	14	94	42.1	1030.3	7.8	1.72
WT12-47-11	840	11	854	12	864	20	34.5	25.1	922	21	3.43
WT12-47-12	1419	14	1431.8	8.9	1486	16	119.1	96	1446.8	9.5	2.2
WT12-47-13	1032.8	8	1046.8	5.4	1007.4	9.5	325	162	1081.2	7.7	2.03
WT12-47-14	965	11	973	16	959	17	39.5	78.7	989	21	3.27
WT12-47-15	978	12	998.5	9.5	1019	17	51.4	33.4	1046	17	2.68
WT12-47-16	1216.9	9.9	1226.4	8.5	1195	18	55.2	52.3	1253	10	2.23
WT12-47-17	1323	13	1328.8	8.4	1259	21	59	37.65	1337	12	2.38
WT12-47-18	1434	18	1439.4	8.8	1390	21	78.5	46.8	1450.7	9.1	2.77
WT12-47-19	1628	21	1669	10	1615	34	45.2	32.2	1714	11	3.58
WT12-47-20	2583	25	2660	11	2605	32	33.1	28.8	2720.2	9.6	4.61
WT12-47-21	1565	13	1598.6	8.4	1552	19	94.2	116.6	1646.9	8.4	2.68
WT12-47-22	880	14	891	9.8	979	13	242	101	930	11	2.32
WT12-47-23	1049	15	1047	12	1053	18	30.1	27.3	1050	16	3.1
WT12-47-24	1048	10	1058.4	7.5	1010	11	125.7	100.6	1074	15	2.31
WT12-47-25	1686	16	1726.1	8.2	1723	17	203	271	1766.7	7.3	2.77
WT12-47-26	1144	13	1127.9	9.1	1137	21	56.8	27.5	1100	14	3.18
WT12-47-27	1017	13	1039.2	9.3	1019	19	103	33	1081	14	3.1

Appendix C: U/Pb Data

Sample	206/207 (Ma)	2σ (Ma)	207/235 (Ma)	2σ (Ma)	208/232 (Ma)	2σ (Ma)	U (ppm)	Th (ppm)	207/206 (Ma)	2σ (Ma)	Disc. (%)
WT12-47-28	1130	10	1153.7	6.7	1167.4	9.3	389	262	1194	6.4	2.17
WT12-47-29	1369	20	1405	12	1463	20	125	70.5	1458.3	9.1	2.98
WT12-47-30	1014	10	1035	11	1112	21	46.6	35.6	1071	15	3.05
WT12-47-31	1025	11	1038.5	5.8	1092	41	176	21.3	1073	11	2.39
WT12-47-32	1095	11	1124.4	7.7	1165	16	40.6	62.7	1186	14	3.53
WT12-47-33	975.6	7.3	987.3	5.2	982	12	183	63.3	1008	11	1.86
WT12-47-34	997.4	9.2	1008.3	6.5	976	12	205	95.8	1018.6	8.1	1.96
WT12-47-35	1148	10	1160.2	5	1139	13	237	96.6	1180.5	9.3	2.33
WT12-47-36	999	13	1005.4	8.4	1000	17	91	56.1	1015	13	2.68
WT12-47-37	1349	15	1353.5	8.4	1283	18	253	78	1358.4	7.7	2.1
WT12-47-38	1181	11	1189.3	8.6	1169	17	55.8	54.6	1220	15	2.99
WT12-47-39	1041	15	1045	11	1037	14	67.8	50.8	1045	17	3.47
WT12-49-1	836	31	891	25	1036	26	63	20.6	1015	13	4.67
WT12-49-2	987	6.7	994.9	4.5	923	10	201	160.4	1009.3	9	1.86
WT12-49-3	1152	11	1165.7	7.1	1140	16	179	94.4	1202	13	2.38
WT12-49-4	1139	12	1143.6	9.5	1075	16	26.9	50.8	1169	18	3.2
WT12-49-5	1155.5	9.9	1155.6	6.5	1088	16	59.3	42.4	1156	12	2.52
WT12-49-6	1122.9	9.4	1132.3	7.3	1083	16	74.2	40.8	1156	10	2.24
WT12-49-7	1445	10	1451.8	7	1374	15	91.6	78.7	1463.6	5.8	1.71
WT12-49-8	1461	10	1460.9	6.1	1387	18	133.5	130.9	1458.4	6.1	1.67
WT12-49-9	935.8	7.7	947.9	5.4	907.2	8.9	336	187.1	968.4	7.9	1.76
WT12-49-10	1135	10	1148.5	6.8	1072	13	50.1	77.6	1168	11	2.58
WT12-49-11	1011.2	8	1029.2	6.9	1142	64	244	20.3	1073	12	1.93
WT12-49-12	1123.7	9.6	1124.5	8.2	1088	12	49.1	49.7	1135	15	2.54
WT12-49-13	1064	18	1079	10	1210	160	241	2.9	1115	11	2.13
WT12-49-14	1339	16	1339.8	9.1	1317	25	121	140	1352	14	2.14
WT12-49-15	1386	12	1407.6	6.6	1351	11	189.5	184	1426.7	9.7	2.43

Appendix C: U/Pb Data

Sample	206/207 (Ma)	2σ (Ma)	207/235 (Ma)	2σ (Ma)	208/232 (Ma)	2σ (Ma)	U (ppm)	Th (ppm)	207/206 (Ma)	2σ (Ma)	Disc. (%)
WT12-49-16	1400	15	1406	11	1314	18	125.2	66.1	1404	11	1.77
WT12-49-17	1149	11	1158.2	6.3	1096	18	63.9	43.5	1182.7	9.2	2.5
WT12-49-18	1419	13	1435.2	7.6	1348	14	123.9	85.6	1452	11	2.35
WT12-49-19	1357.2	9.9	1345.7	6	1288	17	229	121.1	1336.8	7.4	1.87
WT12-49-20	1013	8.1	1009	5.5	953	34	136.1	6.5	995.6	9.9	1.8
WT12-49-21	1047	11	1048.3	6.6	977	10	145.9	110.3	1040.4	8.9	2
WT12-49-22	1447	12	1448.6	6.9	1396	12	204	132.9	1453.1	6.3	1.7
WT12-49-23	1011.1	8.9	1015.1	5.4	971	8.6	108.4	227.7	1021	11	2.08
WT12-49-24	1300	12	1315.5	6.2	1329	13	209.2	136.9	1336.2	7.4	1.97
WT12-49-25	1222	17	1226	14	1235	32	16.12	11.79	1261	23	4.03
WT12-49-26	1033	16	1062	13	1040	19	13.33	26.87	1128	22	4.61
WT12-49-27	994.7	8.7	1003	6.3	1007	11	286	87.6	1026.3	8.1	1.84
WT12-49-28	1136	11	1148.9	8.2	1131	11	76.1	70.4	1161	13	2.51
WT12-49-29	1408	23	1421	13	1487	20	129	93.2	1436.5	9.8	3.21
WT12-49-30	1041	12	1057	11	1035	14	103	124.8	1090	18	3.1
WT12-49-31	1883	17	1914.5	7.8	1898	26	99.9	123.1	1947.4	7.5	2.91
WT12-49-32	1068	11	1071.7	6.6	1048	16	94.1	68.2	1087	13	2.3
WT12-49-33	1007	14	1051	12	1105	18	71.4	54.5	1126	25	4.2
WT12-49-34	1171	16	1201	13	1735	81	111	17.8	1249	16	2.65
WT12-49-35	1060	12	1091.8	8.2	1129	18	61.7	42.9	1161	14	3.09
WT12-49-36	1261	12	1295.6	9.5	1259	13	190	113.9	1346	10	2.55
WT12-49-37	1282	13	1285.7	9.4	1325	21	70.3	54.6	1295	16	2.59
EAB10-11-1	1087	10	1083.9	7.5	982	13	89	119.2	1073	10	2.28
EAB10-11-2	1058	10	1065.8	7.9	996	13	75.8	64.3	1086	13	2.42
EAB10-11-3	1042	12	1043.9	8.7	986	18	52.2	50	1041	19	3.08
EAB10-11-4	1394	19	1460	13	1228	44	111.8	42	1560	12	4.19
EAB10-11-5	1024	8.5	1020	5.4	946	11	263	154	1018.1	9.3	1.85

Appendix C: U/Pb Data

Sample	206/207 (Ma)	2σ (Ma)	207/235 (Ma)	2σ (Ma)	208/232 (Ma)	2σ (Ma)	U (ppm)	Th (ppm)	207/206 (Ma)	2σ (Ma)	Disc. (%)
EAB10-11-6	1029.1	9.3	1017.9	6.3	938	11	136.4	136.8	1002	11	2.12
EAB10-11-7	1115.4	8.1	1115.4	4.5	1068	24	311	32.1	1110.7	8.2	1.8
EAB10-11-8	948	13	953	11	896	21	72.6	41.2	954	16	2.69
EAB10-11-9	1087	15	1086	12	1021	21	30.08	43.65	1079	22	3.98
EAB10-11-10	1071	16	1046	13	1006	24	36.9	29.8	1024	16	3.46
EAB10-11-11	1377	15	1347	9.1	1272	16	93.6	112.1	1315.4	8.6	2.71
EAB10-11-12	1782	21	1754	10	1778	23	97.5	98.3	1736	10	3.13
EAB10-11-13	1447	12	1451.1	7.2	1413	16	81.3	94.5	1462.7	7.8	2.25
EAB10-11-14	1175	9.4	1170.9	7.5	1130	13	97.8	53.5	1168.6	9.8	2.39
EAB10-11-15	1323	14	1349	11	1279	21	120.9	72.3	1399	12	2.25
EAB10-11-16	1137	11	1137.6	7.8	1090	19	74	57.6	1148	12	2.54
EAB10-11-17	1175	12	1167	10	1153	23	26	29.01	1162	17	4.03
EAB10-11-18	1431	11	1442	6.4	1400	17	225.7	91.1	1457.9	7.1	1.85
EAB10-11-19	1072.4	8.7	1069.4	6.9	1047	15	94	79.3	1070	12	2.53
EAB10-11-20	1153	12	1178	13	1148	22	30.4	41.4	1234	24	3.76
EAB10-11-22	1058	11	1058.3	7.4	1010	14	140	76.3	1059.9	8.7	1.94
EAB10-11-23	1224	11	1335	25	1690	100	77.7	45.8	1494	53	7.4
EAB10-11-24	1158	12	1155.6	7.4	1193	23	58.2	41.7	1155	13	2.73
EAB10-11-25	1083	11	1119	12	1048	21	85.3	68.5	1190	22	3.39
EAB10-11-26	991	11	1021.5	9.1	949	23	92	40.3	1091	15	3.41
EAB10-11-27	1157	10	1185.4	6	1142	20	132.5	109.8	1236	12	2.25
EAB10-11-28	1313	11	1314.2	8.9	1339	22	45.4	55.4	1318	13	3.16
EAB10-11-29	1109	14	1115	12	1016	37	49.2	49.3	1116	21	3.11
EAB10-11-30	948	19	992	15	613	38	83.4	165	1094	15	4.07
EAB10-11-31	1425.7	9.8	1437.9	7	1445	18	82.4	49	1457.6	9.6	2.49
EAB10-11-32	2597	18	2636.1	6.9	2743	36	66.2	58.8	2670.4	6.2	3.03
EAB10-11-33	1109	12	1120	8.5	804	46	68.3	42.1	1150	22	3.42
EAB10-11-34	1134	19	1110	14	1011	98	99.7	61	1060	17	3.04

Appendix C: U/Pb Data

Sample	206/207 (Ma)	2σ (Ma)	207/235 (Ma)	2σ (Ma)	208/232 (Ma)	2σ (Ma)	U (ppm)	Th (ppm)	207/206 (Ma)	2σ (Ma)	Disc. (%)
EAB10-11-35	1154	34	2210	130	2140	140	21.1	71	3390	190	87.5
EAB10-11-36	1155.3	7.7	1152.1	5	1161	19	253	55.8	1158	11	1.93
EAB10-11-37	1019	13	1158	19	1128	39	32.9	36.4	1450	57	10.8
CAT-23-1	2055	23	2365	11	2070	48	263	296	2628.1	7.8	18.1
CAT-23-2	1756	21	1801	10	1475	43	361	162.9	1871	11	3.96
CAT-23-3	3035	48	3137	47	6180	440	15.14	15.76	3198	48	6.62
CAT-23-4	1806	50	2676	25	3290	230	177.8	227	3403	30	61
CAT-23-5	1326	20	1723	26	773	36	180.8	486	2226	35	26.5
CAT-23-6	1826	19	1837.9	8.9	1800	24	52.1	30.2	1846.7	9.9	3.32
CAT-23-7	1475	15	1479.4	9.8	1424	19	118.8	106.6	1478	15	2.98
CAT-23-8	1737	16	1777	10	1769	35	72.8	78.9	1829	17	3.7
CAT-23-9	2514	40	2776	33	4220	330	174	230	2973	33	13.9
CAT-23-10	1793	35	1836	20	2125	51	200	244	1885.1	9.8	3.88
CAT-23-11	1991	32	2331	16	2258	84	182	179	2649.9	5.6	20.3
CAT-23-16	1922	19	1930	17	2860	170	119.5	35.7	1931	28	3.67
CAT-23-17	2570	30	2616	11	2695	24	138.7	212	2642.8	5.8	3.5
CAT-23-14	1796	23	2026	52	3210	270	86.9	50.2	2231	84	12.9
CAT-23-15	476	15	993	23	317	18	978	1013	2427	19	55.66
CAT-23-16	741	24	1405	27	827	22	594	1191	2586	30	56
CAT-23-18	2622	20	2645.5	8.8	2591	27	61.7	91.8	2670.5	8.1	2.81
CAT-23-19	2319	20	2480.7	8.9	2480	20	105	227	2621.3	6.4	9.26
CAT-23-20	1934	42	1970	51	2640	320	244.7	201.3	2006	59	4.7
CAT-23-21	1930	64	2182	61	3370	190	172.7	155.7	2469	61	18.1
CAT-23-22	1873	30	1860	16	2255	55	170	49.9	1851.1	8.7	3.32
CAT-23-23	3010	51	2974	46	8070	940	84	27.9	2949	45	3.44
CAT-23-24	964	30	2241	32	2130	150	567	920	3822	30	114.5
CAT-23-25	2001	23	2465	16	1038	26	102	196	2875	14	29

Appendix C: U/Pb Data

Sample	206/207 (Ma)	2σ (Ma)	207/235 (Ma)	2σ (Ma)	208/232 (Ma)	2σ (Ma)	U (ppm)	Th (ppm)	207/206 (Ma)	2σ (Ma)	Disc. (%)
CAT-23-26	2528	46	2617	21	1785	99	175.1	129	2691.1	7.5	6.2
CAT-15-1	1111	15	1253	16	1341	28	33.7	32.2	1525	32	10.8
CAT-15-2	2856	34	2806	15	3360	110	18.1	10.72	2768	15	5.38
CAT-15-3	1190	19	1305	19	1619	73	37.57	19.43	1513	40	8
CAT-15-4	1824	18	1800.8	8.7	1839	22	236	80.4	1785.4	8.7	2.63
CAT-15-5	1810	15	1803.5	6.5	1768	20	82.4	79	1797.2	8.6	2.51
CAT-15-6	2263	50	2575	22	2300	49	161	66.5	2834	13	17.9
CAT-15-7	2111	57	2533	73	7440	670	62.9	35.79	2893	79	25.1
CAT-15-8	2709	37	2789	23	3190	120	53.3	57.4	2841	16	5.19
CAT-15-9	1746	24	1789	16	1750	37	22.8	26.4	1842	23	4.87
CAT-15-10	1757	16	1777.1	8.5	1690	20	243	317	1813	10	2.34
CAT-15-11	1779	27	1767	14	1726	24	64.4	59.3	1766.8	9.9	3.7
CAT-15-12	1735	17	1745.6	9.3	1602	27	87	43.2	1765	11	2.94
CAT-15-13	1853	17	1863.5	8.2	1621	55	198	103.3	1885	10	2.92
CAT-15-14	1677	23	1988	20	259	23	210	1552	2311	37	19.6
CAT-15-15	1803	23	1800	11	1731	24	47.7	40.5	1804	14	3.55
CAT-15-16	1955	23	1926	11	1968	39	56.8	44.6	1883	15	3.93
CAT-15-17	2764	34	2753	11	3149	62	27.7	18.84	2743	11	5.05
CAT-15-18	1481	27	1655	20	745	71	262	364	1880	21	11.1
CAT-15-19	1198	13	1230	16	1297	55	123	62.3	1294	32	3.82
CAT-15-20	1826	16	1853	12	1816	31	63.9	108.3	1882	21	3.72
CAT-15-21	1812	18	1833	18	1885	57	69	73.5	1871	33	4.46
CAT-15-22	1469	14	1467	13	1436	43	44.7	31.3	1472	18	3.06
CAT-15-23	1247	15	1287	16	1333	49	23.2	11.9	1347	32	5.2
CAT-15-24	10490	190	6154	35	4.97E+04	1.40E+03	44	49.1	no value	NAN	88.35
CAT-15-25	1837	19	1841	12	1971	64	65	32.7	1840	15	3.65
CAT-15-26	2813	29	2728	15	2899	83	29.9	45.1	2666	11	5.15

Appendix C: U/Pb Data

Sample	206/207 (Ma)	2σ (Ma)	207/235 (Ma)	2σ (Ma)	208/232 (Ma)	2σ (Ma)	U (ppm)	Th (ppm)	207/206 (Ma)	2σ (Ma)	Disc. (%)
CAT-15-27	2810	22	2737	7.8	2868	50	153	106.9	2681.7	6	4.36
CAT-15-28	1768	18	1832	20	2021	56	36.4	40.5	1920	53	6.8
CAT-15-29	1824	13	1812.4	9	1775	27	54.1	58.2	1802.9	8.8	2.63
CAT-15-30	2473	31	2764	25	1690	250	134.1	730	2982	28	16
CAT-15-31	1928	15	1924	15	2112	85	187.8	120.2	1935	28	3.25
CAT-15-32	1547	49	1708	48	1770	330	349	150	1928	37	11.5
CAT-15-33	1820	11	1904	17	2066	70	92.7	85.6	1991	30	4.82
CAT-15-34	1850	16	1819.4	8	1730	20	93.6	128.8	1785.9	6.8	2.72
CAT-9-1	49.58	0.65	51.7	1.4	51.3	1.5	455	319	260	52	5.51
CAT-9-2	40.61	0.79	48.4	3.1	51.6	3.3	225	297	472	91	11.4
CAT-9-3	49.2	1.2	52.6	2.6	48.5	2.5	103.1	88.5	346	49	8.5
CAT-9-4	1192	11	1185.4	8	1123	15	121	80.2	1173	13	2.27
CAT-9-5	51.53	0.74	61.7	2.5	56.6	2.1	263.2	211.9	560	77	10
CAT-9-6	48.99	0.53	48.9	1	48.4	1.2	538	240.7	121	24	4.06
CAT-9-7	51.95	0.78	52.5	1.2	53.7	1.3	476	351	163	39	4.46
CAT-9-8	49.04	0.76	51.9	1.8	50.6	2	231.5	185.6	290	52	7
CAT-9-9	50.4	1.3	51.4	2.6	51.6	3.7	91.8	53.7	320	56	9.9
CAT-9-10	61.1	1.3	62.6	1.3	63.3	5.8	1527	54	115	18	2.25
CAT-9-11	48.36	0.68	48.5	2	48	2.5	157.1	120.4	257	62	7.6
CAT-9-12	1022	13	1027	12	1048	25	20.2	13.9	1025	22	3.84
CAT-9-13	48.21	0.51	48.87	0.81	48.87	0.98	773	495	124	19	3.23
CAT-9-14	49.62	0.72	55.3	3	50.3	1.9	197	234.6	504	93	11.1
CAT-9-15	1105.6	8.6	1099.7	6.2	1075	17	63.6	47.7	1085	13	2.39
CAT-9-16	1725	12	1748.6	6.2	1682	18	251	163.6	1774.2	6.2	2.11
CAT-9-17	1773	13	1776.7	4.7	1741	24	469	55.7	1779.4	5.3	2.04
CAT-9-18	1948	27	2335	22	9420	360	11.56	2.46	2678	33	23.3
CAT-9-19	49.1	1.2	61.7	3	65.6	4.4	107	73.3	617	64	13.7

Appendix C: U/Pb Data

Sample	206/207 (Ma)	2σ (Ma)	207/235 (Ma)	2σ (Ma)	208/232 (Ma)	2σ (Ma)	U (ppm)	Th (ppm)	207/206 (Ma)	2σ (Ma)	Disc. (%)
CAT-9-20	1173	10	1185.3	7	1171	18	53.6	33.9	1224	12	2.71
CAT-9-21	1201.3	7.4	1188.8	4.9	1187.6	9.7	436	318	1167.8	4.9	1.24
CAT-9-22	49.67	0.65	56	1.6	53	1.8	260	208	368	43	7.2
CAT-9-23	1672	12	1665.9	6.4	1649	21	112.3	73.2	1661	10	1.93
CAT-9-24	433	10	452.7	7.1	503	6.6	113.1	142.6	574	37	5.1
CAT-9-25	1243	11	1248	9.3	1292	24	24.72	25.2	1265	17	3.21
CAT-9-26	1112.2	9.1	1104.9	7.4	1112	20	55.6	43.9	1094	11	2.78
CAT-9-27	1417	21	1402	13	1541	83	63	6.09	1406	19	2.97
CAT-9-28	47.6	1.2	51.6	2.7	50.4	2.5	101.7	87.2	290	46	9.6
CAT-9-29	1095	10	1098.8	7.8	1118	13	71.8	90.1	1124	12	2.49
CAT-9-30	1805	13	1789.9	8.4	1784	32	44.5	39.98	1776	12	2.41
CAT-9-31	1191	15	1202	10	1197	38	27.99	14.66	1223	21	3.81
CAT-9-32	1109	14	1122	14	1195	28	67	47.6	1125	22	2.73
CAT-9-33	1336	11	1339.4	9.5	1394	27	32.17	19.96	1360	15	3.12
CAT-9-34	454.1	4.4	461.2	5.2	494	10	271	74.4	495	19	2.06
CAT-9-35	2001	13	2001.3	5.8	1996	16	269	195	2000.7	6.1	1.88
CAT-9-36	50.33	0.84	58.4	3	55.8	2.6	226.4	195.6	496	98	8.6
CAT-9-37	1078	11	1067	7.6	1068	16	45.8	50.9	1051	18	2.75
CD10-55-1	1363	18	1359	10	1321	26	42.6	35.1	1350	20	4.15
CD10-55-2	1072	13	1069	10	1060	27	37.5	18.3	1086	19	3.6
CD10-55-3	1179.9	9	1179.1	6.6	1225	13	122.2	89.2	1181	10	1.89
CD10-55-4	1339	11	1340.2	5.9	1337	21	156.5	60	1349	11	2.33
CD10-55-5	1371	12	1366.4	7.6	1341	17	50.4	72.3	1364	14	3.06
CD10-55-6	1827	13	1849.1	6.7	1853	24	79.9	60.2	1866	12	2.78
CD10-55-7	1407	13	1423.8	8.5	1087	24	48.4	45.1	1461	13	2.87
CD10-55-8	1078	12	1068.7	7.1	1079	15	195.2	64	1045	13	2.86
CD10-55-9	2695	30	2685	11	2368	38	154.9	71.6	2679	10	4.29

Appendix C: U/Pb Data

Sample	206/207 (Ma)	2σ (Ma)	207/235 (Ma)	2σ (Ma)	208/232 (Ma)	2σ (Ma)	U (ppm)	Th (ppm)	207/206 (Ma)	2σ (Ma)	Disc. (%)
CD10-55-10	2667	24	2677.9	7.9	2730	30	37	62.8	2687.2	8.5	3.87
CD10-55-11	1269	14	1268.4	9	1286	16	68.2	50.6	1287.2	9.6	2.73
CD10-55-12	1423	28	1437	16	1407	24	65.4	62.3	1458	17	4.8
CD10-55-13	1078	27	1116	24	1198	42	10.4	10.3	1188	42	8.7
CD10-55-14	1236	21	1231	12	1241	20	49	45.5	1231	14	4.24
CD10-55-15	1063	15	1077	10	1098	21	55.8	29.23	1105	16	3.11
CD10-55-16	2692	24	2700.7	8.8	2734	38	59	40.6	2705.4	5.7	3.85
CD10-55-17	989	11	992.6	7.2	983	15	103.3	64.8	1005	11	2.21
CD10-55-18	1323	18	1385	22	1515	58	18.2	13.05	1482	40	6.6
CD10-55-19	1807	14	1825.3	9	1843	20	57.3	96.1	1858.2	9.3	2.64
CD10-55-20	2426	32	2624	13	1981	39	29.2	30.6	2788	11	11
CD10-55-21	2357	23	2539.7	9.5	1152	25	49.1	111.2	2692.2	7.9	10.2
CD10-55-22	3316	23	3341.6	8.4	3321	28	124.8	139.7	3352.3	7.8	3.8
CD10-55-23	1202	10	1195.8	7.9	1195	16	85.6	49.9	1193	11	2.23
CD10-55-24	1092	13	1090.9	9	1125	23	36.9	28.01	1099	16	3.33
CD10-55-25	1609	12	1626.1	5.8	1567	16	126.8	171.6	1649.2	9.9	2.56
CD10-55-26	1372	13	1370.6	8.2	1362	18	86.6	75.6	1383	12	2.53
CD10-55-27	1340	12	1330	6.9	1295	15	86.3	69.8	1324	14	2.84
CD10-55-28	922	19	950	16	939	28	8.66	12.39	962	30	6.01
CD10-55-29	1202	15	1206	13	1209	26	22.36	22.6	1212	21	3.69
CD10-55-30	1247	10	1246.9	7.5	1246.8	9.2	279	432	1250.4	7.4	1.99
CD10-55-31	1423	23	1435	13	1136	32	113.9	126.6	1457	12	2.99
CD10-55-32	1449	17	1444.1	7.5	1460	17	263	313.8	1451	11	2.49
CD10-55-33	2727	29	2725	13	2842	74	14.66	9.14	2732	12	5.1
CD10-55-34	1112	17	1121	11	1089	42	55.8	59	1140	18	4.11
CD10-55-35	1905	17	1852.7	7.2	1922	22	196.3	34.3	1790.3	9.8	3.81
CD10-55-36	1461	17	1425	10	1523	20	91.1	64	1370.5	9.5	3.26
CD10-55-37	1370	15	1373.7	8.7	1406	20	121.5	75	1375	14	2.86

Appendix C: U/Pb Data

Sample	206/207 (Ma)	2σ (Ma)	207/235 (Ma)	2σ (Ma)	208/232 (Ma)	2σ (Ma)	U (ppm)	Th (ppm)	207/206 (Ma)	2σ (Ma)	Disc. (%)
CD10-55-38	981	14	982.2	9.7	1001	14	91.3	63	985	18	3.09
CD10-55-39	1076	22	1164	14	486	14	113	316	1336	16	6.61
CD10-59-1	1680	47	2148	28	1818	60	245	260	2627	26	30.2
CD10-59-4	2066	70	2496	36	1979	87	228	392	2881	12	27.8
CD10-59-5	2706	25	2698.6	9	2843	25	98.4	147.3	2697.7	7	3.72
CD10-59-7	2303	35	2476	17	830	46	237	277	2635.3	8.5	9.9
CD10-59-9	1456	40	1337	24	1486	83	11.2	7	1176	27	7.7
CD10-59-10	2376	18	2429.1	7.3	2444	27	79.4	77.5	2474.2	8.3	3.72
CD10-59-11	2583	16	2624.1	8.2	2555	58	204	75.5	2653.4	5.3	2.92
CD10-59-12	2374	20	2504.2	8.4	2420	30	182.2	311	2620.9	5.8	7.27
CD10-59-13	2646	17	2616.9	6.5	2747	27	193.1	92.7	2603.3	5.6	2.63
CD10-59-14	1311	44	1992	29	2660	100	63.2	42.4	2806	16	49.3
CD10-59-16	2380	73	2523	31	2290	140	199	460	2624.9	5.7	8.8
CD10-59-17	789	34	1350	41	664	47	414	723	2406	28	48.2
CD10-59-18	2543	24	2519.7	9.5	2583	23	96.8	90.5	2509.8	7.2	3.39

Note: Analyses excluded for grains with age discordance >10%

References

Adriasola, A. C., Thomson, S., Brix, M., Herve, F., and Stockhert, B., 2006, Postmagmatic cooling and late Cenozoic denudation of the North Patagonian Batholith in the Los Largos region of Chile: International Journal of Earth Science, v. 95, p. 504-528.

Allmendinger, R.W., 1992, Fold and thrust tectonics of the western United States exclusive of the accreted terranes: The Geology of North America, v. G-3, p. 583-607.

Armstrong, R. 1968, Sevier orogenic belt in Nevada and Utah: Geological Society of America Bulletin, v. 79, p. 429-458.

Barton, M. D., 1990, Cretaceous magmatism, metamorphism, and metallogeny in the east-central Great Basin, *in* The Nature and Origin of Cordilleran Magmatism, edited by J. L. Anderson, Geological Society of America Memoir 174, p. 283-302.

Bjerrum, C., and Dorsey, R., 1995, Tectonic controls on deposition of Middle Jurassic strata in a retroarc foreland basin, Utah-Idaho trough, western interior, United States: Tectonics, v. 14, p. 962-978.

Braun, J., Beek, P., Batt, G., 2006. Quantitative thermochronology: numerical methods for the interpretation of thermochronological data. Cambridge: Cambridge University Press.

Burchfiel, B., and Royden, L., 1991, Antler orogeny: A Mediterranean-type orogeny: Geology, v. 19, p. 66-69.

Burtner, R., and Nigrini, A., 1994, Thermochronology of the Idaho-Wyoming Thrust Belt During the Sevier Orogeny: A New, Calibrated Multiprocess Thermal Model: American Association of Petroleum Geologists Bulletin, v. 78, p. 1586-1612.

Cashman, P.L., 1992, Structural Geology of the North-eastern Stansbury Mountains, *in* Wilson, J.R., editor, Field guide to geologic excursions in Utah and adjacent areas: Utah Geological Survey Miscellaneous Publication 92-3, p. 171-178.

Camilleri, P., and Chamberlain, K., 1997, Mesozoic tectonics and metamorphism in the Pequop Mountains and Wood Hills region, northeast Nevada: Implications for the architecture and evolution of the Sevier orogen: Geological Society of America Bulletin, v. 109, p. 74-94.

Camilleri, P., Yonkee, A., Coogan, J., DeCelles, P., McGrew, A., and Wells, M., 1997, Hinterland to foreland transect through the Sevier Orogen, Northwest Nevada to North central Utah: structural style, metamorphism, and kinematic history of a large contractional orogenic wedge: Brigham Young University Geological Studies, v. 42, p. 297-309.

Christie-Blick, N., 1982, Upper Proterozoic and Lower Cambrian rocks of the Sheeprock Mountains, Utah: regional correlation and significance: Geological Society of America Bulletin, v. 93, p. 735–750.

Coogan, J.C., 1992, Structural evolution of piggyback basins in the Wyoming-Idaho-Utah thrust belt: Geological Society of America Memoir 179, p. 55-81.

Crittenden Jr., M. C., 1972, Willard Thrust and the Cache Allochthon, Utah: Geological Society of America Bulletin, v. 83, p. 2871-2880.

Cruz-Uribe, A.M., Hoisch, T.D., Vervoort, J.D., Wells, M.L., Mazdab, F.K., 2014, Linking thermodynamic modeling, Lu-Hf geochronology, and trace elements in garnet: New P-T-t paths from the Sevier hinterland: submitted.

Currie, B., 1997, Sequence stratigraphy of nonmarine Jurassic and Cretaceous rocks, central Cordilleran foreland-basin system: Geological Society of America Bulletin, v. 109, p. 1206-1222.

Currie, B., 1998, Upper Jurassic-Lower Cretaceous Morrison and Cedar Mountain Formations, NE Utah-NW Colorado: Relationships Between Nonmarine Deposition and Early Cordilleran Foreland-Basin Development: Journal of Sedimentary Research, v. 68, p. 632-652.

Currie, B., 2002, Structural configuration of the Early Cretaceous Cordilleran Foreland-Basin System and Sevier Thrust Belt, Utah and Colorado: The Journal of Geology, v. 110, p. 697-718.

Damon, P., and Kulp, J., 1957, Alpha-helium ages of pegmatite zircons: Transactions - American Geophysical Union, v. 38, p. 390.

DeCelles, P., Pile, H. T., and Coogan, J. C., 1993, Kinematic history of the Meade thrust based on provenance of the Bechler Conglomerate at Red Mountain, Idaho, Sevier thrust belt: Tectonics, v. 12, p. 1436–1450.

DeCelles, P., 1994, Late Cretaceous-Paleocene synorogenic sedimentation and kinematic history of the Sevier thrust belt, northwest Utah and southwest Wyoming: Geological Society of America Bulletin, v. 106, p. 32-56.

DeCelles, P., Lawton, T., and Mitra, G., 1995, Thrust timing, growth of structural culminations, and synorogenic sedimentation in the type Sevier orogenic belt, western United States: Geology, v. 23, p. 699-702.

DeCelles, P., and Currie, B., 1996, Long-term sediment accumulation in the Middle Jurassic to early Eocene Cordilleran retroarc foreland-basin system: Geology, v. 247, p. 591-594.

DeCelles, P., and Giles, K., 1996, Foreland basin systems: Basin Research, v. 8.2, p. 102-123.

DeCelles, P., 2004, Late Jurassic to Eocene evolution of the Cordilleran thrust belt and foreland basin system, Western U.S.A.: American Journal of Science, v. 504, p. 105-168.

DeCelles, P., and Coogan, J., 2006, Regional structure and kinematic history of the Sevier fold-and-thrust belt, central Utah: Geological Society of America Bulletin, v. 1187/8, p. 841-

864.

Dickinson, W., Klute, M., and Bilodeau, W., 1988, Tectonic setting and sedimentological features of upper Mesozoic strata in southeastern Arizona: Special Paper - State of Arizona, Bureau of Geology and Mineral Technology, v. 5, p. 266-279.

Dickinson, W., and Gehrels, G., 2003, U/Pb ages of detrital zircons from Permian and Jurassic eolian sandstones of the Colorado Plateau, USA: paleogeographic implications: Sedimentary Geology, v. 163, p. 29-66.

Dickinson, W., 2004, Evolution of the North American Cordillera: Annual Review of Earth and Planetary Sciences, v. 32, p. 13-45.

Dodson, M., 1973, Closure temperature in cooling geochronological and petrological systems: Contributions to Mineralogy and Petrology, v. 40, p. 259-274.

Dumitru, T., Gans, P.B., Foster, D., and Miller, E., 1991, Refrigeration of the western Cordilleran lithosphere during Laramide shallow-angle subduction: Geology, v. 19, p. 1145-1148.

Farley, K., 2002, U-Th/He dating: Techniques, calibrations, and applications: Reviews in Mineralogy and Geochemistry, v. 47, p. 819-844.

Farley K.A., Wolf R.A., Silver L.T., 1996, The effects of long alpha-stopping distances on (U-Th)/He ages:
Geochim Cosmochim Acta, v. 60, p. 4223-4229.

Friedrich, A. M., and Bartley, J. M., 2003, Three-dimensional structural reconstruction of a thrust system overprinted by postorogenic extension, Wah Wah thrust zone, southwestern Utah: Geological Society of America Bulletin, v. 115, p. 1473-1491.

Gentry, A., Yonkee, A., Wells, M., and Eleogram, B., 2013, Patterns of Synorogenic Sedimentation and Unroofing History of the Willard-Paris-Mead Thrust Sheet, Sevier Fold-Thrust Belt: Geological Society of America- Abstracts with Programs, v. 45, p. 5.

Giallorenzo, M. A., Wells, M., Stockli, D., 2013, Two exhumation events of the Wheeler Pass thrust sheet in the southern Sevier fold-thrust belt from U-Th/He thermochronology: Abstracts with Programs – 2013 Cordilleran Section Meeting, v. 64.

Giallorenzo, M. A., 2013, Application of (U-Th)/He and $^{40}Ar/^{39}Ar$ Thermochronology to the age of thrust faulting in the Sevier orogenic belt: University of Nevada, Las Vegas, Ph.D. Dissertation, 270 p.

Guenthner, W., Reiners, P., Ketcham, R., Nasdala, L., and Giester, G., 2013, Helium Diffusion in Natural Zircon: Radiation Damage, Anisotropy, and the Interpretation of Zircon U-Th/He Thermochronology: American Journal of Science, v. 313, p. 1-54.

Hager, C., and Stockli, D., 2009, A New Matlab©-Based Helium Modeling Package (HeMP) for Thermal History Recovery from Single and Multi-Thermochronometer U-Th/He Data and

Data Arrays: Geological Society of America- Abstracts with Programs, v. 487, p. 186-8.

Heller, P., Bowdler, S., Chambers, H., Coogan, J., Hagen, E., Shuster, M., et al., 1986, Time of initial thrusting in the Sevier orogenic belt, Idaho-Wyoming and Utah: Geology, v. 14, p. 288-291.

Hoisch, T., Wells, M., Beyene, M., Styger, S., and Vervoort, J., 2014, Jurassic thrust burial in the Cordilleran retroarc: Linking pressure-temperature paths and Lu-Hf garnet geochronology in the Funeral Mountains, California: Geology, in press.

Hoisch, T., Wella, M., Beyene, M., Kelly, E., and Wills, M., 2013. Unraveling the history of crustal thickening in the Sevier orogenic belt with Lu-Hf garnet geochronology and pressure-temperature paths from metamorphic rocks: Geological Society of America Abstracts with Programs, v. 125, p. 211.

Hourigan, J.K., Reiners, P.W., and Brandon, M.T., 2005, U-Th zonation-dependent alpha ejection in (U-Th)/He chronometry: Geochimica et Cosmochimica Acta, v. 69, p. 3349-3365.

Hudec, M.R., 1992, Mesozoic structural and metamorphic history of the central Ruby Mountains metamorphic core complex, Nevada: Geological Society of America Bulletin, v. 104, p. 1086–1100.

Jordan, T., 1981, Thrust loads and foreland basin evolution, Cretaceous, western United States: American Association of Petroleum Geologists Bulletin, v. 65, p. 12.

Kelly, E., Hoisch, T., Wells, M., and Vervoort, J., 2013, Early Cretaceous Valanginian Crustal Thickening in the Sevier Hinterland from Garnet P-T Paths and Lu-Hf Garnet Geochronology: Geological Society of America Abstracts with Programs, v. 125, p. 211.

Ketcham, R. A., 1996, Distribution of heat-producing elements in the upper and middle crust of southern and west central Arizona: Evidence from the core complexes: Journal of Geophysical Research, v. 101, p. 611-632.

Ketcham, R.A., 2005, Forward and Inverse Modeling of Low-Temperature Thermochronology Data: Reviews in Minerology and Geochemistry, v. 58, p. 275-314.

Lacey, A., Wells, M., Hoisch, T., and Vervoort, J., 2013, Early Eocene Metamorphism in the Sevier Hinterland Constrained by Lu-Hf Garnet Geochronology: Geological Survey of America: Abstracts with Programs, v.45, no. 6, p. 71.

Lawton, T., and Trexler, J.H., 1991, Piggyback basin in the Sevier orogenic belt, Utah: Implications for development of the thrust wedge: Geology, v. 19, p. 827-830.

Lee, J., Hager, C., Wallis, S., Stockli, D., Whitehouse, M., Aoya, M., et al., 2011, Middle to late Miocene extremely rapid exhumation and thermal reequilibration in the Kung Co rift, southern Tibet: Tectonics, v. 30, p. TC002745.

McGrew, A. J., 1992, Tectonic evolution of the northern East Humboldt Range, Elko County,

Nevada [Ph.D. dissert]: Laramie, University of Wyoming, 191 p.

McGrew, A., Peters, M., and ,Wright, J., 2000, Thermobarometric constraints on the tectonothermal evolution of the East Humboldt Range metamorphic core complex, Nevada: Geological Society of America Bulletin, v. 112, p. 45-60.

Miller, D., and Hoisch, T., 1995, Jurassic Tectonics of Northern Nevada and Northwestern Utah from the Perspective of Barametric Studies: Geological Society of America Special Paper, v. 299, p. 267-294.

Miller, E., Gans, P., and Wright, J., 1988, Metamorphic History of the East-Central Basin and Range Province; Tectonic Setting and Relationship to Magmatism: Rubey, v. 7, p. 649-682.

Naeser, C. W., Bryant, B., and Crittenden, M. D., 1983, Fission-track ages of apatite in the Wasatch Mountains, Utah: An uplift study: Geological Society of America Memoir 157, p. 29-36.

Nasdala, L., Reiners, P., Garver, J., Kennedy, A., Stern, R., and Balan, E., 2004, Incomplete Retention of Radiation Damage in Zircon from Sri Lanka: The American Minerologist, v. 89, p. 219-231.

Platt, J. P., and England, P., 1993, Convective removal of lithosphere beneath mountain belts: Thermal and mechanical consequences: American Journal of Science, v. 293, p. 307-336.

Poole, F. G., Steward, J. H., Palmer, A. R., Sandberg, C. A., Madrid, R. J., Ross, R. J., Jr., Hintze, L. F., Miller, M. M., and Wrucke, C. T., 1992, Latest Precambrian to latest Devonian time; development of a continental margin, *in* Burchfiel, B. C., Lipman, P. W., and Zoback, M. L., editors, The Cordilleran Orogen: Conterminous U.S.: Geological Society of America, The Geology of North America, v. G-3, p. 9–56.

Rahl, J. M., McGrew, A. J., and Foland K. A., 2002, Transition from contraction to extension in the northeastern Basin and Range: New evidence from the Copper Mountains, Nevada: Journal of Geology, v. 110, p. 179–194.

Reiners P.W., Farley K.A., and Hickes H.J., 2002, He diffusion and (U-Th)/He thermochronometry of zircon: Initial results from Fish Canyon Tuff and Gold Butte: Tectonophysics, v. 349, p. 247-308.

Reiners, P., 2005, Zircon (U-Th)/He Thermochronometry: Reviews in Mineralogy and Geochemistry, v. 58, p. 151-179.

Royden, L., 1993, The tectonic expression of slab pull at continental convergent boundaries: Tectonics, v. 2, p. 303-325.

Royse Jr., F., 1993a, An overview of the geologic structure of the thrust belt in Wyoming, northern Utah, and eastern Idaho: Geological Survey of Wyoming, v. 5, p. 272-311.

Royse Jr., F., 1993b, Case of the phantom foredeep: Early Cretaceous in west-central Utah:

Geology, v. 21, p. 133-136.

Royse Jr., F., Warner, M., and Reese, D., 1975, Thrust belt structural geometry and related stratigraphic problems Wyoming-Idaho-northern Utah: Deep drilling frontiers of the central Rocky Mountains: Denver, Rocky Mountain Association of Geologists, p. 41-54.

Saleeby, J. B., and Busby-Spera, C., 1992, Early Mesozoic tectonic evolution of the western U.S. Cordillera,in Burchfiel, B. C., Lipman, P. W., and Zoback, M. L., editors, The Cordilleran Orogen: Conterminous U. S.: Geological Society of America, The Geology of North America, v. G-3, p. 107–168.

Sears, J., 2001, Emplacement and denudation history of the Lewis-Eldorado-Hoadley thrust slab in the northern Montana Cordillera, USA; implications for steady-state orogenic processes: American Journal of Science, v. 301, p. 359-373.

Smith, D., Miller, E., Wyld, S., and Wright, J., 1993, Progression and Timing of Mesozoic Crustal Shortening in the Northern Great Basin, Western U.S.: Mesozoic Paleography of the Western United States, v. 71, p. 389-405.

Solum, J., and der Pluijm, B. v., 2007, Reconstructing the Snake River-Hoback River Canyon section of the Wyoming thrust belt through direct dating of clay-rich fault rocks: Geological Society of America- Special Paper, v. 433, p. 183-196.

Speed, R. C., and Sleep, N. H., 1982, Antler orogeny and foreland basin: A model: Geological Society of America Bulletin, v. 93, p. 815-828.

Stewart, J., 1972, Initial Deposits in the Cordilleran Geosyncline: Evidence of a Late Precambrian <850 m.y. Continental Separation: Geological Society of America Bulletin, v. 83, p. 1345-1360.

Stockli, D. F., Linn, J. K., Walker, J. D., and Dumitru, T. A., 2001, Miocene unroofing of the Canyon Range during extension along the Sevier Desert Detachment, west-central Utah: Tectonics, v. 20, p. 289-307.

Sullivan, W. A., and Snoke, A. W., 2007, Comparative anatomy of core-complex development in the northeastern Great Basin, USA: Rocky Mountain Geology, v. 42(1), p. 1-29.

Taylor, W., Bartley, J., Martin, M., Geissman, J., Walker, J., Armstrong, P., 2000, Relations between hinterland and foreland shortening: Sevier orogeny, central North American Cordillera: Tectonics, v. 196, p. 1124-1143.

Turcotte, D. L., and Schubert, G., 2002, Geodynamics, 2nd edition: New York, New York, Cambridge
University Press, p. 456.

Wells, M., Dallmeyer, R., and Allmendinger, R., 1990, Later Cretaceous extension in the hinterland of the Sevier thrust belt, northwestern Utah and southern Idaho: Geology, v. 18, p. 929-933.

Wells, M., 1997, Alternating contraction and extension in the hinterlands of orogenic belts: An example from the Raft River Mountains, Utah: Geological Society of America Bulletin, v. 109, p. 107-126.

Wells, M., Snee, L.W., and Blythe, A.E., 2000, Dating of major normal fault systems using thermochronology: An example from the Raft River detachment, Basin and Range, western United States: Journal of Geophysical Research, v. 105, p. 16,303–16,327.

Wells, M., and Hoisch, T., 2008, The role of mantle delamination in widespread Late Cretaceous extension and magmatism in the Cordilleran orogen, western United States: Geological Society of America Bulletin, v. 120, p. 515-530.

Wells, M., Hoisch, T., Cruz-Uribe, A., and Vervoort, J., 2012, Geodynamics of Synvergent extension and tectonic mode switching: Constraints from the Sevier-Laramide orogen: Tectonics, v. 31, p. 1002.

Wells, M., Vervoort, J., Lacy, A., Cruz-Uribe, A., Beyene, M., and Kelly, E., 2013, The Sevier-Laramide Hinterland: Initial Late Jurassic-Early Cretaceous Shortening, Renewed Early Late Cretaceous Shortening and the Influence of a Delamination Cycle on Wedge Mechanics: Geological Society of America- Abstracts with Programs, v. 125, p. 208.

Wenickie, B., Axen, G., and Snow, J., 1988, Basin and Range extensional tectonics at the latitude of Las Vegas, Nevada: Geological Society of America Bulletin, v. 100, p. 1738-1757.

Wiltschko, D.V., and Dorr Jr, J.A., 1983, Timing of Deformation in overthrust belt and foreland of Idaho, Wyoming, and Utah: American Association of Petroleum Geologists Bulletin, v. 67, p. 1304-1322.

Wright, J. E., and J. L. Wooden, 1991, New Sr, Nd, and Pb isotopic data from plutons in the northern Great Basin: Implications for crustal structure and granite petrogenesis in the hinterland of the Sevier thrust belt, Geology, v. 19, p. 457-460.

Yonkee, A., Parry, W., Bruhn, R., and Cashman, P., 1989, Thermal Models of Thrusting: Contraints from fluid-inclusion observations, Willard thrust sheet, Idaho-Utah-Wyoming thrust belt: Geological Society of America Bulletin, v. 101, p. 304-313.

Yonkee, A., 1992, Basement-cover Relations, Sevier Orogenic Belt, Northern Utah: Geological Society of America Bulletin, v. 104, p. 280-302.

Yonkee, W., DeCelles, P., and Coogan, J., 1997, Kinematics and Synorogenic Sedimentation of the Eastern Frontal Part of the Sevier Orogenic Wedge, Northern Utah: Brigham Young University Geology Studies, v. 42, p. 355-375.

Yonkee, A., 2005, Strain patterns within part of the Willard thrust sheet, Idaho-Utah-Wyoming thrust belt: Journal of Structural Geology, v. 27, p. 1315-1343.

Yonkee, A., and Weil, A., 2011, Evolution of the Wyoming Salient of the Sevier Fold-Thrust Belt, Northern Utah to Western Wyoming: Utah Geological Association Publication, v. 40, p. 1-56.

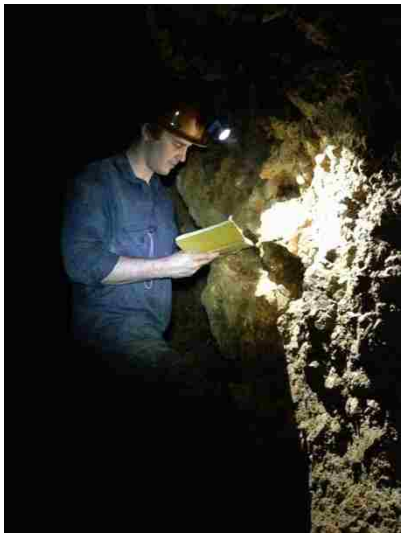

Vita

Bryan R. Eleogram

M.Sc. Geologist
(702)556-5501
Eleogram@unlv.nevada.edu

UNLV
UNIVERSITY OF NEVADA LAS VEGAS

I am graduate student from the University of Nevada, Las Vegas currently on track to graduate in April 2014 with an MSc in geology. I am perusing a career as a Professional Geologist in the **Petroleum Exploration** sector.

My experience includes working on an underground mapping project at Sterling Gold Mine in southern Nevada and participating in the **Imperial Barrel Award** program.

I have been a student athlete and understand the importance of **team work** and a commitment to health and safety.

I believe my set of skills, along with a strong desire to learn are valued assets that will benefit a company in attaining its goals.

Skills:

General

- 2D and 3D seismic interpretation
- Excellent work within individual and team environments
- Overriding commitment to organizational and leadership skills

- High technical communication skills
- French Horn player for over 6 years

Geologic mapping

- Mapping assistant to structural geologist Dr. Michael Wells in the Grouse Creek Quadrangle in northern Utah
- Detailed geologic mapping of structures, lithologies, and alteration within the underground Sterling Gold Mine

Core Logging

- Detailed core logging as a student researcher for structural geologist Dr. Wanda Taylor
- In depth core logging of lithologies, alteration, and mineralization at Sterling Gold Mine

Analytical Background

- Advanced mineral separation using heavy liquids and magnet separators
- Aliquot dissolution using HNO_3 and HF
- Petrel Geophysics Software and B-Mod Basin analysis software by Schlumberger Limited
- Iolite Software for laser ablation ICPMS data reduction
- Equipment operation (Laser Ablation ICPMS, ^4He extraction line, SEM, etc.)

Employment History

- **Geology Internship**
  Sterling Gold Mine
  Advisor: Chuck Stevens (775) 372-5229
  May 2013 – August 2013

- **Undergraduate Assistant**
  University of Nevada, Las Vegas
  Advisor: Dr. Michael Wells (702) 895-0828
  Dr. Wanda Taylor (702) 445-4391
  June 2011 – January 2012

- **Geology Internship**
  National Security Technologies LLC
  Advisor: Robert White (702) 295-0577
  May 2010 – August 2010

- **Civil Engineering & Design Internship**
  National Security Technologies LLC
  Advisor: Steven Gould (702) 295-6252

  June 2009 – May 2010

Honors

- **2012/2013 Imperial Barrel Awards Participant**
- **American Association of Petroleum Geologists Member (Student)**
- **Geological Society of America Member (Student)**
- **Millennium Scholarship Recipient**
- **University of Nevada, Las Vegas Geo-club Member**

Education

Master of Science in Geology
GPA: 3.7/4.0
Structural Geology, Advisor: Dr. Michael Wells
University of Nevada, Las Vegas
Spring 2012 – Fall 2013

Bachelor of Science in Geology
Geology GPA: 3.0/4.0
University of Nevada, Las Vegas
Fall 2006 – Fall 2011

Research

THE APPLICATION OF ZIRCON (U-TH)/HE THERMOCHRONOLOGY TO DETERMINE THE TIMING AND SLIP RATE ON THE WILLARD THRUST, SEVIER FOLD AND THRUST BELT, NORTHERN UTAH

ELEOGRAM, Bryan[1], YONKEE, Adolph[2], WELLS, Michael L.[1], STOCKLI, Daniel F.[3], GENTRY, Amanda[2], and GIALLORENZO, Michael A.[1], (1) Department of Geosciences, University of Nevada Las Vegas, 4505 South Maryland Parkway, Las Vegas, NV 89154-4010, eleogram@unlv.nevada.edu, (2) Department of Geosciences, Weber State University,

2507 University Circle, Ogden, UT 84408, (3) Department of Geological Sciences, University of Texas at Austin, Austin, TX 78712

Although the Sevier belt is one of the best studied fold-thrust systems in the world, timing of motion on dominant western thrust sheets that carry thick Neoproterozoic to Paleozoic strata, including the Willard thrust sheet (WTS) of northern Utah, remains incompletely understood. Interpretations for the age of initial slip on the WTS vary widely from 140 to 115 Ma, reflecting ambiguous relations with foreland basin strata and limited geochronologic data. Large displacement on the WTS (~60 km net slip), wide range of exposed levels (>8 km vertical structural relief), and wide aerial extent (>60 km horizontal length) provided an ideal setting for application of zircon (U-Th)/He thermochronology (ZHe) to evaluate thrust timing. Samples were collected along three pseudo-vertical transects that spanned the eastern leading, east-central, and central parts of the WTS (with ~0.5 to 1 km sample spacing) and along a stratigraphic-parallel (pseudo-horizontal) traverse at an intermediate level across the sheet. Due to relatively slow cooling rates and multi-kinetic zircon populations, grains were prescreened based on similar U-Pb ages and U/Th contents, with 6 grains selected for ZHe analysis at each sample site. Vertical transects capture an Early Cretaceous partial retention zone (PRZ) with slow cooling starting at ~130 Ma. Cooling ages increase systematically upward in the east-central and central transects, yielding an average exhumation rate of 0.12 mm/yr.; only part of the PRZ is preserved along the eastern leading edge of the sheet. Detrital zircon analysis of Aptian to Turonian (~125-90 Ma) synorogenic strata also record protracted, slow exhumation of upper levels of the WTS. The horizontal traverse yields an average slip rate of 1.7 mm/yr. from ~125 to 90 Ma (assuming a constant geothermal gradient), consistent with estimated net slip. $^{40}Ar/^{39}Ar$ UV laser ablation ages of mica in the western, basal part of the WTS are ~145-130 Ma, recording early alteration and internal deformation that preceded large-scale thrust slip. The WTS was subsequently passively uplifted and exhumed during Late Cretaceous development of the Wasatch anticlinorium. Additional work is underway to increase sample density and conduct thermo-kinetic modeling to evaluate potential temporal variations in exhumation and slip rates.

References

Dr. W. Adolph Yonkee
Weber State University
Structural Geology

(801)-626-7419
ayonkee@weber.edu

Dr. Andrew Hanson
University of Nevada, Las Vegas
Sedimentology
(702)895-2263
Andrew.Hanson@unlv.edu

Dr. Patrick McAndles
Vice President Exploration
Imperial Metals Corporation
(604)488-2665
pmcandless@imperialmetals.com

Dr. Wanda Taylor
University of Nevada, Las Vegas
Structural Geology
(702)895-4615
Wanda.Taylor@unlv.nevada.edu

Dr. Stephen M. Rowland
University of Nevada, Las Vegas
Paleontology
(702)895-3625
Steve.Rowland@unlv.edu